ASTR

Science and Engineering Research Council

Rutherford Appleton Laboratory

Chilton DIDCOT Oxon OX11 0QX   RAL-92-084

Proceedings of the Workshop on Astronomy and Astrophysics "Dusty Discs" 26-28 May 1992, The Covener's House, Abingdon

P M Gondhalekar, editor

December 1992

ERRATUM

Proceedings of the RAL Workshop on Astronomy and Astrophysics

Dusty Discs
26-28 May 1992
P M Gondhalekar, editor
RAL 92-084

Note following errors in these proceedings;

- page 3, line 4 should read
  ....stars having detectable inner disc less than 10% of older stars...

- page 3, line 6 should read
  ......yielded a 42% detection rate, and no measurable dependence of the disc mass on the stellar age.

- page 3, line 20 should read
  ......very few discs have $q=3/4$ with most in the range.......

- page 4, line 17 should read
  ....polarization of about 17% between $\theta=15$ and 35 arc sec from the star........

- page 5 has been repeated on page 6

- page 29, bottom three lines have been repeated at the top of page 30.

Rutherford Appleton Laboratory
Workshop on Astronomy and Astrophysics

Dusty Discs

Edited by:

P M Gondhalekar
Rutherford Appleton Laboratory
Chilton, DIDCOT, Oxon
OX11 0QX, England.

26 − 28 May 1992
The Cosener's House, Abingdon.

CONTENTS

PREFACE

Discs are known to exist around many types of star, from the initial stages of their formation to their eventual demise. Data have been gathered using a wide variety of techniques (*IUE*, optical polarimetry, *IRAS*, sub-millimeter, radio masers etc.), and in view of the expected launch of *ISO* in the near future and the plans for *EDISON*, it was an appropriate time to examine the current status of research in this area. Around 30 astronomers/astrophysicists met in the Coseners' House, Abingdon, to discuss Dusty Discs. This was the 9th RAL Workshop on Astronomy and Astrophysics, and followed the established pattern of informal presentations on key topics and lots of discussion 'around-the-table'. The speakers were asked to remember the discussions when writing up their presentations for these proceedings.The workshop aimed to bring together observers from a broad range of wavelengths and theoreticians to survey current knowledge and map future avenues of research. The contents of these proceedings show how well this aim was realised. A very wide range of observational and theoretical topics were addressed and these topics generated a great deal of lively discussion. The organisers are grateful to all the participants for their contributions.

Helen J Walker
November 1992

Acknowledgements

Participants

M J Barlow	University College London, England.
S Beckwith	MPIf Astronomie, Germany.
J Bunn	University of Oxford, England.
H M Butner	NASA Ames Research Center, California, USA.
C Clarke	University of Cambridge, England.
C Clayton	Rutherford Appleton Laboratory, England.
J Cohen	NRAL, Jodrell Bank, England.
L Cornwall	Rutherford Appleton Laboratory, England.
J Drew	University of Oxford, England.
R Emery	Rutherford Appleton Laboratory, England.
P Gondhalekar	Rutherford Appleton Laboratory, England.
B J Kellett	Rutherford Appleton Laboratory, England.
A Heske	ISO, Science Operations Team/ESA, The Netherlands.
M Hoare	University of Oxford, England.
V Mannings	Queen Mary & Westfield College, England.
P Podsiadlowski	University of Cambridge, England.
H Pongracic	University of Wales, College of Cardiff, Wales.
J Porter	Univeristy of Oxford, England.
M Scarrott	University of Durham, England.
R Sylvester	University College London, England.

E Szuszkiewicz   Queen Mary & Westfield College, England.

H Walker   Rutherford Appleton Laboratory, England.

D Ward-Thompson   MRAO, University of Cambridge, England.

R Warren-Smith   Rutherford Appleton Laboratory, England.

D Whitmire   University of South Western Louisiana, USA.

R Wolstencroft   Royal Observatory, Edinburgh, Scotland.

D Wonnacott   Rutherford Appleton Laboratory, England.

J Yates   NRAL, Jodrell Bank, England.

Dusty Stellar Discs : An Overview

Ramon D Wolstencroft
Royal Observatory
Edinburgh EH9 3HJ

1   INTRODUCTION

My task is to set the scene, *i.e.* to briefly review the field of dusty stellar discs focussing particularly on areas where our current understanding and observational data need to be clarified and improved. I plan to cover the ground in a chronological sequence, and will discuss not only pre-main sequence discs and the discs that survive onto the main sequence, but also the evidence for post main-sequence discs, which may not be generically related to the discs seen around young and middle aged stars. The review will cover (some of) what we know of the properties of discs and what we understand about the processes which act on the discs during their lifetime.

2   FORMATION OF STARS AND DISCS

2.1   Low Mass Stars

It is widely believed that circumstellar discs are a natural and perhaps inevitable by-product of the low mass ($M \leq 2\ M_\odot$) star formation process. The broad theoretical outlines of how discs may form have been described by Shu, Adams & Lizano (1987). They identify four main stages (see their fig. 1): (a) dense cores within a molecular cloud slowly collapse under the constraints of ambipolar diffusion; (b) an individual core collapses from the inside outwards with low angular momentum material building an accreting protostar and material of high angular momentum forming a nebular disc; (c) a strong stellar wind starts up along the rotation axis of the star-disc system, reversing the infall in the polar directions and sweeping up material to form a CO bipolar outflow; and (d) the solid angle of the outflow grows and the central star becomes visible either directly or indirectly via scattered light; eventually the infall stops. The timescales for these processes are believed to be $\sim 10^6$ yr for phase (a) (timescale before dynamical collapse) and $\sim 10^5$ yr for (b) to (d). The main phase of disc evolution takes place as viscous forces cause matter to migrate inwards and angular momentum to be transported outwards: during this phase classical T Tauri stars evolve into weak-line T Tauri stars as inner disc accretion slows and the wind weakens. The crucial question of what drives the neutral wind, which in turn is thought to drive the CO outflow, is most probably answered in terms of MHD forces acting on matter accreting at the inner edge of the disc: either the matter arriving at the inner edge of the disc becomes part of the neutral wind directly (see e.g. Pudritz and Norman, 1986), or material flows inwards from the inner edge of the disc towards the stellar equator before being accelerated away from a

boundary layer in an MHD driven wind by the so-called X-celerator mechanism (Shu et al. 1988; 1991).

The above view applies of course only to single stars and since the majority of main sequence stars are known to be in binary or multiple systems (Duquennoy & Mayor, 1991) it is evidently incomplete: the subject of interacting and merging protostar-disc systems and the formation of binary systems needs to make considerable progress before we have complete confidence that the above outline scenario applies to most stars.

2.2 Evidence for young discs around high mass stars

Current theories of the formation of higher mass stars ($M > 2~M_\odot$) do not, as far as I am aware, allow for the effects of rotation or magnetic fields so that the possibility of disc formation is precluded (see e.g. Palla & Stahler 1991). Nevertheless there is some evidence for discs in some higher mass stars which theory will need to explain in due course.

Ultracompact (UC) HII regions ($< 10^{17}~cm$) are presumed to be energised by newly formed O and B stars. The discovery of CO bipolar outflows associated with some UC HII regions suggests that collimating discs may be present around at least some high mass YSO's: examples are G5.89 - 0.39, GGD27, DR21 and NGC2024 (IRS5). In some cases the molecular disc has been detected in the transitions of high density tracer molecules such as NH_3 and CS. A good example is G35.2 - 0.7N, studied by Brebner et al. (1987) who find a massive $150M_\odot$, slowly rotating molecular disc whose major axis is orthogonal to the outflow: OH masers, which trace the inner parts of the disc, are seen and define a position angle which is also orthogonal to the outflow.

Intermediate mass Herbig Ae/Be stars ($M \sim 2M_\odot to 5M_\odot$) as a class exhibit a strong infrared excess which is associated with circumstellar dust (see, e.g. Catala, 1989). Evidence concerning the spatial distribution of this dust is only available for ~ 10 of the 57 known Ae/Be stars. In the case of RMon and RCrA, optical polarization maps show a polarization disc (Ward-Thompson et al., 1985; Scarrott et al., 1989) which can be interpreted in terms of a physical disc (Bastien and Menard, 1988; Gledhill, 1991). For LKHα234 Dent et al. (1989) interpret their 1100μm JCMT continuum maps in terms of a dust ring that may have evolved from a dust disc. Finally, Corcoran et al. (1992) find that the high velocity forbidden lines in 6 Ae/Be stars are always blue-shifted implying that the red-shifted component of the optical outflow is obscured by a disc: this is exactly analogous to the result found by Apenzeller et al. (1984) for T Tauri stars and cited as evidence for discs.

3   PROPERTIES OF PRE-MAIN-SEQUENCE DISCS AROUND LOW MASS STARS

In section 2.1 we briefly described how discs may form as a normal, and perhaps inevitable, accompaniment to the low mass star formation process: we now use this as a framework to examine and discuss what is known about these discs and in particular the frequency of occurrence of discs. Thermal emission from discs allows us to study the innermost discs of T Tauri stars at short wavelengths (2 to 5μm) and the cool outer parts at 1mm. If outflows are driven by accretion and if gradual erosion of the inner disc region occurs as a result,

we expect older discs preferentially to show a decrease of near infrared excess but little change of mm wave emission. The study of over 80 T Tauri stars in the Taurus-Auriga dark clouds by Skrutskie et al. (1990) at 2.2μm and 10μm confirmed this effect with 50% of young ($< 3 \times 10^6$ yr) stars having detectable inner discs but ¡ 10% of older stars having discs ($> 10^7$ yrs); 1.3mm continuum measurements of 86 T Tauri stars also in the Taurus-Auriga dark clouds by Beckwith et al. (1990) yielded a 42of the disc mass on the stellar age. The gradual erosion of the inner disc or growth of the inner dust free zone with age could in principle have an alternative explanation, namely the growth of planetisimals, and it is not yet clear how to distinguish between the alternatives. Another factor noted in section 2.1. that could influence disc occurrence is the presence of a binary companion: Beckwith et al. (1990) found statistical evidence that stars with close companions have very small or no detectable disc masses.

The micron to millimetre spectral energy distribution may be modelled to yield the temperature and mass distribution within the disc (see Beckwith et al., 1990). The disc is assumed to be thin and flat, to follow a power law for temperature $T(r) = T(r_o)(r/r_o)^{-q}$ and surface mass density $\sigma(r) = \sigma(r_o)(r/ro)^{-p}$, and to be optically thin or thick at $\lambda >$ or$< 100\mu m$. Such a disc, either passively heated by the parent star or heated by viscous frictional jostling of disc particles (reprocessing disc), should have q $=3/4$ and $\nu F_\nu \propto \nu^\alpha$ where $\alpha = 4 - 2/q = 4/3$. However Beckwith et al. (1990) find that very few discs have q $=$ with most in the range 0.50 to 0.65 $i.e.$ flat νF_ν spectra. Various suggestions have been made to explain this slower decline in T(r) than predicted, e.g. in terms of flared discs which would be preferentially heated at large r (Kenyon & Hortmann, 1987); however it is not clear which if any of these suggestions is correct. Model fits yield dust temperatures at ro $= 1$AU in the range 50 to 250K for the Beckwith et al. sample with a median value of about 100K.

Disc masses may be deduced from the optically thin millimetre emission provided the grain emissivity, K_ν , disc radius, R_D, and the parameters $(p, T(r_o), q)$ are known. K_ν is the most difficult of these quantities to estimate (Beckwith & Sargent, 1991) and as a result the masses deduced are uncertain by a factor of about 5. Assuming that the gas to dust ratio of 100 typical of the interstellar medium also applies to the discs, the total disc masses for the Beckwith et al. (1990) sample fall in the range 0.001 to 1 $M\odot$.

4   DISCS AROUND MAIN SEQUENCE STARS

How many of the discs seen around low mass YSO's have survived by the time the parent stars have reached the main sequence, and what processes dominate the evolution of discs in the late pre-main-sequence phase? To answer these questions we require a survey of the infrared excesses and A_v values of a large well defined sample of main sequence stars : this would provide (a) information on the frequency of occurrence of dust shells and discs for different spectral types and (b) constraints on the timescale for the evaporation of discs. The possible mechanisms involved include the accretion of dust particles onto the star (e.g. by the Poynting Robertson effect combined with the effect of grain-grain collisions), grains swept up by stellar winds and the growth of planetisimals to form planets and comets: each process will have a characteristic timescale which should act as a discriminant in deciding whether one process dominates.

Apart from the well known evidence from IRAS of dust discs around β Pictoris, Vega

3

and Fomalhaut a number of IRAS-based lists of candidate stars with possible discs have been published (e.g. Sadakane & Nishida, 1986; Aumann, 1985; Walker & Wolstencroft, 1988) and are being followed up (see e.g. Barlow & Skinner, this conference). Early type stars tend to dominate these lists because of "luminosity bias" (T^4 dependence), but after due allowance for this selection effect, Aumann (1988) concludes that the incidence of dust shells, and by inference dust discs left over from their pre-main-sequence phase, is about equal around main sequence A, F and G stars, and that discs are the rule rather than the exception: this result was based on a volume limited sample of stars within 25pc. On the other hand a magnitude limited sample of 5706 high latitude B to M stars taken from the SAO catalogue yielded only 379 stars with a significant infrared excess (Stencel and Backman, 1991).

The disc around *beta* Pictoris is unique in having the largest infrared excess associated with any main sequence star and in being seen optically as a nearly edge-on disc as a result of light from the star scattered by the disc particles (Smith & Terrile, 1984). Models of the disc have been developed by various authors based on a variety of data and are not readily reconciled. For example optical imaging polarimetry by Gledhill, Scarrott & Wolstencroft (1991) shows a relatively constant polarization of about $17\theta = 15$ and 35 arcsec from the star (240 to 560 pc) and a surface brightness $\propto \theta^{-4}$: modelling these data with an edge-on disc having power law size and number density distributions yields $n(a) \propto a^{-4.0}, \rho(r) \propto r^{-2.75}$ and an average grain size $\sim 0.2\mu m$. Scattered light from such a grain population ought to be blue but the disc has a neutral colour according to Paresce and Burrows (1987), and Artymowicz et al. (1989) have concluded that the grains must therefore be larger than $1\mu m$. On the other hand the grain temperature at 80 AU derived from 10.8 and $19.2\mu m$ imaging by Telesco et al. (1988) is 130K, considerably higher than the black body temperature of 50K at that distance implying small ($0.2\mu m$) silicate grains (see also Telesco and Knacke, 1991). It appears that a hybrid model is needed to reconcile these anomalies: Backman, Gillett & Witteborn (1992) suggest a two component model with sub-micron grains and a relatively low total density within 80 AU, and a sharp transition beyond 80 AU to a higher density disc with an average grain size $\sim 3\mu m$. Note that in these models the grain temperature at 80 AU lies in the range 90 to 140K corresponding to the sublimation temperature for ice, suggesting a physically plausible reason for the two zone model. If this disc is typical it is clear that considerable caution will be needed in fitting acceptable models to other discs where there is less data.

5   POST MAIN SEQUENCE DISCS

In pre-main-sequence objects the presence of optical or molecular outflows is a clear sign that discs may be present to collimate the outflow or even perhaps to be a vital element in its generation. Bipolar flows are also often seen in post AGB objects with about 60% and 15% of planetary nebulae showing respectively a weakly or strongly bipolar morphology implying the current or past existence of such flows. Many proto-planetary nebulae are likewise known to be strongly bipolar. If discs are responsible for these post main sequence bipolar flows it seems very unlikely that they are relics of the main sequence discs. Morris (1981, 1987) first drew attention to this problem and suggested that where the central star is a close binary an accretion disc may naturally form in the orbital plane of the binary when both stars are sources of a stellar wind. The frequency of

main sequence binaries of all separations is sufficiently high (60%) (Duquennoy & Mayor, 1991) to lend support to this idea. Examples of systems where there is strong evidence for a disc include the planetary nebulae NGC2346 and NGC6302 which exhibit molecular tori oriented normal to the bipolar lobes (Zuckerman & Gatley, 1988; and Payne, Phillips & Terzian, 1988 respectively): the suggestion here is that a central dust disc may be shielding the molecules of the torus from dissociation. OH231.8 + 4.2 is an evolved star at the centre of a bipolar nebula which exhibits a polarization disc (Scarrott, Rolph & Wolstencroft, 1990) which is strong evidence for the presence of a circumstellar disc.

A final postscript to this overview of stellar discs concerns the fate of planetary systems during the post-main-sequence phase of stellar evolution. Stern, Shull and Brandt (1990) argue that the comets of the Kuiper disc and the Oort cloud will be partially evaporated during this luminous phase of evolution and provide large amounts of H_2O, OH and complex molecules in the envelopes of these stars and that the time variable OH and H_2O maser structures seen within 10 to 100 AU of the star may be associated with orbiting, evaporating comets. In a similar vein Struck-Marcell (1988) argues that SiO masers in Mira-type stars may be associated with the magnetospheres and orbital wakes of Jovian planets.

6 CONCLUSIONS

In this very active field there are naturally a multitude of questions that need to be addressed. Arising out of this overview I have selected a handful of questions that I believe deserve special attention at this workshop:

1. how can we improve our understanding of the role of disc accretion and MHD forces in the generation of outflows?

2. how does the presence of a binary companion influence the formation, survival and properties of a CS disc?

3. do most low mass stars lose most or all of their disc mass by the time they reach the main sequence, and if so what role does planetisimal formation play?

4. do most high mass ($M > 2M_\odot$) stars have discs?

5. why does the disc temperature profile T(r) decline more slowly than predicted?

6. why is β Pic the only main sequence star with an optically visible disc?

7. how common are post main sequence discs and do they only form in close binary systems?

main sequence binaries of all separations is sufficiently high (60%) (Duquennoy & Mayor, 1991) to lend support to this idea. Examples of systems where there is strong evidence for a disc include the planetary nebulae NGC2346 and NGC6302 which exhibit molecular tori oriented normal to the bipolar lobes (Zuckerman & Gatley, 1988; and Payne, Phillips & Terzian, 1988 respectively): the suggestion here is that a central dust disc may be shielding the molecules of the torus from dissociation. OH231.8 + 4.2 is an evolved star at the centre of a bipolar nebula which exhibits a polarization disc (Scarrott, Rolph & Wolstencroft, 1990) which is strong evidence for the presence of a circumstellar disc.

A final postscript to this overview of stellar discs concerns the fate of planetary systems during the post-main-sequence phase of stellar evolution. Stern, Shull and Brandt (1990) argue that the comets of the Kuiper disc and the Oort cloud will be partially evaporated during this luminous phase of evolution and provide large amounts of H_2O, OH and complex molecules in the envelopes of these stars and that the time variable OH and H_2O maser structures seen within 10 to 100 AU of the star may be associated with orbiting, evaporating comets. In a similar vein Struck-Marcell (1988) argues that SiO masers in Mira-type stars may be associated with the magnetospheres and orbital wakes of Jovian planets.

6   CONCLUSIONS

In this very active field there are naturally a multitude of questions that need to be addressed. Arising out of this overview I have selected a handful of questions that I believe deserve special attention at this workshop:

1. how can we improve our understanding of the role of disc accretion and MHD forces in the generation of outflows?

2. how does the presence of a binary companion influence the formation, survival and properties of a CS disc?

3. do most low mass stars lose most or all of their disc mass by the time they reach the main sequence, and if so what role does planetisimal formation play?

4. do most high mass ($M > 2M_\odot$) stars have discs?

5. why does the disc temperature profile T(r) decline more slowly than predicted?

6. why is β Pic the only main sequence star with an optically visible disc?

7. how common are post main sequence discs and do they only form in close binary systems?

REFERENCES

Apenzeller, I., Jankovics, I. and Ostreicher, R., 1984. *Astr. Astrophys.*, **141**, 108.

Artymowicz, P., Burrows, C., and Paresce, F., 1989. *Astrophys. J.*, **337**, 494.

Aumann, H.H., 1985. *Publs. astr. Soc. Pacif.*, **97**, 885.

Aumann, H.H., 1988. *Astr. J.*, **96**, 1415.

Backman, D.E., Gillett, F.C. and Witteborn, F.C., 1992. *Astrophys. J.*, **385**, 670.

Bastien, P. & Menard, F., 1988. *Astrophys. J.*, **326**, 334.

Beckwith, S.V.W., Sargent, A.I., Chini, R.S. and Gusten, R., 1990. *Astr. J.*, **99**, 924.

Beckwith, S.V.W. and Sargent, A.I., 1991. *Astrophys. J.*, **381**, 250.

Brebner, G.C., Heaton, B., Cohen, R.J. and Davies, S.R., 1987. *Mon. Not. R. astr. Soc.*, **229**, 679.

Catala, C., 1989. *In: Low Mass Star Formation and Pre-Main-Sequence Objects ,.* ed. B Reipurth, ESO Conf. Publn. No. 33, p471.

Corcoran, D., Ray, T.P. and Mundt, R., 1992. *In: Stellar Jets and Bipolar Outflows ,.* Proceedings of the 6th International Workshop of the Osservatorio Astronomico di Capodimonte (in press).

Dent, W.R.F., Sandell, G., Duncan, W.D. and Robson, E.I., 1989. *Mon. Not. R. astr. Soc.*, **238**, 1497.

Duquennoy, A. and Mayor, M., 1991. *Astr. Astrophys.*, **248**, 485.

Gledhill, T.M., 1991. *Mon. Not. R. astr. Soc.*, **252**, 138.

Gledhill, T.M., Scarrott, S.M. and Wolstencroft, R.D., 1991. *Mon. Not. R. astr. Soc.*, **252**, 50P.

Kenyon, S.J. and Hartmann, L., 1987. *Astrophys. J.*, **323**, 714.

Morris, M., 1981. *Astrophys. J.*, **249**, 572.

Morris, M., 1987. *Publs. astr. Soc. Pacif.*, **99**, 1115.

Palla, F. and Stahler, S.W., 1991. *Astrophys. J.*, **375**, 288.

Paresce, F. & Burrows, C., 1987. *Astrophys. J.*, **319**, L23.

Payne, H.E., Phillips, J.A. & Terzian, Y., 1988. *Astrophys. J.*, **326**, 368.

Pudritz, R. and Norman, C., 1986. *Astrophys. J.*, **301**, 571.

Sadakane, K. and Nishida, M., 1986. *Publs. astr. Soc. Pacif.*, **98**, 685.

Scarrott, S.M., Draper, P.W. and Warren-Smith, R.F., 1989. *Mon. Not. R. astr. Soc.*, **237**, 621.

Scarrott, S.M., Rolph, C.D. and Wolstencroft, R.D., 1990. *Mon. Not. R. astr. Soc.*, **243**, 462.

Shu, F.H., Lizano, S., Ruden, S.P. and Najita, J., 1988. *Astrophys. J.*, **328**, L19.

Shu, F.H., Ruden, S.P., Lada, C.J. and Lizano, S., 1991. *Astrophys. J.*, **370**, L31.

Smith, B.A. and Terrile, R.J., 1984. *Science.*, **226**, 1421.

Smith, R.F., 1989. *Mon. Not. R. astr. Soc.*, **237**, 621.

Stencel, R.E. and Backman, D.E., 1991. *Astrophys. J. Suppl.*, **75**, 905.

Stern, S.A., Shull, J.M. and Brandt, J.C., 1990. *Nature*, **345**, 305.

Struck-Marcell, C., 1988. *Astrophys. J.*, **330**, 986.

Telesco, C.M., Becklin, E.E., Wolstencroft, R.D. and Decher, R.. 1988, *Nature*, 335. 51

Telesco, C.M. and Knacke, R.F., 1991. *Astrophys. J.*, **372**, L29.

Ward-Thompson, D., Warren-Smith, R.F., Scarrott, S.M. and Wolstencroft, R.D., 1985. *Mon. Not. R. astr. Soc.*, **215**, 537.

Zuckerman, B. and Gatley, I., 1988. *Astrophys. J.*, **324**, 501.

An Investigation of Circumstellar Discs using an Imaging Polarimeter

S.M.Scarrott, P.W.Draper & T.M.Gledhill
Physics Department,
University of Durham,
South Road, Durham, DH1 3LE .

Abstract

Optical polarization studies of nebulous stars in all stages of evolution show unexpected features which are attributed to the effects of circumstellar discs, possibly of solar system dimensions, and we discuss the various mechanisms which could account for these observations. We also present a simple scattering model to explain the polarization characteristics of the nebula surrounding the main- sequence star β Pictoris which suggests that the disc-like structure contains a population of dust grains which is not untypical of the general interstellar medium.

1 INTRODUCTION

Many stars in pre-, post- and main-sequence evolutionary stages act as illuminators of reflection nebulae created by the scattering of the central starlight by surrounding dusty material. In this scattering process the light is polarized such that the E-vector of the emergent radiation is perpendicular to the scattering plane and this leads to the characteristic circular pattern of vectors seen in polarization maps of reflection nebulae.

Fig. 1 shows a polarization map of the well-known cometary reflection nebula NGC2261 illuminated by the pre-main-sequence star R.Mon seen as the star-like knot in the contour map. At offsets ≥ 20 arcsec from the illuminating star the vector pattern is quite circular and centred on R.Mon; this is the expected pattern for a simple reflection nebula illuminated from within by a single point-like source. However, in the immediate neighbourhood of R Mon this circular pattern breaks down and is replaced by a band of polarization vectors forming a near parallel array across the head of the nebula which terminates in null points (zero levels of polarization) on either side of the star. This pattern is not expected in the simple reflection scenario and has become known as the polarization disc since it appears to be related to an assumed circumstellar disc of material surrounding the central illuminator.

Fig. 2 shows a large scale map of the RNO91/L43 nebulosity which again shows the regular circular pattern of a simple reflection nebula, this time illuminated by the T-Tauri star (RNO91) seen as the bright central knot in the contour map. However, in the high spatial resolution map of the very central region (Fig. 3) the circular pattern again gives way to create the polarization disc with parallel vectors and null points. Although the intensity contours (left hand frame) are approximately circular the polarized intensity contours (right hand frame) are quite different and show a "pinching" effect which suggests the level of polarization is systematically reduced on either side of the star. The line

R Mon I-band
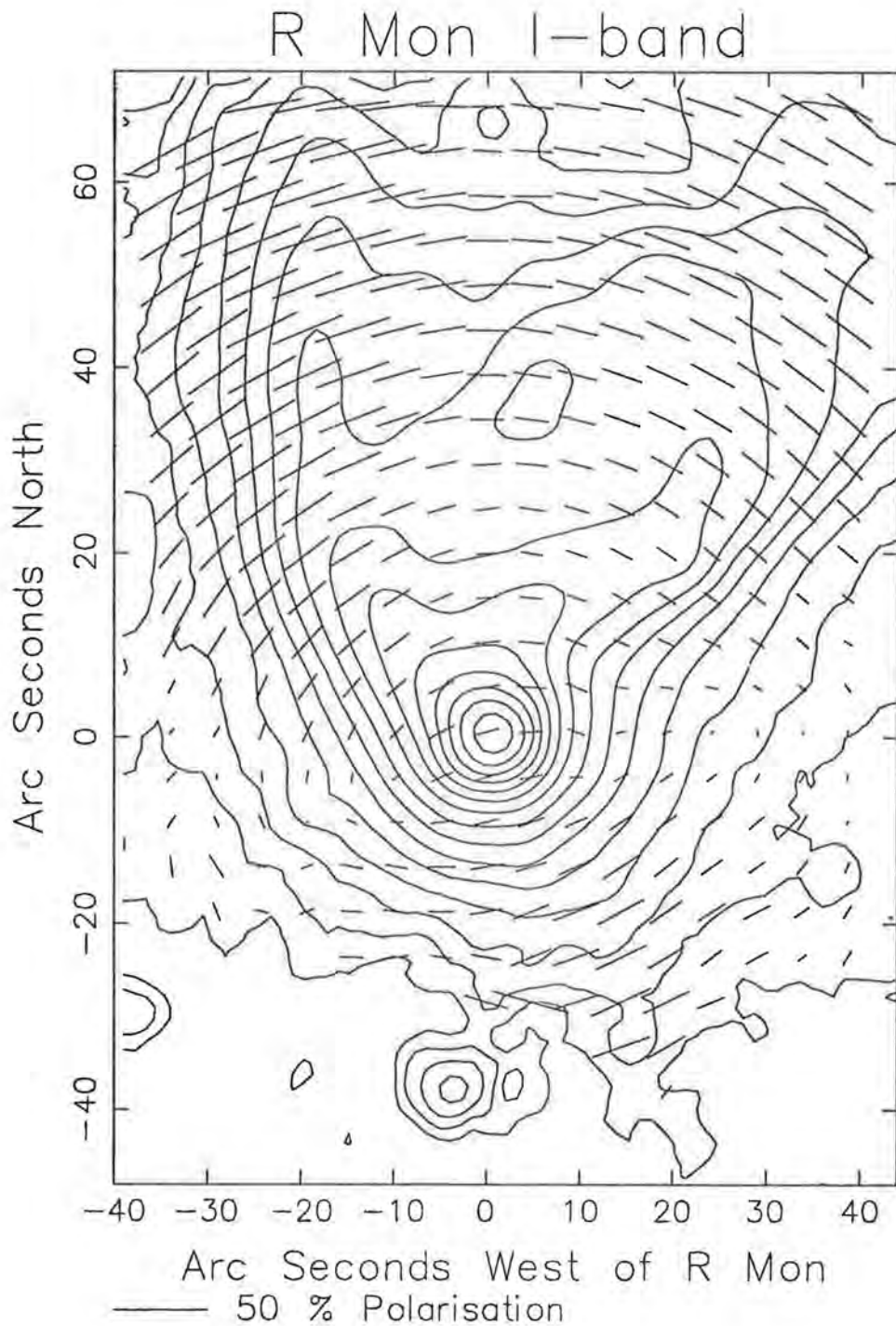
Figure 1: Polarization and intensity contour maps of the cometary nebula NGC2261 illuminated by the star R.Mon. At large offsets from the star the polarization pattern is generally circular and is representative of a simple reflection nebula illuminated by a single star. In the region of R.Mon the circular pattern breaks down to be replaced by a band of polarization vectors which form a near parallel array across the head of the nebula terminating in null points on either side of the star. This pattern is not expected for a simple reflection nebula and has become known as the polarization disc.

9

joining the null points (which also defines the plane of the pinching) is perpendicular to the major axis of the optical nebula which is elongated towards the northeast. Does this imply that there is a physical link between the two features - for instance, does the disc collimating the optical outflow also give rise to the polarization disc in some manner?
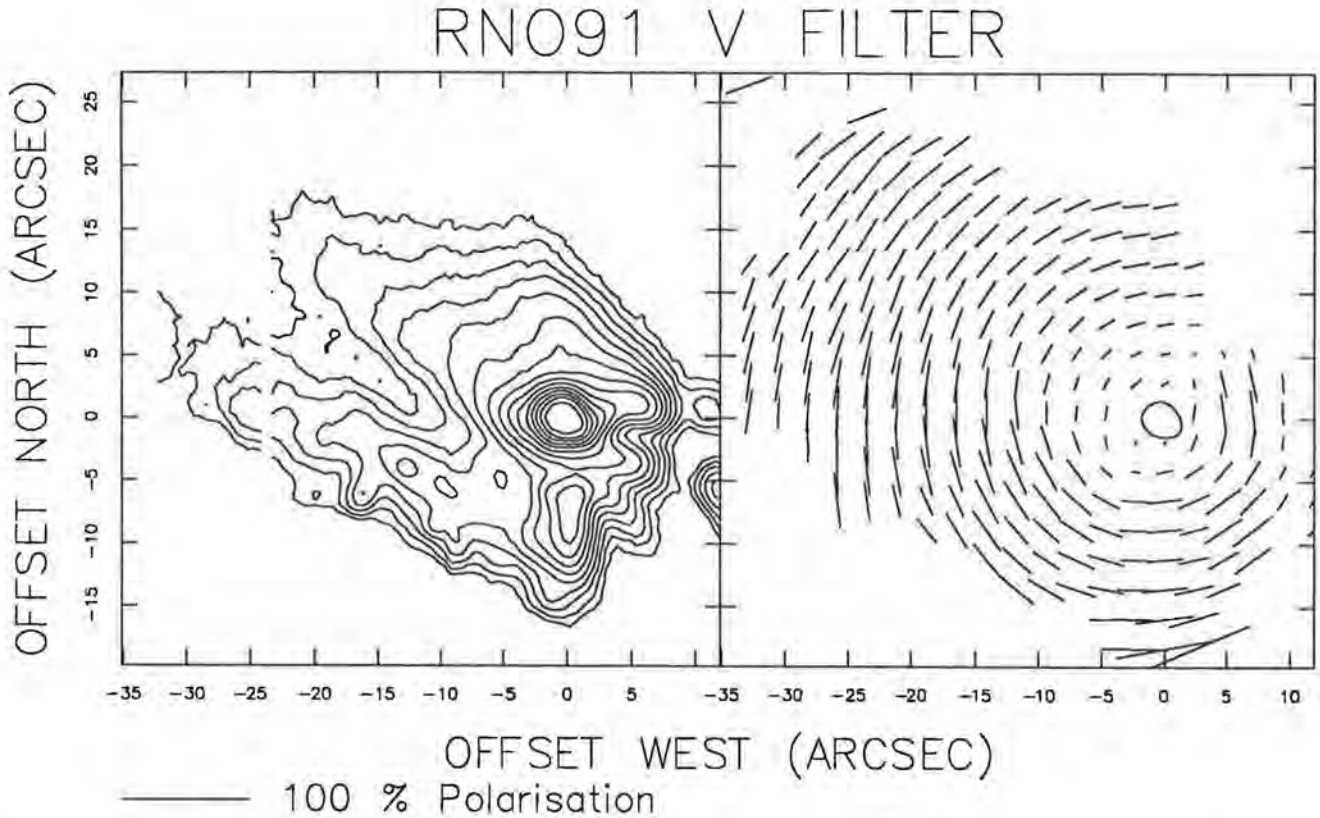

Figure 2: Polarization and intensity contour maps of the nebulosity in the L43 dark cloud illuminated by the T-Tauri star RNO91. Note the regular circular polarization pattern typical of a simple reflection nebula.

The polarization disc is seen in the majority of pre-main-sequence nebulae associated with outflows in star forming regions. It is also seen in some post-main-sequence systems such as bipolar proto- planetary and planetary nebulae. In Table 1 we give a compilation of systems known to have polarization discs and note some of the salient features of individual objects. The list is not exhaustive and the limited number in the post-main-sequence group is indicative of the fact that there are fewer known examples of the cometary/bipolar phenomenon due to the brief transitory nature of this stage of evolution.

2 FEATURES OF THE POLARIZATION DISC

The salient features of the polarization disc are summarized as follows:

i) The polarization disc consists of an anomalous band of polarization centred on the illuminating star of cometary and bipolar reflection nebulae.

ii) This band is normally present regardless of the direct visibility of the central source.

10

Object	Illuminator	Features
		Pre-main-sequence objects
HL Tau Neb	HL Tau*	Jet emanating from central star.
HH46/47	HH46IRS	Bipolar nebulosity, HH objects.
Pars 21	Pars 21*	Cometary nebula in dark cloud.
NGC2261	R.Mon*	Cometary nebula, slight vestige of counter lobe. Orientation of polarization disc changed by 20° in 2 years. Circular polarization also observed.
HH102	L1551IRS5	Stellar jet, bipolar molecular outflow. Polarization parallel to bright rim in inner region.
HH34	HH34IRS	Stellar jet surrounded by nebulosity. Source polarized perpendicular to jet axis.
GM29	PV Cep*	Source polarized, polarization parallel to bright rim. Bipolar. Polarization pattern changes in months.
Serpens	SVS2*	Bipolar nebula.
HH100	HH100IRS?	Comma shaped optical nebulosity offset from possible source.
NGC6729	R/T CrA*	Cometary nebula with polarization discs around the stars R & T CrA. RCrA disc changed orientation by 80° in ten years.
LkHa233	LkHa233*	Bipolar nebula.
RNO91/L43	RNO91*	Outflow region in dark cloud, similar to morphology to L1551/HH102/IRS5 and HH46/47.
Par22	Central star*	Bipolar nebula.
GGD30	Hidden star	Outflow region in dark cloud, similar to RNO91/L43.
		Post-main-sequence objects
M2-9	Central star*	Emission line planetary nebula, bipolar geometry.
Boomerang	Central star*	Highly polarized proto- planetary bipolar nebula.
Nebula		
OH231.8+4.2	Hidden star	Vaguely bipolar. Has Herbig- Haro knots.

Table 1: A summary of cometary and bipolar nebulae with polarization discs. Illuminators marked with an asterisk are visible stars.
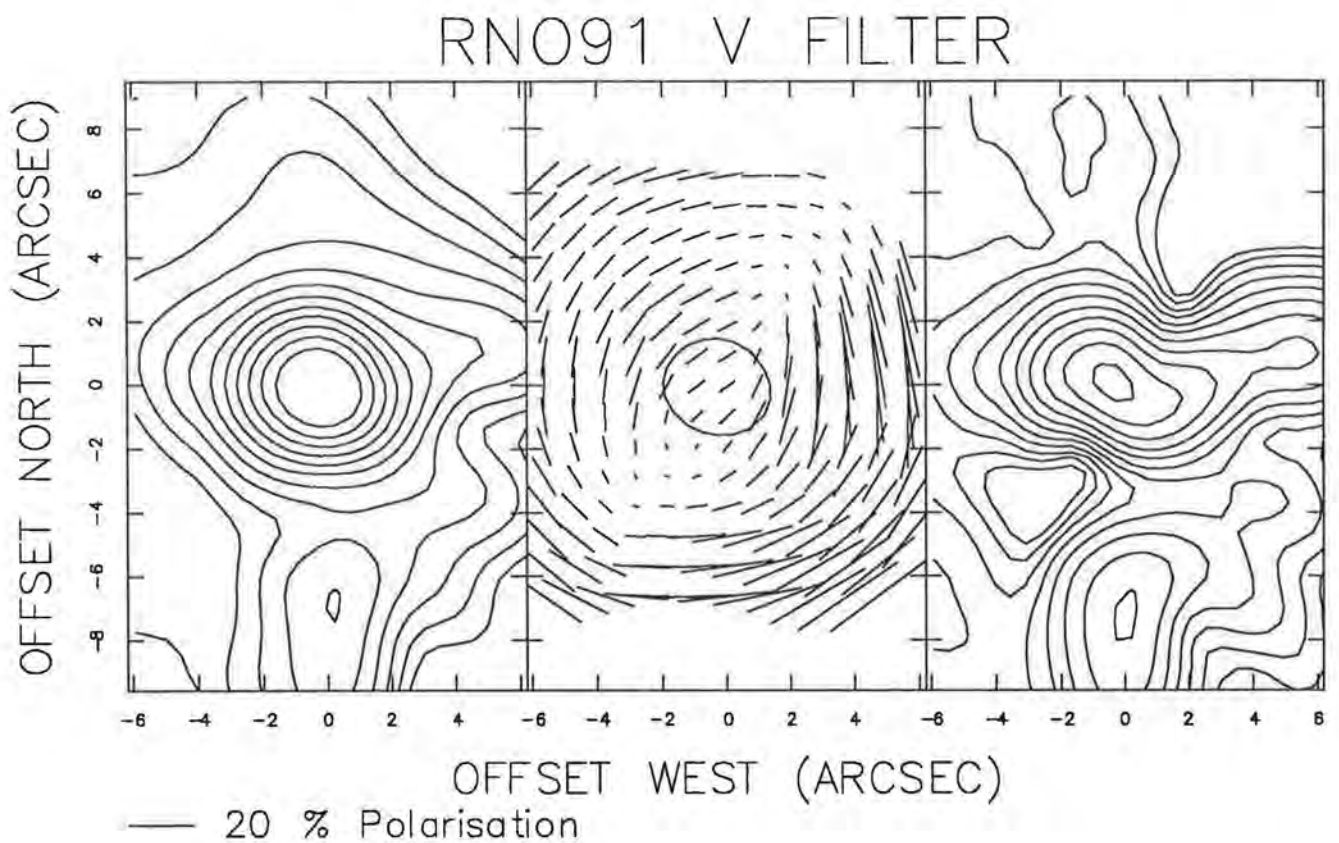
Figure 3: Intensity contour(left), polarization vector(centre), and polarized intensity contour (right) maps for the inner parts of the RNO91 nebulosity. The polarization disc with its null points is clearly visible in the innermost part of the system. Note how the intensity contours are approximately circular whereas the polarized intensity ones are "pinched". These features are well reproduced in the model calculations shown in Fig.5.

iii) When the central source is apparently visible it is significantly linearly polarized in a similar manner to the surrounding anomalous band of polarization in the nebula.

iv) The position angle of the polarization of the central object varies with wavelength.

v) Circular polarization in the central source and disc region has been found in some circumstances.

vi) In cases where molecular bipolar outflows are present the polarization disc is not necessarily perpendicular to this outflow axis. The disc is usually perpendicular to the optical axis.

vii) In systems with small scale stellar jets it is found that the inner parts of the jet and the source (where visible) are polarized with orientations perpendicular to the jet axis.

viii) The extremities of the polarization disc show null points.

x) In the case of NGC2261 and NGC6729 the polarization disc has been found to change orientation on time scales of months/years.

3 POSSIBLE ORIGINS OF THE POLARIZATION DISC

The features of the polarization disc seem to provide circumstantial evidence for associating it with a circumstellar disc of dusty material but before we can pursue this idea any further we must consider the processes which lead to the polarization.

There are two main mechanisms for inducing polarization in starlight: one is simple scattering which has already been discussed and leads to the simple circular vector patterns, the other is dichroic extinction. In this latter process non-spherical dust grains are aligned in a magnetic field such that their long axis is perpendicular to the field direction. If initially unpolarized light passes through a region containing aligned grains the transmitted light is found to have a net polarization with its orientation parallel to the component of the magnetic field perpendicular to the line of sight. The polarization arises because the grains extinguish the vibrations in the incident light parallel to the long axis of the grain in preference to the other vibrations. This process accounts for the polarization of many of the stars in the Galaxy and $\sim 1-3\%$ polarization per magnitude of extinction is typically observed.

From the outset we know that the polarization disc cannot arise from single scattering of unpolarized light from a central source - the simple reflection nebula hypothesis - since the observed pattern of vectors lacks the required centro-symmetry and the central star itself is observed to be polarized on a par with the surrounding band of polarization in the nebula. We must accept that at least two polarized components are present and compete with each other in specific regions so that their cancellation effects produce the observed null points. The three most obvious combinations are - scattering and dichroic extinction, multiple scattering (the scattering of light previously polarized by scattering elsewhere in the nebula) and the scattering of light polarized at source. Various models have been proposed based on these combinations and we will briefly discuss their individual merits and drawbacks.

3.1 Scattering and dichroic extinction

This was the original explanation of Gething, Warren-Smith, Scarrott and Bingham (1983) to account for the polarization disc in the cometary nebula NGC2261. In this model the grains in a circumstellar disc are aligned by a toroidal magnetic field so that the light from the central star is both scattered and extinguished in the disc. Since the field lies in the plane of the disc then the dichroic polarization will be in the plane of the disc whereas the scattered polarization will be perpendicular to the disc; these polarization orientations are orthogonal and can therefore cancel to give null points. In addition, the direct light from the central object is extinguished and not scattered so it is polarized parallel to the disc as defined by the null points as observed. In this model the circumstellar disc must at least have the dimensions of the polarization disc.

This explanation was preferred until the polarization discs of the cometary nebulae NGC2261 and NGC6729 were found to change orientations with time. This creates a problem with reorienting the magnetic field and a hybrid model involving a polarized source in addition to scattering and dichroism was proposed (Scarrott, Draper and Warren-Smith 1989).

3.2 Multiple Scattering

If the circumstellar disc is optically thick then the emergent radiation may have been multiply scattered with polarization induced in each scattering. However, the resultant polarization pattern should still be centro-symmetric but with reduced levels of polarization.

Bastien and Menard (1988) produced a model in which the disc is so dense that it is opaque in the equatorial plane and radiation can only escape along the disc's axis. This polar radiation is then scattered by the optically thin lobes and illuminates the periphery of the disc where it is scattered again. This "double" scattering automatically produces the band of polarization associated with the polarization disc due to the assumed geometry. This model fails to explain one of the main observations which is that the central object, when seen directly as a star-like object, is polarized in the same sense as in the polarization disc. It also has difficulty in accounting for the observed temporal changes in the orientation of the polarization disc.

3.3 Scattering of light polarized at source

In this situation the (apparent) central and unresolved source emits linearly polarized light which, when scattered by the dust grains within the nebula, leads to the observed pattern. Notni (1985) proposed the idea and and it was considered in detail by Draper (1988) for the NGC2261/RMon complex. The scattering of partially polarized light is equivalent in some ways to having competing polarizing processes and cancellation may occur.

Gledhill (1991) carried out model calculations based on this concept. He assumed that the nebula was a simple cylinder uniformly filled with optically thin dust and with a mini bipolar nebula on the cylinder axis acting as the polarized source. Fig. 4 shows a schematic diagram of his model whose main features are:

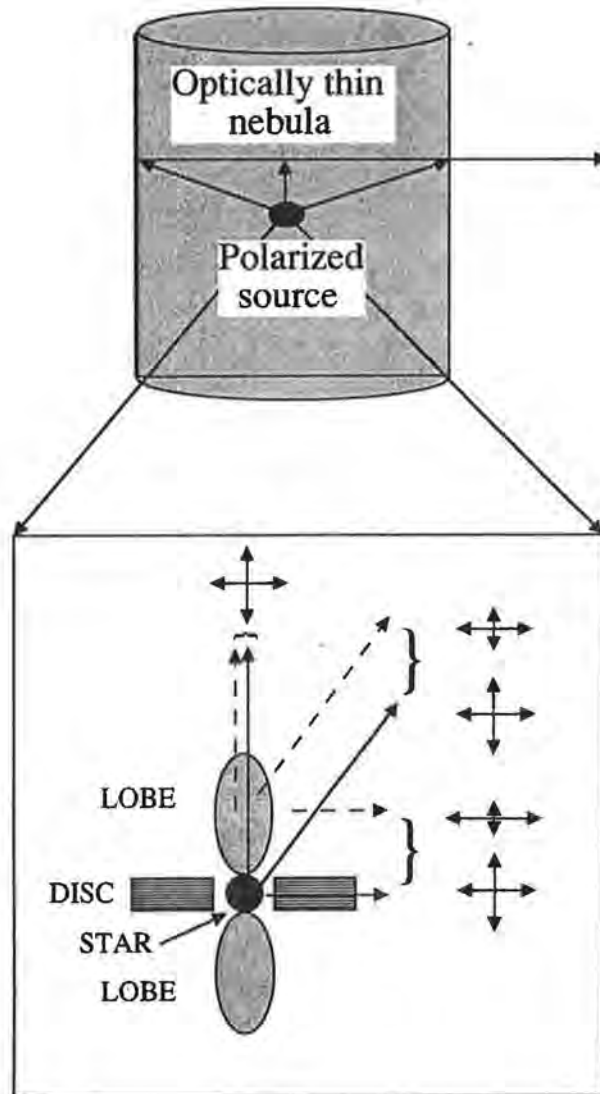i) There is no large scale dust disc, just a uniform and optically thin assembly of scattering centres.

Figure 4: A schematic diagram of the polarized source model. The upper part shows the simple cylindical geometry of a uniform and optically thin distribution of scattering centres illuminated by a central polarized source. For any offset position from the star the light we receive is the sum of the scattering along our total line of sight in the cylindrical nebula. The lower part shows the geometry of the polarized source; it is a mini bipolar nebula which is spatially unresolved and illuminates the nebula with a combination of (unpolarized) direct starlight and (polarized) light which has been scattered off the lobes. The level of polarization of the light from the source depends on the viewing angle and the diagram illustrates how maximum polarization occurs in the equatorial plane while the light emerging along the bipolar axis is unpolarized. Intermediate levels of polarization are seen at other viewing angles.

ii) The mini bipolar, which is spatially unresolved, illuminates the nebula with a combination of (unpolarized) direct starlight and (polarized) light which has been scattered off the lobes. The level of polarization from the source as seen by a grain in the nebula depends on the relative orientation of the line of sight to the star and the axis of the bipolar nebula. Maximum source polarization, as seen by a scattering centre, occurs when it is located in the equatorial plane of the bipolar.

Fig. 5 shows predictions for this model for various combinations of source strength and tilt of the large scale nebula. It is quite clear that the model can account for most of the observed properties of polarization discs and, although it is simplistic in many ways, its basic message is that it is the scattering process and geometry that creates the polarization feature rather than a large scale accumulation of scattering material in the form of a disc around the illuminating stars of cometary and bipolar nebulae.

With this polarized source model we still have to account for the mini bipolar nebula which acts as the unresolved polarized source. We propose that it is created by collimation very close to the star by a circumstellar disc which must be quite small relative to the extent of the polarization disc as defined by the location of the null points. In the case of RNO91 where the polarization disc is $\sim 1000 AU$ this collimating disc would have to be $\sim 10's AU$ in size , i.e. of solar system dimensions. Based on the time scale of the variations in the orientation of the polarization disc in NGC2261 Draper (1988) proposed that the size of an appropriate disc should be $\sim 15 AU$. Rudnitskij (1987) proposed a model to explain the brightness variability of cometary nebulae such as NGC2261 and NGC6729 in which he had a small circumstellar disc ($\sim 10 AU$) precessing in the gravitational potential of a much larger and more massive disc ($1000's AU, 100's M_{\odot}$) with periods of the order of tens of years. This disc produces a collimated optical outflow and its precession creates variable illumination. We expect that our bipolar is of similar ilk but now the precession produces a polarized source whose axial direction changes with time and so permits the polarization disc to vary in orientation in time scales of years.

This polarized source model creates the polarization disc purely on geometrical grounds without recourse to a dust disc with dimensions similar to the separation of the null points ($1000's AU$). Observationally we do not see a visible disc in direct intensity images and this is in agreement with this model. The absence of a visible disc has always remained a problem with the scattering/dichroism and multiple scattering models which required enhanced dust density on the spatial scale of the polarization disc.

At the present time it appears that the polarized source model is most able to account for the polarization disc around the illuminating stars of cometary nebulae but we cannot rule out that the larger scale discs, which are seen in molecular line studies, have a dichroic effect on the polarization in the off-nulcear regions of these nebulae where the effect of the polarized source is less manifest (Draper 1988).

4 THE β PICTORIS DISC

In contrast to the polarization discs discussed in the previous sections the main sequence A5 star β Pic is surrounded by a visible nebula (~ 50 arcsec $= 250 AU$ in extent) which is widely believed to be produced by light from the central star scattered by dust grains distributed in a highly flattened disc viewed almost edge-on (Smith and Terrile, 1984; Paresce and Burrows, 1987; Gledhill, Scarrott & Wolstencroft 1991).
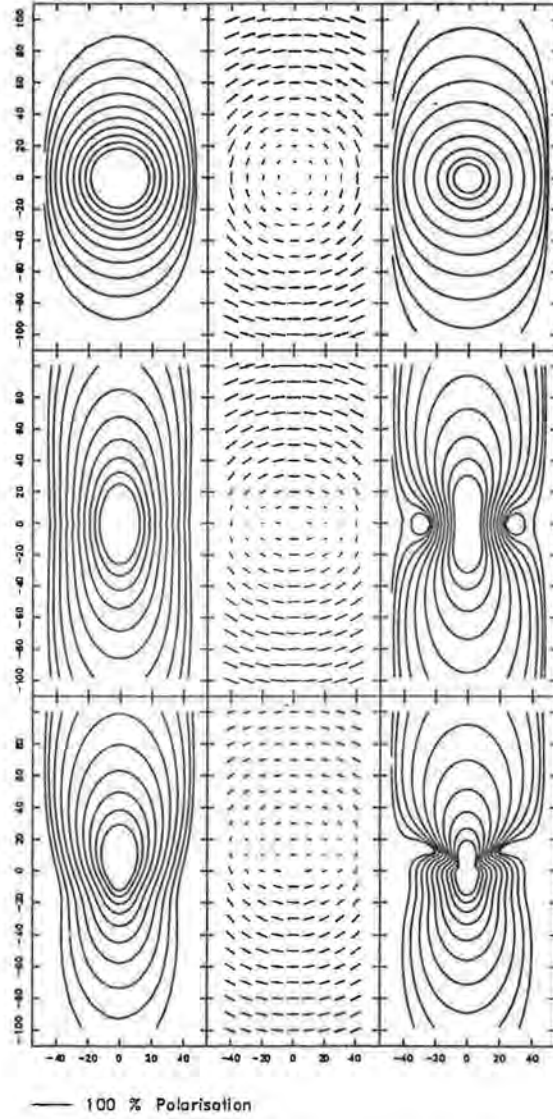
—— 100 % Polarisation

Figure 5: Predictions from the model illustrated in Fig. 4. Each of the frames (left to right) shows maps of intensity, polarization and polarized intensity respectively. The top frames show the results if the source is unpolarized (i.e. we have switched off the scattered component) and the axis of the cylinder is in the plane of the sky: the contour maps (left and right) have circular inner isophotes and the polarization vectors have the circular pattern expected for a simple reflection nebula. The centre frames show the results if 98% of the light is scattered (i.e.virtually all the light is coming from the nebular lobes) and the axis of the cylinder is in the plane of the sky: the intensity contours (left) become elongated while the polarized intensity ones (right) show the "pinching" in the equatorial plane. The polarization pattern (centre) is no longer circular, we have a polarization disc with null points. These figures show features very similar to those displayed in Fig. 3 for RNO91. The lower frames have the same parameters as for the centre frames except that the nebular axis is tilted at 30° to the plane of the sky so that the top and bottom parts of the nebula are seen mainly by forward and backward scattered light respectively. The polarization disc and "pinching" of the polarized intensity isophotes still persist.

17

Currently there is a considerable difference between grain size estimates based on various observations in the optical, NIR, IR and FIR domains. Detailed modelling of the combined optical imaging and the (unresolved) IRAS fluxes led Artymowicz, Burrows & Paresce (1989) to suggest grain radii in the range 1 to 20 μm while imaging of the disc at $10\mu m$ and $20\mu m$ by Telesco et al. (1988) indicates sub-micron grain sizes. The detection of the $10\mu m$ silicate feature in emission in β Pic by Telesco and Knacke (1991) can be interpreted in terms of grain radii $\sim 0.2\mu m$. Observations of the β Pic disc at $800\mu m$ led Becklin & Zuckerman (1990) to suggest that two grain populations are present.

Gledhill, Scarrott and Wolstencroft (1991) have mapped the optical polarization in the β Pic disc and their results confirm that the nebulosity is seen by reflected light originating in the central star. The level of polarization in such situations is a sensitive measure of the size of the scattering particles and in the next section we present a model which predicts the optical polarization, brightness distributions and colour in the β Pic nebula. A comparison with observations will then enable us to place constraints on the grain sizes in the disc.

4.1 A scattering model for the β Pic nebula

The geometry of our model is illustrated in Fig. 6 and consists of an assembly of grains confined to a thin disc centred on the illuminating star and viewed edge-on. We assume that the scattering grains have size and number density distributions which are both power laws *viz*,

$n(a) \propto a^{-h}$, where $n(a)$ is the number of grains of size a and h is the size index, and

$\rho(r) \propto r^{-k}$, where $\rho(r)$ is the total number of grains per unit volume at a radial distance r from the central star and k is the number density index.

We have assumed the grain material to be silicate (m = 1.63 -0.05i) on the basis of the presence of the 10 μm feature although it is not expected that the model predictions will be over sensitive to the precise choice of grain composition. The calculations used Mie scattering throughout and full integrations along the line of sight were made with due regard to the varying grain number density; it was assumed that the nebula is optically thin and that the radius of the disc was 50 arcsec (the exact size of the disc is not important as the model may be spatially scaled to the data as necessary). Our philosophy in judging the model predictions was to fit the polarization, brightness fall off and colour in that order. In the model we assumed that grains with sizes between 0.01 and 3 μm were all present and their relative contributions would be decided by the size index h.

We ran the model for a range of values of the indices h and k. As expected, we found that the polarization was most sensitive in limiting the size index to the range 4 ± 0.3 while the brightness fall off was most influential in constraining the number density index k to 2.75 ± 0.25. Fig. 7 shows the model fits to the experimental data using these optimum values and the fits are quite acceptable.

The model colours for the nebula in terms of the colour parameters defined by Paresce and Burrows[1] are as follows

---

[1]The relative colours, Q_r, Q_v and Q_b of the nebula are $Q_r = (R_n/R_*)/(I_n/I_*)$; $Q_v = (V_n/V_*)/(I_n/I_*)$; $Q_b = (B_n/B_*)/(I_n/I_*)$ where B_n, V_n, R_n, I_n and B_*, V_*, R_*, I_* are the brightnesses in the standard filters for the nebula and the central star respecrively.

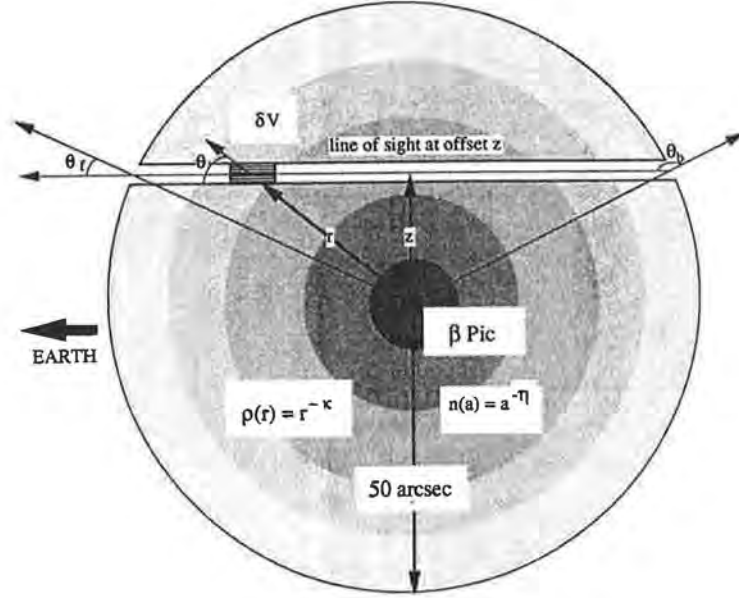Figure 6: A schematic diagram of our scattering model for the β Pic nebula. We assume that the disk is seen edge-on and that the dust number density and grain size distribution are power laws given by $\rho(r)$ and $n(a)$ respectively. For any offset distance we integrate the scattering along our line of sight in the nebula to predict the surface brightness and polarization for comparison with our observations.

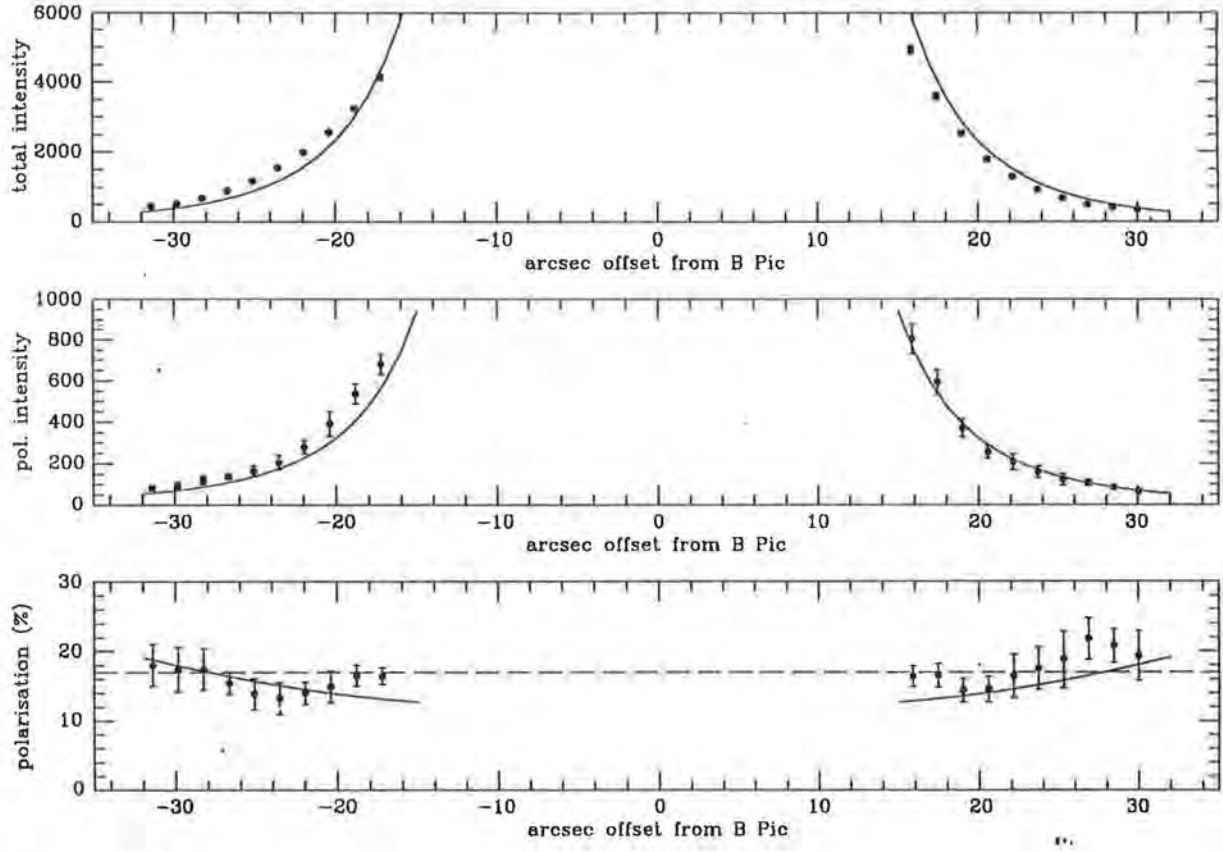Figure 7: A comparison between the model predictions (solid lines) and our data for the variation with offset distance from the central star for the surface brighness (top) , polarized intensity (centre) and polarization (bottom). The optimum values for the two model parameters are h = 4 ± 0.3 and k = 2.75 ± 0.25 where h and k are the indices for the grain size and grain number density power laws respectively.

	Q_b	Q_v	Q_r
Paresce & Burrows	0.84 ± 0.28	1.00 ± 0.22	1.24 ± 0.24
Our model	1.77	1.47	1.23
Rayleigh particles	9.8	4.29	2.28

Values of $Q < 1$, $Q = 0$ and $Q > 0$ corresponds to red, neutral and blue nebular colours respectively. For comparison we give the colours expected for Rayleigh particles and it is clear that our model colours are considerably more neutral than one might expect from a system which has a large component of very small grains. This is due to two factors; first, the most effective grain size is much larger than the small Rayleigh particles and, secondly, in Mie scattering the colour of the scattered light depends on the scattering angles with the forward scattered radiation being blue and backward scattered radiation red to neutral. In our model, and for that matter in any model with a strong grain number density fall off, small angle scattering is severely inhibited and hence the nebula is redder than one might expect. Our model predicts slightly bluer values for Q_b and Q_v than observed but we could redden our results by allowing for extinction in the nebula.

The optical data for polarization, surface brightness and colours for the β Pic nebula are well described by a population of silicate grains with a power law size distribution and a sub-micron mean grain size, typical of the ISM. However, it is known that when considering scattering from grains with a power law size distribution the most effective scatterers are those with sizes approximately equal to the wavelength of the observations. Our proposed size distribution does contain super-micron sized grains and it may well be that measurements at longer wavelengths select out these larger grains and that the apparent discrepancies between the size of grains required to account for various observations may well represent this selection effect.

The fact that the optical observations of the β Pic nebula are explained in terms of grains with properties typical of the general ISM suggests that the circumstellar material surrounding this star may be the leftovers from the original star formation process rather than material condensing out of any mass loss processes from β Pic itself; we make this statement in view of the fact that recently condensed grains, e.g. those found in nebulae surrounding mass losing AGB stars, tend to be much smaller than those in the ISM.

5 CONCLUSION

The ubiquitous polarization disc which is seen in cometary and bipolar nebulae regardless of their evolutionary state appears to be a geometrical effect produced when a source emitting polarized light illuminates the nebula. We propose that the source is a mini bipolar nebula which is spatially unresolved and is created by the collimating effect of a circumstellar disc of solar system proportions.

We have modelled the nebular disc around the main-sequence star β Pic and find that we can explain the optical polarization, surface brightness distributions and colour with a power law size distribution of silicate grains. The grains giving rise to these optical features are sub-micron in size and are typical of those in the ISM. It may well be that

the larger super-micron grains within this distribution are responsible for the IR and FIR emissions.

REFERENCES

Artymowicz, P., Burrows, C., and Paresce, F. 1989. Astrophys. J. 337, 494.

Bastien,P. & Menard,F., 1988. Astrophys.J., 326, 334.

Becklin, E.E., and Zuckerman, B. 1990. "Submillimetre Astronomy"
ed. G.D. Watt and A.S. Webster, Kluwer Academic Publishers, p147.

Draper,P.W., 1988. PhD Thesis, University of Durham.

Gething,M.R., Warren-Smith,R.F., Scarrott,S.M. & Bingham,R.G., 1982.
Mon.Not.R.astr.Soc., 198, 881.

Gledhill,T.M., 1991.Mon.Not.R.astr.Soc., 252, 138.

Gledhill,T.M., Scarrott,S.M. & Wolstencroft,R.D., 1991.Mon.Not.R.astr.Soc. 252, 31p

Notni,P., 1985. Astr.Nachr., 306, 265.

Paresce, F., and Burrows, C. 1987. Astrophys. J. 319, L23

Rudnitskij, G.M., 1987. in IAU115, "Star forming regions"
eds. Peimbert,M. & Jugaku,J, p398. Reidel Publishing Company, Dordrecht.

Scarrott,S.M, Draper,P.W. & Warren-Smith,R.F., 1989 Mon.Not.R.astr.Soc. 237, 621.

Smith, B.A., and Terrile, R.J. 1984. Science 226, 1421.

Telesco, C.M., Becklin, E.E., Wolstencroft, R.D. and Decker, 1988. Nature 335, 51.

Telesco, C.M. and Knacke, R.F. 1991. Ap.J. Letters (in press).

Maser Discs around Massive Young Stars

R. J. Cohen, G. C. Brebner & A. H. Prestwich
University of Manchester
Nuffield Radio Astronomy
Laboratories, Jodrell Bank,
Macclesfield, Cheshire SK11 9DL, UK.

Abstract

Observational evidence for the existence of maser discs around massive young stars is presented, with particular emphasis on sources with bipolar molecular outflows. In several cases molecular line data indicate a massive disc or toroid orthogonal to the outflow, with OH masers tracing the inner (disrupted) portions of the disc, on scales of 1000 A.U. In Orion-KL H_2O and SiO masers have been found to trace disc structure on scales smaller than 100 A.U.

1 Introduction

One of the most important discoveries in the field of star-formation has been the recognition that young stars exceeding a solar mass undergo a phase of energetic outflow (Bally & Lada 1983; Lada 1985; Bachiller & Gomez-Gonzalez 1992; and references therein). The outflow is typically bipolar. The outflow occurs while the young star is deeply embedded in its parent molecular cloud, and is recognized by its disruptive effect on the surrounding gas. Outflow velocities of typically 30 km s^{-1} are observed in the cool molecular gas, while the ionized gas in Herbig-Haro objects and optical jets can have velocities an order of magnitude greater than this. The outflow phase is important for the evolution of both the young star and the molecular cloud. However many of the basic physical processes have yet to be identified. There is no agreed model of the outflow mechanism, the collimation mechanism, or the parameters of the outflowing wind. One of the observational difficulties is the high visual extinction to the central source, which is usually many tens of magnitudes.

Molecular masers offer the possibility to address some of these questions. The maser lines are excited close to the young stars, in regions which are heavily obscured at optical and near-infrared wavelengths, but too compact to be detected at mm and far-infrared wavelengths with current technology (Cohen 1989, and references therein). Masers produce bright, readily detectable signals, and they can be studied at milliarcsecond resolution using radio interferometers. Water masers are known to have large proper motions, and to participate in the outflow (Genzel et al. 1981). The hydroxyl (OH) masers generally cover a smaller velocity range, and may trace shocks in the ambient molecular gas (Elitzur & de Jong 1978). The newly discovered methanol masers fall into two spectral classes, one of which appears to be closely associated with OH masers near the young star, and the other (Class I methanol masers) which appear to be associated with the outer lobes of the bipolar molecular outflow (Menten 1991; Plambeck & Menten 1990).

outer lobes of the bipolar molecular outflow (Menten 1991; Plambeck & Menten 1990). SiO and other maser species are too poorly studied at present for any general conclusions to be drawn.

At this workshop I would like to present results from a systematic study of OH masers associated with bipolar molecular outflows (Brebner 1988). The main part of the project dealt with the Bally & Lada (1983) sample of molecular outflow sources. In addition two further sources were studied: G35.2-0.7N, which is known to have a well developed bipolar outflow and orthogonal molecular disc (Little et al. 1985), and W75N, a well-known maser and molecular outflow source. One of the aims of the project was to search for evidence of collimated outflow or disc structure on the small scales probed by the OH masers.

2   Single Telescope Observations

The 45 sources in the Bally & Lada (1983) sample were searched for OH maser emission in 1984/5 using the MkII telescope at Jodrell Bank. The 1612, 1665 and 1667 MHz lines were searched to a limit of 1 Jy in order to identify sources suitable for interferometric study (Prestwich 1985). Ten maser sources were detected. In addition three further OH maser sources are known which were below the detection level of this survey (Evans et al. 1976; Pankonin et al. 1977; Cohen, unpublished data). Most of the OH masers were previously known, the only new discoveries being M8E and S140. It is notable that the OH masers detected in our survey are much less luminous, as a group, than the strong OH-HII region masers which have been mapped hitherto (e.g. Gaume & Mutel 1987).

A literature search for 22 GHz water masers associated with the Bally & Lada sources was also conducted. The results of these two surveys are shown in Figure 1. OH masers are found in only the most massive systems, namely those massive enough to produce detectable HII regions. All the sources with OH masers also have H_2O masers (upper histogram). H_2O masers (without OH) are also found in some, but not all, of the low luminosity systems (middle histogram). Sources without OH or H_2O maser emission are generally low luminosity objects (lower histogram).

3   Interferometer Observations

Absolute positions for most of the OH maser sources were measured in 1986 using the VLA in A-configuration. Details of these measurements will be published in the Monthly Notices of the Royal Astronomical Society. In all cases but one the OH maser sources were found to coincide closely with the geometrical centre of the bipolar outflow. The exception was DR21, where the main OH maser cluster lies 3 arcmin to the North of DR21, at the postion designated DR21(OH) or W75S, with no OH 18cm maser emission at the position of DR21 itself. (For this reason DR21 was excluded from the statistics in Figure 1).

MERLIN maps were made of the OH 18 cm maser sources W3(OH), W3-IRS5, MonR2, M8E, G35.2-0.7N, AFGL2591, DR21(OH), W75N, CepA and NGC7538, in 1984/6 (Brebner 1988). The results on G35.2-0.7N have been published by Brebner et al. (1987), and provide a clear case of a maser disc. In this source the OH masers have an elongated distribution which exactly mimics, on a much smaller scale, the enlongated molecular disc observed by Little et al. (1985) in the ammonia (1,1) and (2,2) lines. The density of
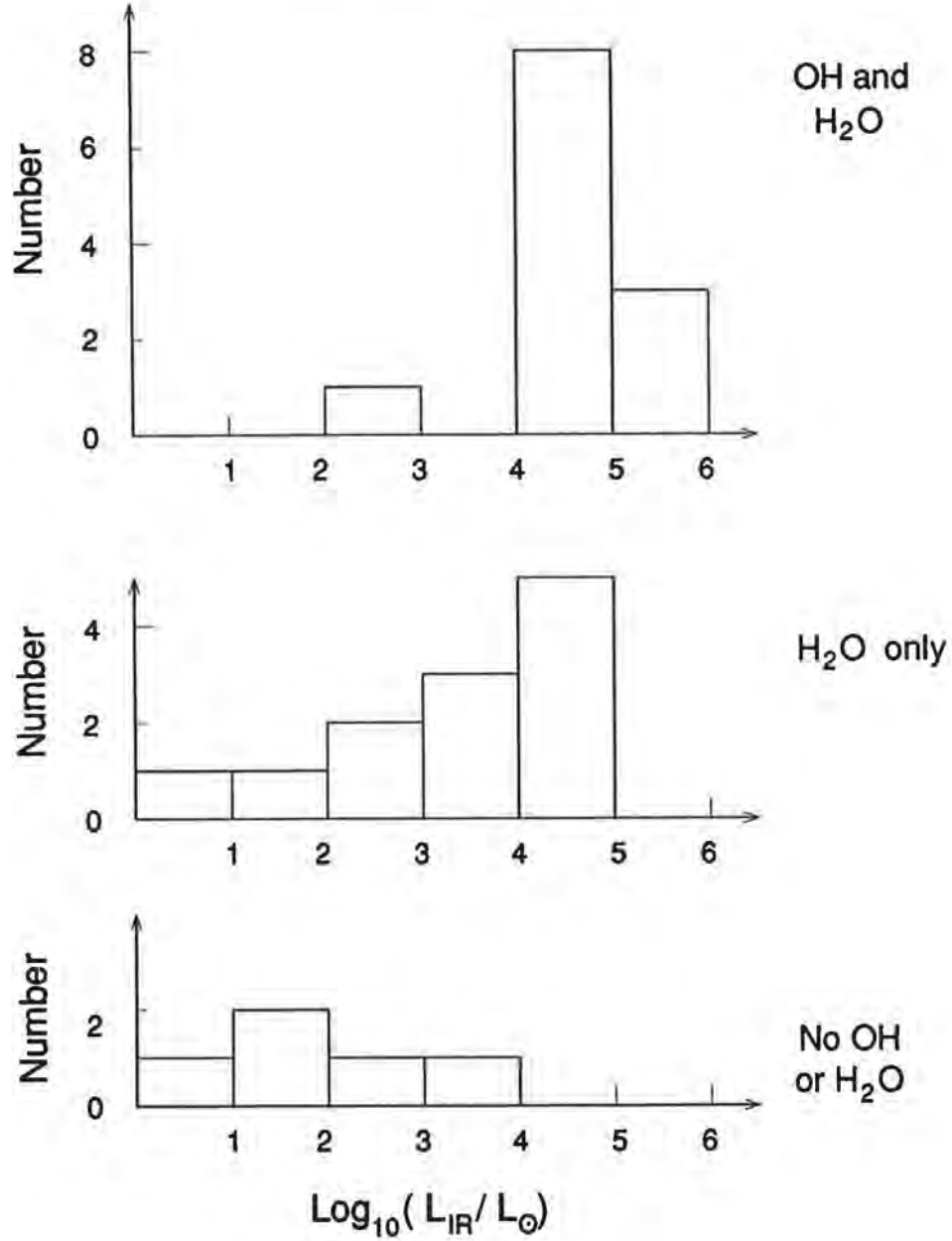
24

Bally & Lada (1983) Sample

Figure 1: OH and H_2O maser detections for the Bally & Lada (1983) sample of bipolar outflow sources, shown as functions of the source luminosity. The upper histogram shows the OH masers. These sources also have H_2O masers. The middle histogram shows H_2O masers without OH detection, and the lower histogram shows sources not detected in OH or H_2O.

the disc increases towards the centre. The ammonia lines trace gas densities of about 6 x $10^{11}m^{-3}$ at a radius of 5 x $10^{15}m$, and the OH masers trace gas densities of about $10^{13}m^{-3}$ at a radius of about 3 x $10^{14}m$. The progressively smaller distributions of ammonia (1,1), (2,2) and (3,3) emission provide evidence for central heating of the disc. However whereas the ammonia data have a regular velocity pattern which allow a disc rotation curve to be measured, and a disc mass to be calculated (150 solar masses), the OH masers have a chaotic velocity pattern. The large spread in OH maser velocities shows that the masers cannot be gravitationally bound to the cental source: radio continuum data suggest a central B0.5 star, with a mass of 14 solar masses, whereas a mass of 100 solar masses would be needed for bound motion. This is consistent with recent proper motion measurements of OH masers in CepA (Migenes et al. 1992) and W3(OH) (Bloemhof et al., in press), which indicate that the OH masers are in a zone of expansion. Such a zone could be produced by the disruption of the inner part of a molecular disc by an energetic stellar wind, as envisaged in some models for bipolar outflow, or simply by the expansion of the HII region, as in the model by Elitzur & de Jong (1978).

There are several other candidates for similar OH maser discs in our sample. Data on the source W3-IRS5 are reproduced in Figure 2. As in G35.2-0.7N we see an elongated maser distribution with a chaotic velocity field. In this source the maser distribution is also orthogonal to an E-W bipolar molecular outflow (Claussen et al. 1985). AFGL2591 and W75N provide further examples of this phenomenon. In AFGL2591 the OH masers are associated with the inner edge of the ammonia cavity found by Torelles et al. (1989), and are distributed orthogonal to the well-known molecular outflow. In W75N the OH masers have a curious arrow-shaped distribution which points along the molecular outfow (Fischer et al. 1985). In all these cases the OH masers lie at projected distances of about 1000 A.U. from the central source and compact HII region.

In some other cases the maser results are inconclusive. The case of DR21 has already been mentioned. In addition to DR21(OH), the MERLIN maps reveal a new OH maser centre which lies a further 2 arcmin to the North of DR21(OH). Discs or outflows at these OH maser sites have yet to be identified. In M8E only a single maser spot was measured; in MonR2 there are several maser centres close to the centre of the outflow; and in NGC7538 there are now several outflows known, as well as several maser centres. Further details on these sources will be published in Monthly Notices of the Royal Astronomical Society (Brebner & Cohen, in preparation). Clearly no one simple disc scenario can apply to the diversity of bipolar outflow sources. However it is clear that maser discs can be identified in a substantial fraction of cases.

Finally I would like to mention Orion-KL, a source which we did not reobserve, but one which provides the nearest and perhaps the most interesting maser disc. The H_2O masers in Orion-KL have long been known to partake in the molecular outflow (Genzel et al. 1981). The centre of the outflow coincides, within the errors of measurement, with IRc2. The OH masers have a complex distribution which may be interpreted in terms of an inner cavity in a molecular disc (Johnson, Migenes & Norris 1989). The OH distribution is fairly extensive. Interior to it are a separate population of "shell" H_2O masers, which are distributed NE-SW orthogonal to the outflow and centred on IRc2 (Genzel & Stutzki 1989). Finally SiO masers are found in the innermost part of the maser disc, also distributed NE-SW, and also centred on IRc2. The SiO masers have a regular velocity pattern which can be interpreted in terms of an expanding and rotating ring (Plambeck et al. 1990). The ring is only 40 A.U. in radius. The pattern seen
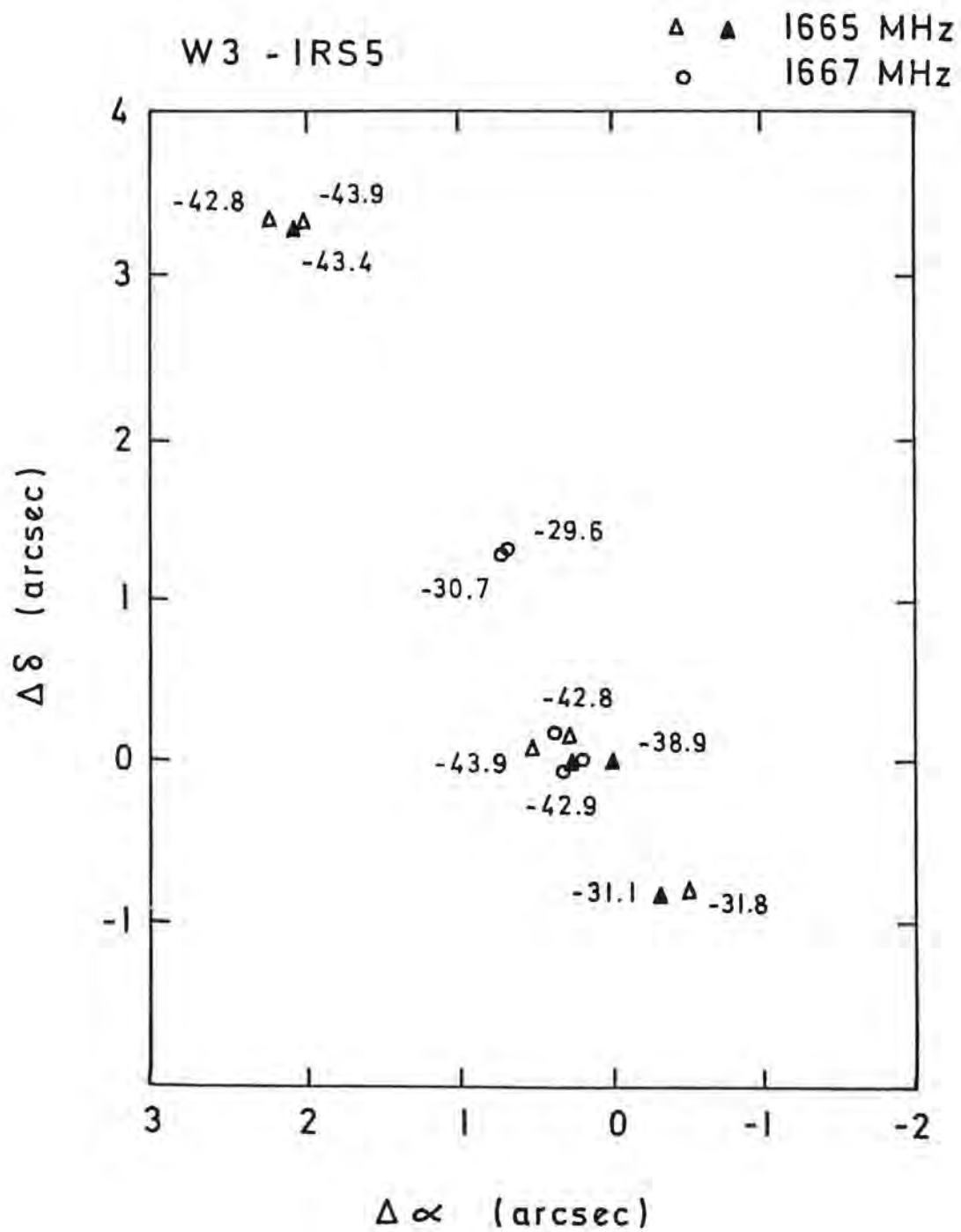
Figure 2: OH maser distribution for W3-IRS5, as mapped with the MERLIN and VLA interferometers (Brebner 1988). The reference position is 02:21:53.14 +61:52:19.3 (1950 coordinates). The radial velocities with respect to the local standard of rest are indicated.

here is very reminiscent of the regular excitation sequence of masers seen in circumstellar envelopes of red giants. In that case OH masers occur furthest from the star, H_2O masers occur nearer, and SiO masers occur nearest of all (Cohen 1989, and references therein). There is a simple physical explanation in terms of excitation temperatures of the different molecular transitions. It may be that the same basic sequence is present in star-forming regions, but that it is confused because H_2O masers are too easily excited, and so occur not only in the molecular disc, but also in the high-velocity outflow.

References

Bachiller, R. & Gomez-Gonzalez, J., 1992. *Astr. Astrophys. Rev.*, **3**, 257-287.

Bally, J. & Lada, C., 1983. *Astrophys. J.*, **265**, 824-847.

Bloemhof, E. E., Reid, M. J. & Moran, J. M., 1992. *Astrophys. J.*, in press.

Brebner, G. C., 1988. *Ph.D. thesis*, University of Manchester.

Brebner, G. C., Heaton, B., Cohen, R. J. & Davies, S. R., 1987. *Mon. Not. R. astr. Soc.*, **229**, 679-689.

Claussen, M. J., Berge, G. L., Heiligman, G. M., Leighton, R. B., Lo, K. Y., Masson, C. R., Moffet, A. T., Phillips, T. G., Sargent, A. I., Scott, S. L., Wannier, P. G. & Woody, D. P., 1985. *Astrophys. J.*, **285**, L79-L83.

Cohen, R. J., 1989. *Rep. Prog. Phys.*, **52**, 881-943.

Elitzur, M. & de Jong, T., 1978. *Astr. Astrophys.*, **67**, 323-332.

Evans, N. J. II & Crutcher, R. M., 1976. *Astrophys. J.*, **206**, 440-442.

Fischer, J., Sanders, D. B., Simon, M. & Solomon, P. M., 1985. *Astrophys. J.*, **293**, 508-521.

Gaume, R. A. & Mutel, R. L., 1987. *Astrophys. J. Suppl.*, **65**, 193-253.

Genzel, R., Reid, M. J., Moran, J. M. & Downes, D., 1981. *Astrophys. J.*, **244**, 884-902.

Genzel, R. & Stutzki, J., 1989. *Ann. Rev. Astr. Astrophys.*, **27**, 41-85.

Johnston, K. J., Migenes, V. & Norris, R. P., 1989. *Astrophys. J.*, **341**, 847-856.

Lada, C. J., 1985. *Ann. Rev. Astr. Astrophys.*, **23**, 267-317.

Little, L. T., Dent, W. R. F., Heaton, B., Davies, S. R. & White, G. J., 1985. *Mon. Not. R. astr. Soc.*, **217**, 227-238.

Menten, K., 1991. In *Atoms, Ions and Molecules: New Results in Spectral Line Astrophysics*, ed. A. D. Haschick & P. T. P. Ho, pp. 119-136 (San Francisco: Astronomical Society of the Pacific).

Migenes, V., Cohen, R. J. & Brebner, G. C., 1992. *Mon. Not. R. astr. Soc.*, **254**, 501-508.

Pankonin, V., Winnberg, A. & Booth, R. S., 1977. *Astr. Astrophys.*, **58**, L25-L26.

Plambeck, R. L. & Menten, K., 1990. *Astrophys. J.*, 364, 555-560.

Plambeck, R. L., Wright, M. C. H. & Carlstrom, J. E., 1990. *Astrophys. J.*, **348**, L65-L68.

Prestwich, A. H., 1985. *M.Sc. thesis*, University of Manchester.

Torelles, J. M., Ho, P. T. P., Rodriguez, L. F. & Canto, J., 1989. *Astrophys. J.*, **343**, 222-228.

What Can We Learn from Millimetre/Submillimetre Continuum Observations of T Tauri Systems?

V. Mannings
Department of Physics,
Queen Mary and Westfield College,
Mile End Road,
London, E1 4NS

Abstract

We present calculations of model spectral energy distributions for dusty circumstellar disks in low-mass pre-main sequence systems, and we compare these results with new millimetre and submillimetre continuum observations. Beckwith and Sargent (1991) observed many of the T Tauri systems studied here at 600, 800 and 1100 μm and we have extended this coverage down to 350 μm and up to 2 mm in the hope that disk parameters (e.g. mass and dust opacity) might be better constrained. We investigate model-fitting by sampling in a 2-dimensional parameter space to illustrate the ambiguity of the simultaneous determination of disk masses and dust grain opacities. The answer to the question posed in the title of this report is: much, but with due regard for the inherent uncertainties involved.

1   Introduction

We consider low-mass (T Tauri) stars which have recently ($t < 10^7$ yr) become optically visible and which are still on their pre-main sequence vertical convective tracks. T Tauri stars are typically observed to have effective temperatures $T_{eff} \approx 4200$K (e.g. Cohen and Kuhi 1979), for which a blackbody spectrum would peak at a wavelength $\lambda \sim 1$ μm. However, it is often the case that infrared fluxes which are far in excess of those expected from a single-temperature blackbody are observed and, for some T Tauri stars, there is little or no decline in the spectrum with increasing wavelength until λ exceeds ~ 100 μm. Mendoza (1966, 1968) was first to explain this excess IR emission by suggesting the existence of circumstellar dust grains which are in thermal equilibrium with the radiation field of a given host star; i.e. grains which absorb optical and UV photons emitted at the stellar surface and then radiate copiously at longer wavelengths. (The alternative hypothesis is free-free emission from ionized material near the photosphere: however, it has been shown — e.g. Cohen and Kuhi (1979) and Beckwith *et al.* (1990) — that this process is incapable of generating sufficient fluxes to account for the observed NIR and millimetre continuum excesses). The question of the geometrical distribution of the dust

has been shown — e.g. Cohen and Kuhi (1979) and Beckwith *et al.* (1990) — that this process is incapable of generating sufficient fluxes to account for the observed NIR and millimetre continuum excesses). The question of the geometrical distribution of the dust grains has until recently been rather controversial — see Shu, Adams and Lizano (1987) — but it is now generally agreed that they probably reside in circumstellar disks whose orbital axes are parallel (and coincident) with the rotational angular momentum vectors of the central stars (Kenyon and Hartmann 1987, Adams, Lada and Shu 1987, 1988, Strom *et al.* 1988, 1989, Cohen, Emerson and Beichman 1989, Weintraub, Sandell and Duncan 1989, Adams, Emerson and Fuller 1990, Beckwith *et al.* 1990, and Beckwith and Sargent 1991).

Adams, Lada and Shu (1987, 1988) have developed a theoretical treatment of continuum emission from dusty disks in low-mass systems. The principal observational input is the fact that the optically thick infrared (10 μm $\leq \lambda \leq$ 100 μm) spectral energy distributions ($\log \nu F_\nu$ v. $\log \nu$) of T Tauri systems with IR excesses often follow a power law, always with a positive (and sometimes near-zero) spectral index (n). A power law infrared spectral energy distribution is consistent with a power law distribution of temperature (T_D) with radius (ω) in a circumstellar disk, i.e. $T_D \propto \omega^{-q}$, where $^1/_2 \leq q \leq {}^3/_4$, corresponding to $0 \leq n \leq {}^4/_3$. These disks can be divided into two broad categories: (1) *passive* disks (n = $^4/_3$) which have negligible intrinsic luminosity but which absorb and re-radiate up to $^1/_4$ of the stellar luminosity; (2) *active* disks (n < $^4/_3$) which reprocess stellar photons *and* which have an intrinsic energy source. Active disk emission dominates the bolometric luminosity of the flat spectrum (n $\approx$ 0) sources. Adams, Lada and Shu (1988, hereafter ALS) concentrated on the flat-spectrum sources and assembled spectral energy distributions for a small sample of T Tauri systems for comparison with their model spectral energy distributions. The long-wavelength ($\lambda >$ 100 μm) portion of a spectral energy distribution is of particular importance, for it is at these wavelengths that some/all of a disk might be optically thin; in this situation, estimates of the mass of a disk may therefore be made using millimetre observations, once the frequency-dependent dust grain opacity is specified. Above the IRAS long-wavelength limit (135 μm), ALS had access only to detections/upper limits at 1.3 and 2.6 mm for three of their sources, but they were able to provide some estimates of disk masses. Adams, Emerson and Fuller (1990, hereafter AEF) improved on this by making broad-band photometric observations of about a dozen T Tauri systems in Taurus-Auriga and Ophiuchus in the wavelength range 350 μm to 1100 μm. (Their sample included most of those studied by ALS). They compared spectral energy distributions predicted by the ALS model with the data on 9 of their sources and obtained estimates of disk masses. We have extended this work with 350 μm to 2000 μm broad-band photometry of 21 T Tauri systems in Taurus-Auriga, eight of which were members of the sample studied by AEF (HL Tau, DG Tau, GM Aur, T Tau, DO Tau, HK Tau, UY Aur, and DK Tau). AEF have already found evidence for the presence of circumstellar disks in six of the sources observed by us. We have confirmed many of their measurements of flux densities and, in most cases, provide new measurements at 850, 1300 and 2000 μm. All but two (SAO 76411A and V819 Tau) of the 13 new sources we observed are included in a catalogue compiled by Cohen, Emerson and Beichman (1989, hereafter CEB), who listed details of the composite spectral energy distributions of 72 T Tauri systems in Taurus-Auriga; ratios of bolometric luminosity (L_{bol}) to stellar luminosity (L_*) are listed for some 8 of these new sources (GG Tau, RY

Tau, CI Tau, UZ Tau, CY Tau, Haro 6-37, DM Tau, and DN Tau). Although $L_{bol}/L_* \approx$ 0.91 for CY Tau, which is indicative of no significant dust emission in this system, the remaining 7 sources have L_{bol}/L_* in the range 1.10 to 2.44; some of these may therefore possess appreciable disks.

This report is arranged as follows. In Section 2 we describe our photometric observations and the corrections we have made for atmospheric extinction. We present flux densities and upper limits in Section 3 and we combine our measurements with IRAS photometry and the results of NIR observations to construct spectral energy distributions for each of our sources. Section 4 provides a brief outline of the ALS continuum emission model. In section 5 we compare the observed spectral energy distributions with those generated by the model and in Section 6 we investigate the implications for the masses of disks. Our conclusions are given in Section 7.

2 Observations

2.1 Instrument and Method

All observations were performed with the common user broad-band detector UKT14 (Duncan *et al.* 1990) at the Nasmyth focus of the 15m James Clerk Maxwell Telescope[1] on Mauna Kea, Hawaii. UKT14 is a ^{3}He-cooled one-channel bolometer with a filter wheel and a variable iris; the filter bandpasses encompass atmospheric transmission windows from 350 to 2000 μm. Our observations were made on 1990 December 30 and 31 (UT) and on 1991 January 1 and 3. The atmospheric opacity during the first two nights was unusually low and permitted observations of stellar sources down to 350 μm with good signal-to-noise. Although the opacity was higher on 1991 January 1, detections could still be made down to 600 μm. Atmospheric conditions degraded considerably by 1991 January 3, but we were able to make several detections at the longer wavelengths.

The data were sky-chopped to eliminate atmospheric emission and beam-switched to reject local background. Sky-chopping on all sources was performed at a frequency of 7.8125 Hz. The chop throw for the target (stellar) sources was nominally 60″ R.A.; this was executed at constant declination to ensure that the reference beam remained in the same position on the sky.

The typical pointing accuracy of the JCMT (Matthews 1991, *JCMT Guide*) is approximately 2″ rms in both azimuth and elevation under stable conditions (i.e. steady temperatures in the carousel). The usual tracking accuracy is less than half this amount over periods of about an hour. We peaked up on Mars using a five-point routine at the beginning of each night and made any necessary adjustments. (Mars was in Taurus throughout our observations). The pointing was then checked in the same way on at least three further occasions each night to correct for any error accumulated as targets were tracked on

---

[1]The James Clerk Maxwell Telescope is operated by the Royal Observatory Edinburgh on behalf of the Science and Engineering Research Council of the United Kingdom, the Netherlands Organisation for Scientific Research, and the National Research Council of Canada.

the sky; we found that the average pointing adjustments required were less than $0''.5$ in azimuth and elevation.

We used an aperture of 65 mm FWHM throughout the observations, which is the maximum permitted by the UKT14 Fabry lens. Circumstellar disks in T Tauri systems are expected to be $\sim$ 100 AU, so that the angular diameters are expected to be approximately $2''$ at the distance (140 pc) of the Taurus molecular cloud. The telescope beam sizes corresponding to the maximum detector aperture vary between $16''.8$ (HPBW) at 800 μm and $27''.5$ at 2000 μm and should therefore have been adequate to collect most of the emission from disks.

Observations were made with broad bandpass filters at nominal wavelengths of 350, 450, 600, 800, 850, 1100, 1300 and 2000 μm. These filters are matched to the corresponding atmospheric transmission windows, but the effective frequencies and the band-passes are dependent on the water vapour content of the atmosphere at the time of any given observation, particularly for the shorter wavelength windows. Centre frequencies, bandwidths, beamwidths and responsivities are listed in Table 1.

λ (μm)	Centre ν (GHz)	Bandwidth (GHz	Beamwidth[a] (arcsec;FWHM)	Responsivity (Jy mV^{-1}
2000	150	40	27.5	36.7
1300	233	64	19.5	15.1
1100	264	75	18.5	14.1
850	354	30	17.8	16.9
800	394	103	16.8	8.4
600	480	119	17.5	9.8
450	685	84	17.5	18.0
350	870	249	18.5	26.8

Table 1: UKT14/JCMT System Characteristics

[a]For 65 mm aperture

2.2 Correction for Atmospheric Extinction

We need to be able to correct for extinction in the atmosphere before we can determine the flux density of a source at any given zenith angle. On none of our four nights was the transmission of the atmosphere sufficiently stable to permit accurate determination of optical depths from plots of logarithm of signal strength against air mass. However, if we know the UKT14 responsivity in each of the filter bandpasses, we can go on to determine optical depths directly. Sandell (1991, private communication) has provided values for the UKT14 system responsivity. The presence of deep atmospheric absorption lines in the band-pass of the 600 μm filter means that the responsivity of UKT14 at 600 μm is very sensitive to the amount of water vapour in the atmosphere at any given time. It is therefore difficult to calibrate, since particularly stable conditions (i.e. constant optical depth) are required. The most stable of our four nights was that of 1991 January 1. A

plot of the logarithm of signal strength against air-mass using our 600 μm measurements of Mars on this date yields a value of 9.8 ± 3.1 Jy mV^{-1} for the 600 μm responsivity. In the absence of any other knowledge of the responsivity on the three remaining nights, we have used this value for all our 600 μm observations. We note that the resulting 600 μm flux densities fit very smoothly onto the continuum spectra of the T Tauri systems (see below), which suggests that our 600 μm calibration is approximately correct.

This is not the forum for detailed discussion of the minutiae of the determination of atmospheric opacities and the application of extinction corrections. However, full details are given by Mannings and Emerson (1992). Briefly: we observed Mars using the full set of filters on four occasions during each night. Expected values of flux densities for Mars in each of the filter bandpasses have been calculated, which were then used in combination with the above values for responsivity to obtain the optical depths in each bandpass. We also observed the proto-planetary nebula CRL 618 and the data from these observations have been used to check the atmospheric opacities determined from the Mars photometry. On average, the zenith optical depths determined using the Mars photometry and the CRL 618 photometry differ by less than three standard deviations. Table 2 shows for each night the average atmospheric transmission at the zenith and the corresponding average optical depth for each filter bandpass determined using the Mars photometry. Also shown are the ranges over which the zenith optical depths varied during each night.

3 RESULTS

3.1 Flux Densities and Upper Limits

Table 3 presents our determinations of flux densities and their uncertainties for the T Tauri systems we observed. All upper limits to flux density entered in the Table are 3σ and all entries with $3 <$ signal-to-noise ≤ 5 are indicated. The remaining entries in the Table have signal-to-noise ratios in excess of 5. Often we made several observations of a given source in the same filter. Where this was the case, we have computed the weighted mean flux density and uncertainty. All uncertainties listed in Table 3 are propagations of both the statistical uncertainty in the measurement of signal voltage at the detector and the uncertainty in the determination of atmospheric opacity at the time of any given observation. The uncertainties in the Table do *not* include any systematic errors arising from (small) uncertainties in the computation of the flux densities of Mars or from the uncertainties in the knowledge of the UKT14 responsivities. Six of the T Tauri systems we observed were also detected by AEF in 1989 January (approximately two years before our observations) using the same instrument. Repeated detections were made of HL Tau at 600, 800 and 1100 μm, DG Tau at 350, 450, 600, 800 and 1100 μm, GM Aur at 1100 μm, and T Tau at 350, 450 600, 800 and 1100 μm; the two sets of measurements of flux densities agree to within two standard deviations.

Date	Filter (μm)	% Transmission	Mean τ at Zenith	Range in τ
1990 Dec 30	350	41	0.90	0.80 - 1.01
1990 Dec 31		48	0.74	0.66 - 0.78
1991 Jan 01		17	1.76	1.35 - 1.93
1991 Jan 03		14	1.96	1.72 - 2.42
1990 Dec 30	450	45	0.80	0.71 - 0.88
1990 Dec 31		51	0.67	0.60 - 0.71
1991 Jan 01		20	1.62	1.24 - 1.78
1991 Jan 03		17	1.79	1.46 - 2.26
1990 Dec 30	600	53	0.63	0.59 - 0.67
1990 Dec 31		59	0.53	0.49 - 0.57
1991 Jan 01		26	1.33	1.07 - 1.47
1991 Jan 03		26	1.34	0.75 - 1.85
1990 Dec 30	800	75	0.29	0.25 - 0.34
1990 Dec 31		79	0.23	0.22 - 0.25
1991 Jan 01		58	0.54	0.47 - 0.60
1991 Jan 03		51	0.67	0.50 - 1.06
1990 Dec 30	850	78	0.24	0.20 - 0.28
1990 Dec 31		82	0.20	0.16 - 0.22
1991 Jan 01		68	0.39	0.36 - 0.44
1991 Jan 03		67	0.41	0.32 - 0.52
1990 Dec 30	1100	96	0.04	0.02 - 0.07
1990 Dec 31		95	0.05	0.04 - 0.06
1991 Jan 01		88	0.12	0.10 - 0.16
1991 Jan 03		90	0.10	0.06 - 0.17
1990 Dec 30	1300	98	0.02	0.002-0.05
1990 Dec 31		96	0.04	0.003 - 0.10
1991 Jan 01		89	0.11	0.09 - 0.14
1991 Jan 03		92	0.08	0.05 - 0.14
1990 Dec 30	2000	98	0.02	0.006 - 0.04
1990 Dec 31		98	0.02	0.003 - 0.03
1991 Jan 01		93	0.07	0.07 - 0.09
1991 Jan 03		89	0.12	0.09 - 0.18

Table 2: Transmission properties of atmosphere derived from Mars photometry

Source	F_ν:(2000) (Jy)	(1300) (Jy)	(1100) (Jy)	(850) (Jy)	(800) (Jy)	(600) (Jy)	(450) (Jy)	(350) μm (Jy)
HL Tau	0.32±0.04	1.07±0.05	1.27±0.06	2.63±0.05	3.02±0.04	4.89±0.08	10.98±0.30	16.10±1.06
GG Tau	0.23±0.04	0.71±0.07	0.85±0.05	1.62±0.07	1.75±0.03	2.38±0.13	4.27±0.24	6.40±0.29
DG Tau	0.14^b±0.03	0.70±0.13	0.57±0.07	1.10±0.10	1.19±0.03	1.62±0.11	3.95±0.35	5.19±0.54
GM Aur	¡0.20	-	0.23^b±0.07	0.50±0.07	0.70±0.03	1.09±0.06	2.88±0.23	2.60±0.46
DL Tau	0.12^b±0.03	0.19^b±0.06	0.26±0.03	0.44±0.04	0.55±0.05	0.67±0.05	1.28±0.17	1.39±0.18
V819 Tau	-	-	-	-	¡0.04	-	-	-
T Tau	0.11^b±	0.35±0.04	0.34±0.05	0.92±0.05	0.80±0.04	1.35±0.16	3.23±0.41	7.54±0.97
DO Tau	¡0.27	-	-	0.31±0.03	-	-	1.06±0.14	1.08^B±0.24
RY Tau	0.13^b±0.04	-	0.28^b±0.09	0.56±0.03	0.54±0.06	0.96±0.04	1.92±0.16	2.43±0.33
CI Tau	-	-	-	¡0.11	-	¡0.19	-	-
H6-13	0.17^b±0.05	-	0 26±0.04	0.34±0.07	0.34±0.03	0.64±0.04	1.10±0.10	2.01±0.18
DR Tau	¡0.17	-	0.18^b±0.04	0.49±0.07	0.35±0.03	0.61±0.05	1.34±0.24	1.85±0.38
SAO 76411A	-	-	-	¡0 08	-	-	-	-
HK Tau	-	-	-	0.12^b±0.03	-	0.39±0.08	-	¡1.76
UZ Tau	¡0.19	-	0.27±0.04	0.42±0.04	0.34±0.03	0.66±0.08	1.11±0.22	¡1.10
CY Tau	¡0.10	-	0.186±0.04	0.17±0.03	0.19^b±0.06	0.19^b±0.06	¡0.60	-
H6-37	-	0.10^b±0 03	0.19±0.03	0.25±0.03	-	0.42^b±0.11	-	-
UY Aur	-	-	-	-	¡0.12	¡0.80	-	-
DK Tau	-	-	-	¡0.11	-	-	-	-
DM Tau	-	-	0.12^b±0.03	0.17^b±0.04	-	¡1.22	-	-
DN Tau	-	-	-	0.19^b±0.04	-	-	-	-

Table 3: Measured flux densities[a] for T Tauri systems

[a]Upper limits are 3σ [b]N.B. 3¡signal-to-noise≤5.

3.2 Spectral Energy Distributions

Figures 1-14 show plots of the spectral energy distributions of those T Tauri systems we observed at signal-to-noise ratios in excess of 5. The millimetre and submillimetre data points are taken from the present work; our reference sources for all other data points are listed below each Figure. The plots show smooth declines in luminosity with increasing wavelength in the low frequency region; the slopes of our long-wavelength composite spectra are also often in agreement with those we would anticipate by extrapolating from the IRAS far-infrared measurements, which suggests that the system calibrations we used and the determinations we made of optical depths are approximately correct and that any remaining uncertainties due to systematic error are small. The plotted curves are the predictions of the model discussed below.

4 Theory of Emission from Circumstellar Disks

We assume that the dust particles responsible for the observed submillimetre emission reside in circumstellar disks. These disks are assumed to be spatially thin (scale height H $<<$ radius, ω) — in which case any line-of-sight cutting an inclined disk will sample only a single radius — and to be isothermal in the vertical direction. The radiative transfer equation can then be integrated to give the monochromatic specific intensity,

$$I_\nu(\omega, \theta) = B_\nu[T_D(\omega)]\left[1 - e^{[-\tau_\nu^D(\omega,\theta)]}\right] \qquad (1)$$

where ω is radius from the centre of the host star, θ is the angle of inclination of the disk plane to the plane of the sky, B_ν is the Planck function, T_D is the radius-dependent absolute temperature in the disk, and τ_ν is the optical depth in the disk along the line-
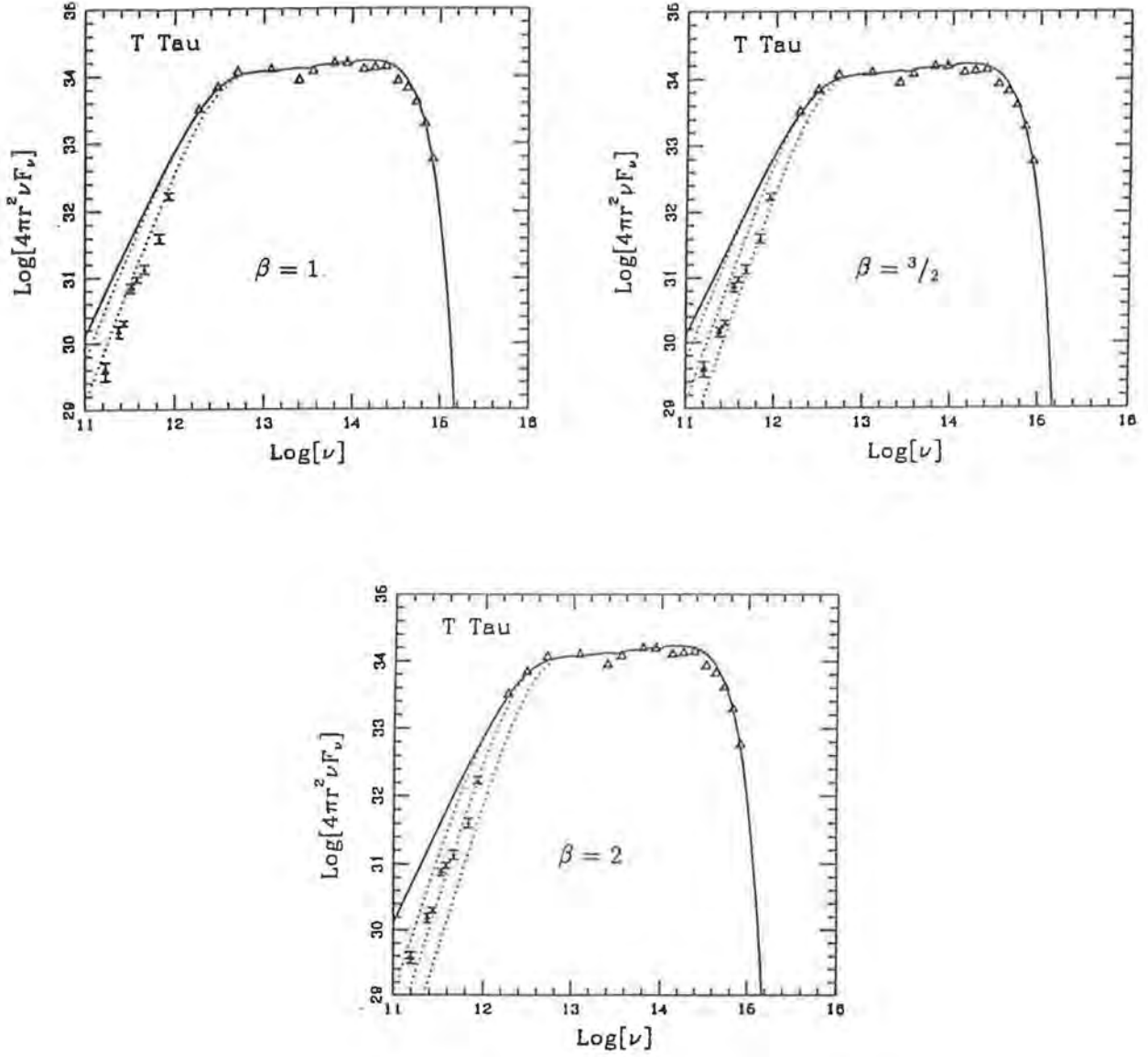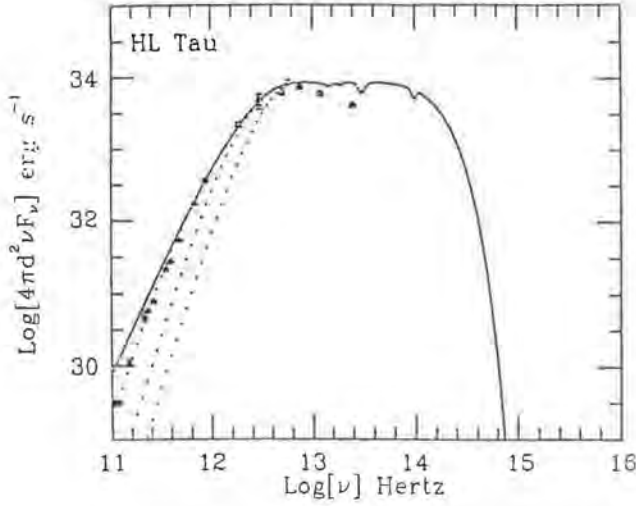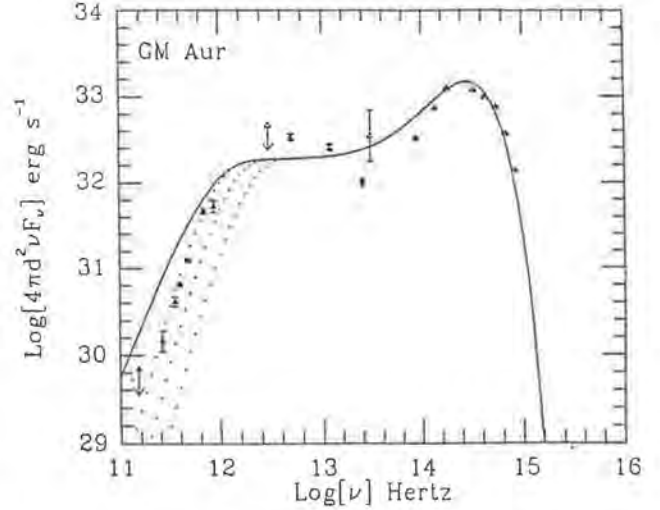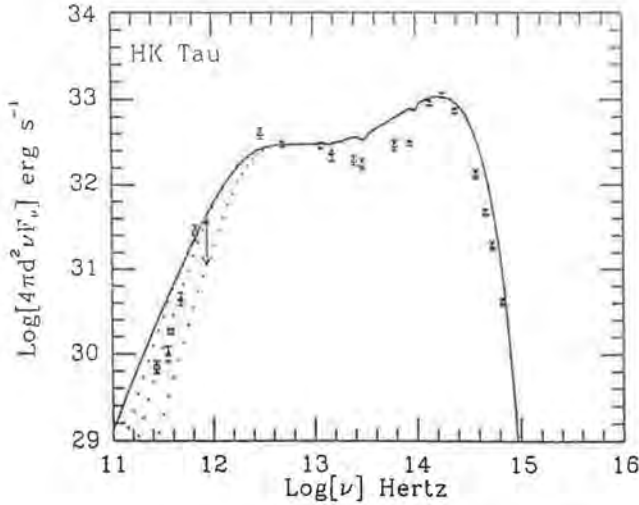
35

Figure 1. Spectral energy distribution of T Tauri. Solid triangles are the data points from this paper. Other data (open triangles) are from Cohen and Schwartz (1976), Rydgren, Strom and Strom (1976) and Harvey, Thronson and Gatley (1979). Dotted curves: from right to left, the model spectra for $M_D = 0.01$, 0.1, and 1 $M_\odot$. Solid curve is the model spectrum in the optically thick limit.
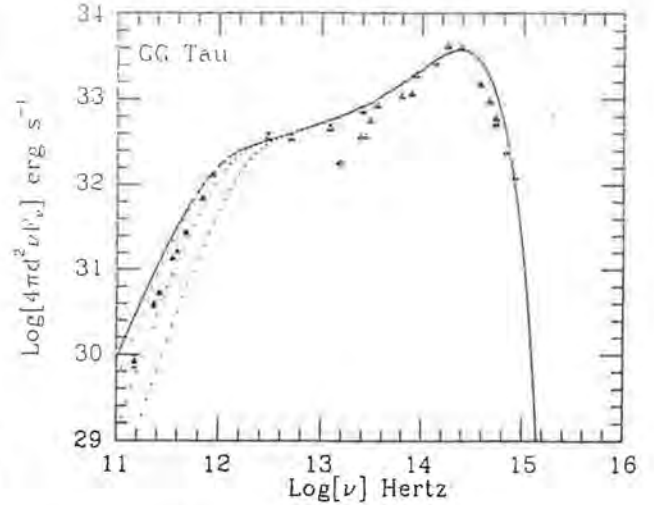
Figure 2. Spectral energy distribution of HL Tauri. Solid triangles are the data points from this paper. Optical and near-infrared data (open triangles) are from Rydgren *et al.* (1984); other infrared data (also open triangles) are from Cohen (1983), CEB, and the IRAS point source catalogue. The open squares (1.4 and 2.7 mm) are from Woody *et al.* (1989). The dotted curves show, from right to left, the model spectra for M_D = 0.01, 0.1, and 3 $M_\odot$ (β = 2). The solid curve is the model spectrum in the optically thick limit.
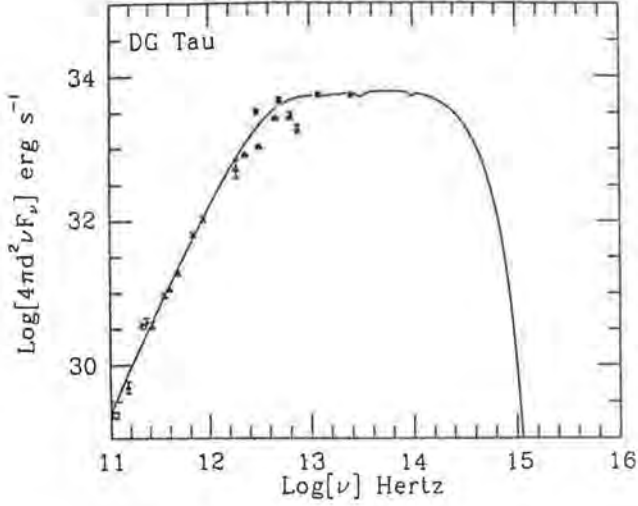

Figure 3. Spectral energy distribution of GM Aurigae. Solid triangles are the data points from this paper. Optical and NIR data (open triangles) are from Cohen (1974), Cohen and Kuhi (1979), and Rydgren and Vrba (1983). The 12 μm data point (solid square) is from CEB; other FIR data (open triangles) are from the IRAS point source catalogue. The dotted curves show, from right to left, the model spectra for M_D = 0.01, 0.1, and 1 $M_\odot$ (β = 2). The solid curve is the model spectrum in the optically thick limit.

Figure 4. Spectral energy distribution of HK Tauri. Solid triangles are the data points from this paper. Optical and infrared data (open triangles) are from Myers *et al.* (1987). The 12, 25, 60, and 100 μm data points (also open triangles) are from CEB. The 450, 800, and 1100 μm points (open squares) are from AEF. The dotted curves show, from right to left, the model spectra for M_D = 0.01, 0.15, and 1 $M_\odot$ (β = 2). The solid curve is the model spectrum in the optically thick limit.
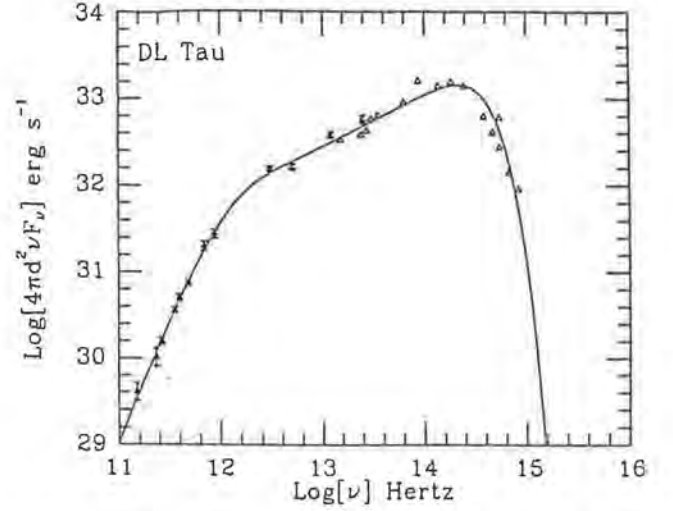

Figure 5. Spectral energy distribution of GG Tauri. Solid triangles are the data points from this paper. Optical and infrared data (open triangles) are from Cohen and Kuhi (1979), Rydgren *et al.* (1984), and Herbig and Bell (1988); far-infrared data (also open triangles) are from the IRAS point source catalogue. The dotted curves show, from right to left, the model spectra for M_D = 0.01, 0.1, and 1 $M_\odot$ (β = 1). The solid curve is the model spectrum in the optically thick limit.

37

Figure 6. Spectral energy distribution of DG Tauri. Solid triangles are the data points from this paper. Solid squares are FIR data from the IRAS point source catalogue. Open triangles are MIR and FIR data from Cohen et al. (1985). The 1.4 and 2.7 mm data points (open squares) are from Woody et al. (1989). The solid curve shows the model spectrum in the optically thick limit.
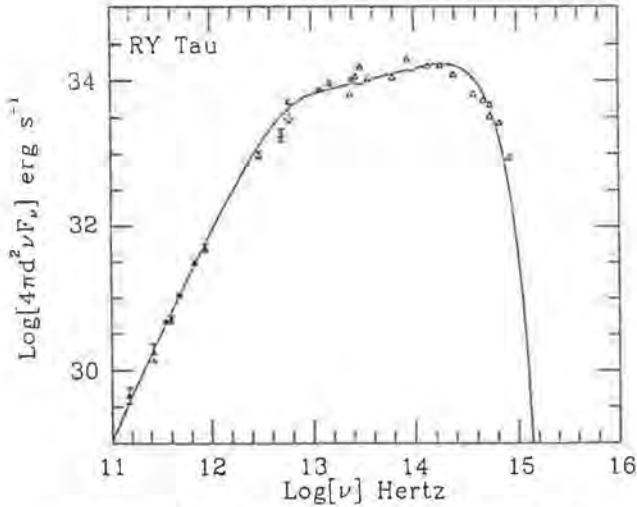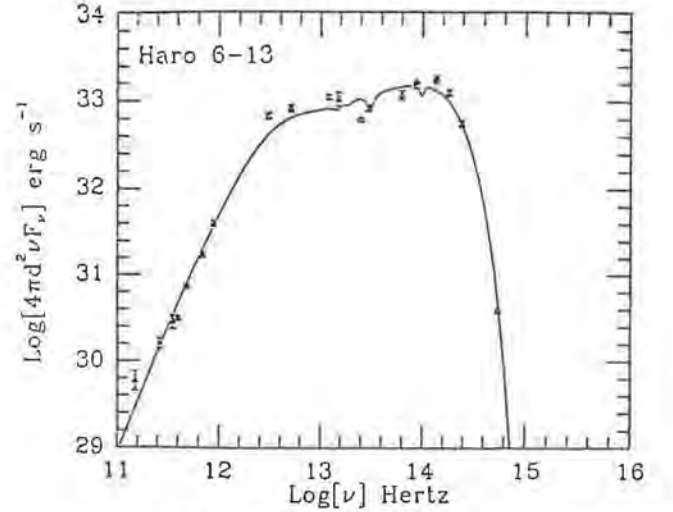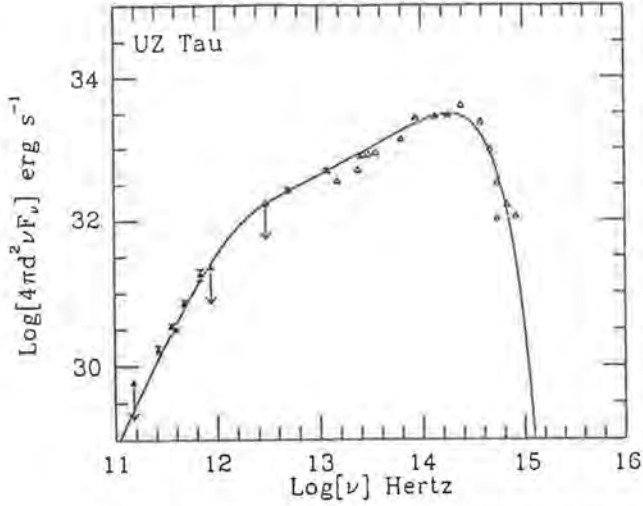

Figure 7. Spectral energy distribution of DL Tauri. Solid triangles are the data points from this paper. Optical and infrared data (open triangles) are from Cohen and Kuhi (1979), Rydgren et al. (1984), and Herbig and Bell (1988). The 100 μm data point is from CEB; other far-infrared data (open triangles) are from the IRAS point source catalogue. The solid curve shows the model spectrum in the optically thick limit.

Figure 8. Spectral energy distribution of RY Tauri. Solid triangles are the data points from this paper. Optical and NIR data (open triangles) are from Cohen and Kuhi (1979), Rydgren et al. (1984), and Herbig and Bell (1988). The 50 μm upper limit is from Harvey et al. (1979). Other far-infrared data points are from the IRAS point source catalogue. The solid curve shows the model spectrum in the optically thick limit.

Figure 9. Spectral energy distribution of Haro 6-13. Solid triangles are the data points from this paper. Optical and NIR data (open triangles) are from Cohen and Kuhi (1979), Myers et al. (1987), and Herbig and Bell (1988). Far-infrared data points (also open triangles) are from the IRAS point source catalogue. The solid curve shows the model spectrum in the optically thick limit.

Figure 10. Spectral energy distribution of UZ Tauri. Solid triangles are the data points from this paper. Optical and infrared data (open triangles) are from Cohen and Kuhi (1979), Rydgren *et al.* (1984), and Herbig and Bell (1988). The 12, 25, 60, and 100 µm data points (also open triangles) are from the IRAS point source catalogue. The solid curve shows the model spectrum in the optically thick limit.

Figure 11. Spectral energy distribution of Haro 6-37. Solid triangles are the data points from this paper. Optical and infrared data (open triangles) are from Cohen and Kuhi (1979), Rydgren *et al.* (1984), and Herbig and Bell (1988); far-infrared data (also open triangles) are from the IRAS point source catalogue. The solid curve shows the model spectrum in the optically thick limit.
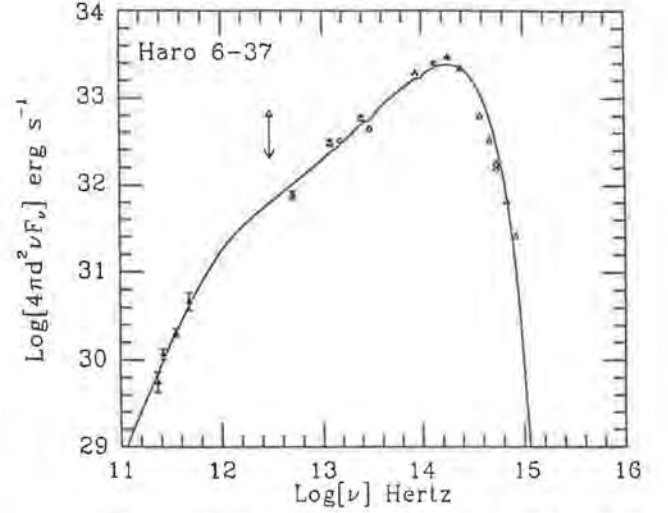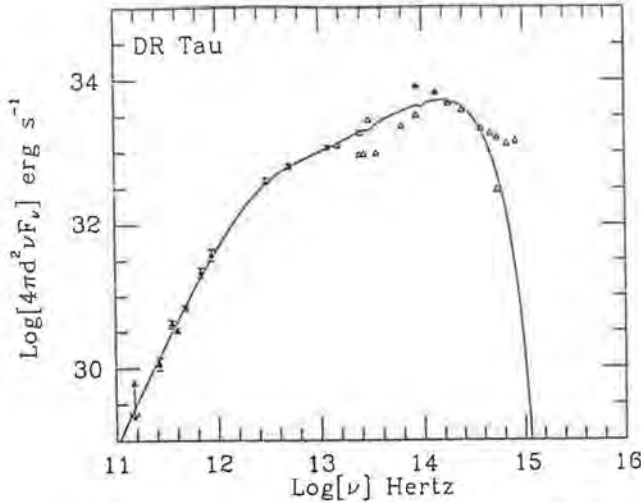

Figure 12. Spectral energy distribution of DR Tauri. Solid triangles are the data points from this paper. Optical and infrared data (open triangles) are from Cohen and Kuhi (1979), Rydgren *et al.* (1984), and Herbig and Bell (1988). Far-infrared data points (also open triangles) are from the IRAS point source catalogue. The solid curve shows the model spectrum in the optically thick limit.
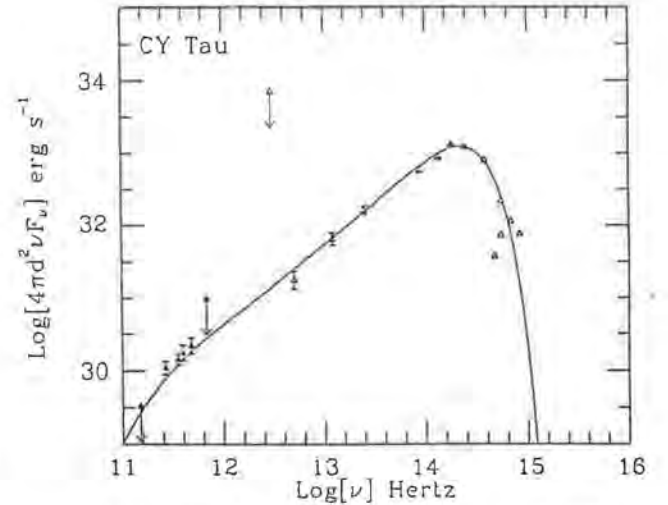

Figure 13. Spectral energy distribution of CY Tauri. Solid triangles are the data points from this paper. Optical and infrared data (open triangles) are from Cohen and Kuhi (1979), Rydgren *et al.* (1984), and Herbig and Bell (1988). The FIR data points (also open triangles) are from CEB. The solid curve shows the model spectrum in the optically thick limit.
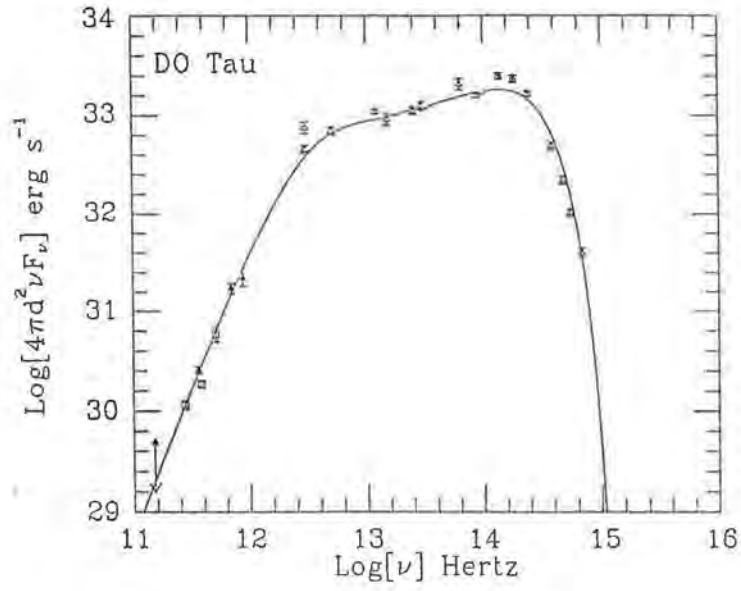
Figure 14. Spectral energy distribution of DO Tauri. Solid triangles are the data points from this paper. Optical and NIR data (open triangles) are from Myers *et al.* (1987). The 12, 25, and 60 μm data points and the lower 100 μm point (also open triangles) are from the IRAS point source catalogue. The upper 100 μm point is from Evans *et al.* (1986). The 600, 800 and 1100 μm points (open squares) are from AEF. The solid curve shows the model spectrum in the optically thick limit.

of-sight. The latter quantity is, by definition, given by

$$\tau_\nu^D \equiv \frac{\kappa_\nu \Sigma(\omega)}{cos\theta} \qquad (2)$$

where κ_ν is the mass opacity of the disk material and Σ is the radius-dependent surface column density in the vertical direction. If we build a disk from an infinite set of annuli with radii from some inner value R_o out to the full disk radius R_D then the flux density F_ν^D due to the entire disk observed at distance d is given by

$$
\begin{aligned}
4\pi d^2 F_\nu^D &= 4g_*(\theta)e^{-\tau_\nu^{ISM}}cos\theta \\
&\times \int_{R_o}^{R_D} \pi B_\nu[T_D(\omega)] \\
&\times \left[1 - e^{[-\tau_\nu^D(\omega,\theta)]}\right] 2\pi\omega d\omega
\end{aligned}
\qquad (3)
$$

where $g_*(\theta)$ is the mean shadowing function describing occultation of part of the disk by the star (ALS) and τ_ν^{ISM} is the interstellar optical depth along the line-of-sight to a given T Tauri system.

The above formulation is quite general and is applicable to any circumstellar disk. Our aim is to use the observed spectral energy distributions to constrain disk quantities such as mass and opacity index; it can be seen from equation 3 that if we are to make any headway then we must specify the form of the radial distribution of temperature in the disk. In the case that observed emission is optically thin, we must also write down the radial distribution of the surface column density. For these functions we adopt the disk emission model of ALS. In this model both the temperature and the surface column density take power law radial dependencies — a form which is also adopted by Beckwith et al. (1990) — i.e.

$$T(\omega) = T_o \left(\frac{R_o}{\omega}\right)^q \qquad (4)$$

$$\Sigma(\omega) = \Sigma_o \left(\frac{R_o}{\omega}\right)^p \qquad (5)$$

where T_o and Σ_o are the absolute temperature and surface column density, respectively, at the inner radius of the disk. The indices, q and p, are both real and > 0. Consider the temperature distribution in equation 4. Disk emission dominates the total radiative flux observed at wavelengths in excess of ~ 10 μm. (T Tauri stars have effective photospheric temperatures typically ≈ 4200 K, for which the Planck spectrum peaks at about 1 μm). This disk emission will be optically thick at all radii for wavelengths less than about 100 μm ($\nu \leq 10^{14}$ GHz); it is then easy to demonstrate that substitution of a power law temperature distribution into equation 3 likewise produces a power law spectral energy distribution, $\nu F_\nu^D \propto \nu^n$, over the same wavelength interval, with

$$n = 4 - \frac{2}{q} \qquad (6)$$

(Note that 100 μm is also approximately the wavelength of the peak of the Planck spectrum at the minimum disk temperature, which corresponds to the outer edge of the disk. See also below). The majority of the T Tauri systems studied in this paper clearly exhibit power law spectral energy distributions from the near-infrared (NIR) to the far-infrared (FIR); see Figures 1 to 14. Adams and Shu (1986) and Adams, Lada and Shu (1987) demonstrated that so-called *passive* disk emission, which originates solely in the reprocessing of photons intercepted from the radiation field of a central host star, can produce a temperature index of q = 3/4, which leads to an infrared spectral slope n = 4/3. Such a temperature distribution is also generated by Keplerian accretion which gives rise to so-called *active* disk emission. This can be seen by balancing the blackbody radiation through the top and bottom surfaces of a given disk annulus with the work done by a torque exerted on the annulus by disk material within the radius of the annulus (see Lynden-Bell and Pringle 1974 and Adams, Lada and Shu 1987); the distinction between passive reprocessing and active radiation by viscous accretion therefore lies in the level of the observed emission rather than in the slope of the spectral energy distribution observed in the infrared. Though we expect both these processes to be operating in any disk which is accreting, examination of many of the spectral energy distributions we observe indicates that the foregoing does not completely account for the infrared excesses in all T Tauri systems: all the systems considered here have infrared spectral slopes which are *less* than 4/3. Indeed, several have flat (n $\approx$ 0) spectra, which implies q $\approx$ 1/2, i.e. it would appear that the disk temperature often falls off with increasing radius much more slowly than expected. Kenyon and Hartmann (1987) suggested that the assumption of a flat disk be dropped for such systems; they proposed a flared disk, leading to enhanced reprocessing of stellar photons. ALS point out that whilst such flaring is quite adequate to explain infrared slopes down to n $\approx$ 2/3, the great infrared excesses of the flat-spectrum sources cannot be entirely generated in this way unless the bulk of the reprocessing dust surface exists at altitudes significantly above the scale height of the gas, which is very unlikely because of dust settling. A third emission process is therefore required for the extreme flat-spectrum systems: one possibility is the propagation of spiral density waves in the disk, generated by gravitational instabilities (Adams, Ruden and Shu 1989). We proceed here with the assumption that all disks are flat and we postulate that any infrared slope n < 4/3 requires a second dissipative torque acting on the material within a disk. Adams, Lada and Shu (1987) showed that a power law temperature function will result regardless of the mechanism(s) actually producing the dissipative torque(s) (be they viscous, magnetic or gravitational), so long as the assumption of axial symmetry is appropriate. Given the uncertainty in the nature of the infrared excesses, we will assume only that a temperature power law holds and, rather than attempting to predict a value for q *ab initio*, we will determine its value by direct inspection of the spectral energy distribution observed for each T Tauri system. It is important to emphasise that the results we present here depend only on the power law forms we adopt for the temperature distributions, and *not* on the details of the *origin* of such power laws.

We assume that any given element of the surface of a circumstellar disk radiates both the energy intercepted from the stellar radiation field, and the flux produced by (unspecified)

active emission processes in the disk. Following ALS — who provide a rigorous treatment of mutual heating and mutual shadowing of a star and flat-disk system — the resulting disk temperature distribution can be expressed using the dimensionless variable $u \equiv R_* / \omega$:

$$
\begin{aligned}
\sigma T(u)^4 = & \left(\frac{L_{\text{intrinsic}}}{4 \pi R_*{}^2 f} \right) u^{4q} \frac{1}{\pi} \sigma T_*{}^4 [sin^{-1} u \\
& - u(1 - u^2)^{1/2}].
\end{aligned}
\tag{7}
$$

T_* in this equation is the effective photospheric temperature. R_* is the stellar radius, obtained from knowledge of T_* and the bolometric stellar luminosity, L_*. σ is the Stefan-Boltzmann constant. The quantity $L_{\text{intrinsic}}$ is the bolometric luminosity of the disk generated by active disk emission processes. Analytically, $L_{\text{intrinsic}}$ can be obtained in terms of T_o, R_o, R_D, and q by integrating $\sigma T_D{}^4(\omega)$ over all ω using the power law distribution in equation 4. The dimensionless quantity f arises when we integrate across the disk to obtain $L_{\text{intrinsic}}$ and is given by

$$
f = \frac{1}{4q - 2} \left[1 - \left(\frac{R_o}{R_D} \right)^{4q-2} \right].
\tag{8}
$$

We see that $f \sim$ unity when $q > {}^1/_2$; $f \longrightarrow \ln(R_D/R_o)$ (~ 10) as $q \longrightarrow 1/2$;

We will therefore employ equation 7 for the temperature distribution[2] when we generate model spectral energy distributions (using equation 3) for comparison with our observed spectral energy distributions. The exponential optical depth term in the flux density equation cannot be neglected at wavelengths for which disk material is *optically thin*, which appears to be the case for a few of the systems studied here at millimetre wavelengths (see also below). We must then consider the normal surface column density, $\Sigma(\omega)$, and the frequency-dependent mass opacity κ_ν. (Note that we lose the dependency on the inclination angle of the disk, as expected for optically thin structures). The power law distribution of Σ postulated by ALS has a proportionality constant which is determined by the total mass of the disk (M_D) and the power law index p (equation 5):

$$
\Sigma_o = \frac{(2 - p)M_D}{2 \pi R_o{}^2 [(R_D/R_o)^{2-p} - 1]}.
\tag{9}
$$

ALS show that the model spectra are insensitive to the value of p. AEF employed p = 7/4 when considering optically thin emission; this was simply a representative value and was taken from the protostellar theory described by Cassen and Moosman (1981). We will adopt the same value for p here whenever we observe optically thin emission. Substituting for $\tau_\nu(\omega)$ in equation 3 in the case $\tau_\nu(\omega) \longrightarrow 0$,

---

[2]Reprocessing of stellar photons provides a relatively small contribution to the emission observed at millimetre/submillimetre wavelengths for disks which have high active luminosities. At such low frequencies, equation 4 can be used in equation 3 without making an appreciable difference to the emergent spectral energy distribution.

$$4\pi d^2 F_\nu^D = \frac{(\kappa_\nu M_D)4\pi(2-p)R_o{}^{p-2}}{[(R_D/R_o)^{2-p} - 1]}$$

$$\times \int_{R_o}^{R_D} B_\nu[T_D(\omega)]\omega^{1-p}d\omega \qquad (10)$$

i.e. with $T_D(\omega)$ specified by equation 7,

$$F_\nu^D \propto \kappa_\nu M_D \qquad (11)$$

Optically thin emission can therefore allow a determination of the mass of a disk if we know the mass opacity, κ_ν. The latter is commonly taken to be a power law at low frequencies, i.e.

$$\kappa_\nu \propto \nu^\beta \qquad (12)$$

(e.g. Draine and Lee 1984, ALS). We will specify the opacity index (β) and employ the scaling adopted by AEF — see below — to estimate disk masses from optically thin emission at millimetre wavelengths.

5 Comparison of Model Predictions with Observations

We begin by listing the various relevant quantities. T_* (photospheric temperature), A_V, (extinction), q (temperature index) and θ (disk inclination) are fixed, and no adjustments are made to their values. L_* (stellar luminosity) is adjusted to fit the short-wavelength data, but its value is of no consequence when fitting the long-wavelength observations. For those disks which appear to be optically thick even out to $\lambda \sim 1$ mm (see below), only 2 quantities are adjusted, namely $L_{intrinsic}$ (disk luminosity) and R_D. A total of 4 quantities are adjusted when we consider observed long-wave spectral energy distributions which can be fitted only by optically thin spectra: $L_{intrinsic}$ (disk luminosity), R_D, M_D, and κ_ν (mass opacity). The number of observed long-wavelength data points (60 μm to 2mm) for each T Tauri system is typically ≈ 10.

1. T_*, the effective photospheric temperature. This quantity is required by equation 7 for specification of the temperature distribution in the disk. It is also combined with the bolometric stellar luminosity to estimate the stellar radius. A catalogue of pre-main sequence stars compiled by Cohen and Kuhi (1979) includes data for the majority of our T Tauri systems. They supply both spectral classifications and a scale for the conversion of spectral class to effective temperature. Cohen and Kuhi (1979) caution that the definition of T_{eff} is unclear for a star with various emitting regions, each of which might contribute

44

significantly to the bolometric stellar luminosity (e.g. photosphere, chromosphere, extended atmosphere and the disk itself). The use of spectral type is therefore the crudest way in which one may characterise the effective temperature of a T Tauri system. With this caveat, and in the absence of other knowledge of T_*, we use the catalogued spectral classes.

2. L_*, the bolometric stellar luminosity. Its value is required in order to estimate stellar radius (using T_*); its value has no bearing on the long-wavelength model spectrum. For more than half our sources we have employed the luminosities catalogued by CEB as initial estimates; indeed, we found that several of the CEB stellar luminosity values required no further adjustment. CEB adopted a distance of 160 pc to the Taurus-Auriga complex. We employ a distance of 140 pc throughout the present work and have therefore scaled down all CEB luminosities accordingly. This also permits direct comparison of our results with those of AEF.

3. $L_{intrinsic}$, the bolometric luminosity of the disk arising from active emission processes. We need a value for $L_{intrinsic}$ in order to compute the run of $T_D(\omega)$ across the disk. Initial estimates for each of the T Tauri stars in our sample were made in the following way: we summed the (scaled-down) integrated luminosity listed by CEB in the 3 bands 0.44 to 0.67 μm, 0.67 to 3.5 μm, and 3.5 to 7 μm; to these we added the 7 to 135 μm luminosity determined from IRAS observations (where available) by summing across the 4 contiguous IRAS bandpasses; finally we trapezoidally integrated from 135 μm to the longest wavelength at which we detected a given T Tauri system with UKT14 (typically 1100 μm). (All luminosity components were estimated assuming spherically symmetric emission at a distance of 140 pc). The bolometric luminosity so estimated needed to be adjusted downwards by an average of 45% to obtain agreement between the predicted and the observed spectral energy distributions.

4. A_V, the visual extinction. Knowledge of this quantity is needed only to generate a realistic model spectral energy distribution in the visible part of the spectrum, which is dominated by stellar emission rather than disk emission. Its value is of no consequence when considering the mass and radius of a circumstellar disk. The average value for our sample of T Tauri systems is $A_V = 1.2$ magnitudes (from the catalogue of Cohen and Kuhi 1979). Interstellar K-band extinction will be about 10% of this value, and is therefore negligible, whilst we expect essentially no interstellar extinction at millimetre wavelengths. We employ the values of A_V listed by Cohen and Kuhi (1979); no adjustments are made to this quantity.

5. q, the disk temperature index. For most of the T Tauri systems we observed, we have estimated the temperature index by fitting a straight line to the NIR photometry and the IRAS FIR data-points, and then relating the infrared slope to q via equation 6; where statistical uncertainties in flux densities are available, we have made a weighted fit. Values of q estimated in this way range from 0.515 (T Tau) to 0.684 (CY Tau); only CY Tau has a value of q which is greater than the minimum ($q \approx 2/3$; see above) which can be reasonably accounted for by disk flaring. By far the majority of our sample would appear to have infrared excesses indicative of active disk radiation processes. These estimates of q were used, with no adjustment, when computing model spectral energy distributions.

6. θ, the angle of inclination of the disk plane. We have no knowledge of this quantity for any of the systems in our sample and we assume a value of 45° throughout this work. Since θ enters our calculations as a cosine term, any flux densities computed for disks which are, in reality, inclined at angles in the range $0° \leq \theta \leq 45°$ will be underestimated by a maximum of only about 30%. We must have disks inclined by $\theta > 82°$ before our assumption of $\theta = 45°$ overestimates the flux densities by factors ≥ 5. A value of 45° is therefore a good working assumption, since we expect the majority of our sample of disks to be inclined at $< 82°$ if they are drawn from a parent population which is randomly orientated.

7. κ_ν, the mass opacity. All disks are optically thick to radiation up to wavelengths of at least $\lambda \sim 100$ μm. Some disks might have regions which are optically thin to emission at longer wavelengths (AEF, Beckwith and Sargent 1991) and for these we must specify the long-wavelength mass opacity of dust grains if we are to compute model spectral energy distributions and estimate disk masses using our millimetre flux densities. We employ the dust opacity profile used by ALS and AEF, which assumes a mixture of silicate and graphite grains. The opacity of the grains is well determined for wavelengths up to ~ 20 μm, at which $\kappa_\nu = 7.2$ cm^2 g^{-1}. Though it is generally agreed that the grain opacity falls off as a power law — $\kappa_\nu \propto \nu^\beta$ — at wavelengths > 20 μm, the precise value of the index is not known. (See Emerson 1988 for an elementary review of emission from dust grains in star-forming regions). ALS proposed a value $\beta = 2$, which is the same as that computed for interstellar dust grains by Draine and Lee (1984). However, the grains in warm, dense circumstellar disks may be different from those in the interstellar medium; AEF briefly review other proposals for the value of β, all of which lie in the range $1 \leq \beta \leq 2$. Taking the above value of κ_ν at $\lambda = 20$ μm, the extremes of this range in β lead to values of κ_ν at 1100 μm which differ by a factor of 55; it can be seen from equation 11 that estimates of disk masses using our millimetre flux densities will differ by the same amount.

8. Disk mass (M_D) and outer radius (R_D). Where emission is optically thin we have attempted to fit our millimetre flux densities by adjusting M_D. R_D is treated as a free parameter in all cases.

5.1 Results

Model spectral energy distributions (SEDs) generated for our T Tauri systems are plotted in Fig. 1 to 14.

Consider the long-wavelength data ($\lambda \geq 60$ μm): it is apparent that 9 of the 14 observational SEDs can be fitted very well by SEDs computed for disks which are optically thick at all observed wavelengths, even out to 2 mm. Neither the disk mass nor the dust opacity enter the calculations for such disks and one can set only a lower bound to the value of M_D. These lower limits are listed in Table 4. The remaining SEDs (i.e. those for T Tau, HL Tau, GG Tau, GM Aur, and HK Tau) can be fitted only by spectra computed for disks which are optically thin at millimetre/submillimetre wavelengths.

Source	R_D (AU)	M_{min} ($M_\odot$)
DG Tau	42	0.05
RY Tau	25	0.02
UZ Tau	40	0.01
DL Tau	52	0.06
H6-13	33	0.03
H6-37	50	0.05
DR Tau	33	0.02
CY Tau	150	0.3
DO Tau	25	0.006

Table 4: Lower limits to masses of optically thick disks[a]

[a]Note. for $\beta = 1$ and $\kappa_\nu = 0.1[\lambda(\mu m)/250]^{-\beta}$ cm^2 g^{-1}
(cf. Beckwith and Sargent 1991)

6 Discussion

Clearly, the five SEDs which can be fitted only when we consider optically thin long-wave emission are those which show the greatest promise for extracting information on disk properties. However, one must be cautious. Recall from equation (10) that, not surprisingly, the disk mass and the dust opacity enter as a product in our calculations of flux densities at long wavelengths. We can therefore determine M_D from a model fit only once we specify the opacity profile, κ_ν. This situation would be relieved somewhat if we were to find that the observed long-wavelength flux densities lie in the Rayleigh-Jeans region of the (composite modified blackbody) SED; then, with $\nu F_\nu \propto M_D \nu^{3+\beta}$, the long-wave opacity index could be obtained directly from inspection of the slope of the SED. However, for the typical outer disk temperatures[3] found here ($T_D \approx 35$ K), the Rayleigh-Jeans approximation to the Planck law is valid only when $\lambda \geq 1100$ μm and cannot therefore be used. Instead, we make no such assumption and we determine instead a likely range of disk masses for the anticipated range in dust opacities. This is illustrated in a crude fashion in Figure 1 (T Tauri), where we have plotted model spectra for $M_D = 0.01$, 0.1 and 1 $M_\odot$ and $\beta = 1$, $^3/_2$, and 2.

Can we identify some combination of M_D and β which provides a markedly better fit to the long-wave data for T Tauri (e.g.) than other combinations? Clearly it would be a hopeless task to attempt to answer this by simply inspecting the SEDs and judging by eye. Observe the '3-dimensional' surface plots in Figure 15, where reduced χ^2 is plotted against both M_D and β. We have restricted our values of β to the range 1 to 2 (see also AEF for discussion on this point). (For these calculations, R_D was fixed *a priori* at the upper limit value determined *not* from the model but by simply assuming the disk is optically thick at 60 μm). Note the wedge-shaped distribution of reduced χ^2 in Figure

---

[3]Remember that the cool, outer regions of a disk will make by far the dominant contribution to the long-wavelength portion of a SED
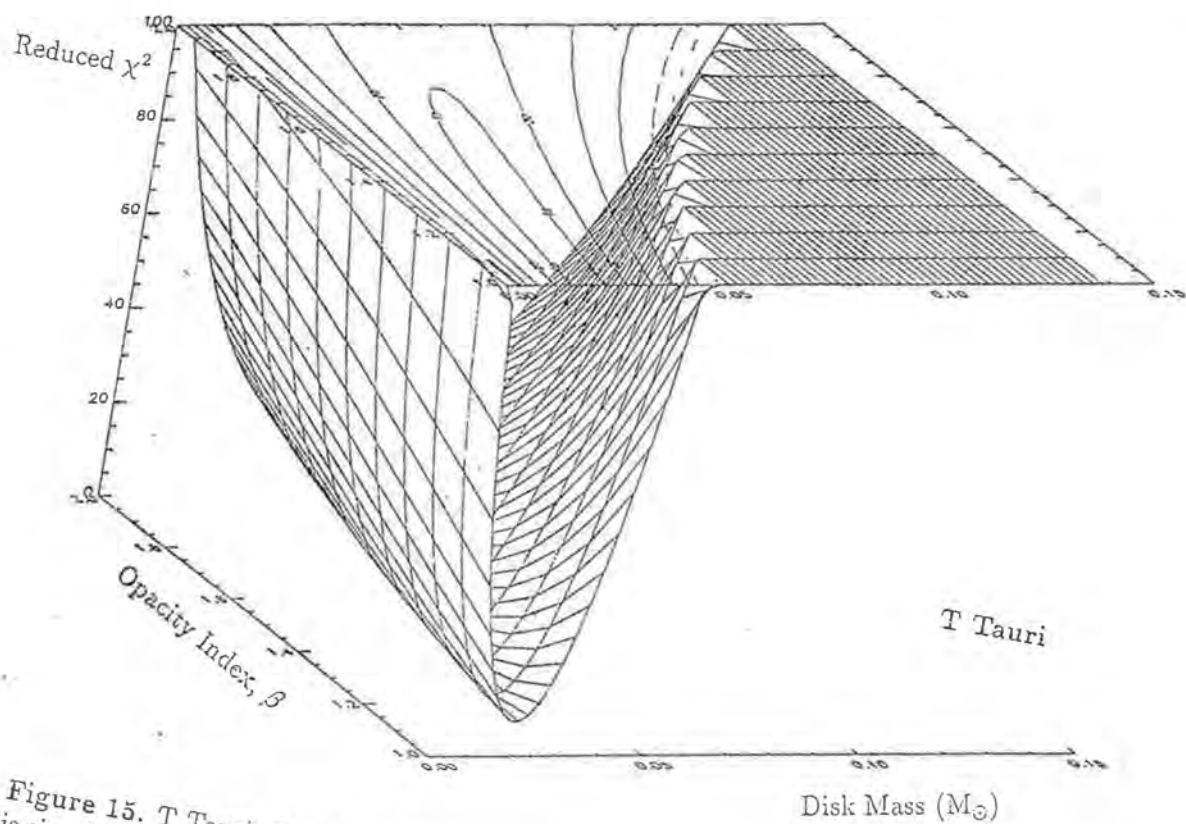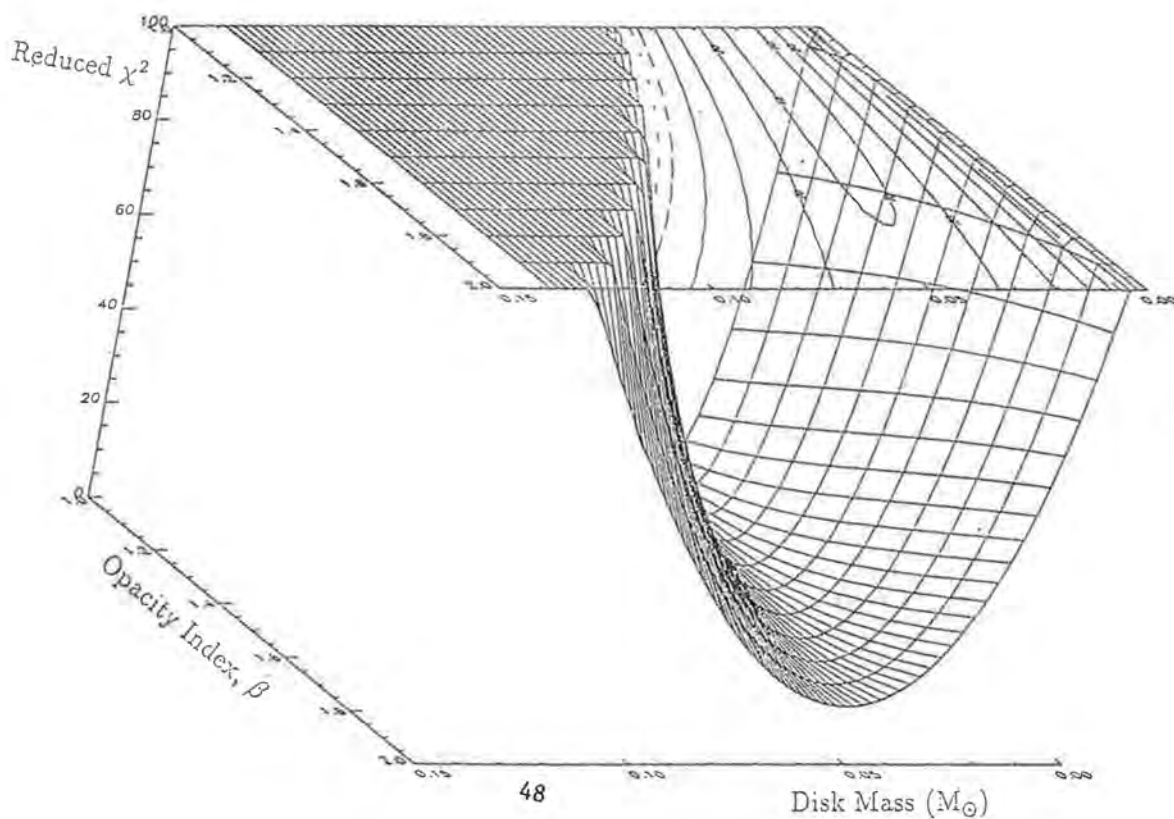
Figure 15. T Tauri. Results of χ^2 fitting to 60-2000 μm observations. (The diagram below is simply a reverse view of the upper picture)

15, which opens out along the M_D dimension as we move in the β dimension from $\beta=$ 1 to 2. We would clearly gain little by selecting the overall best fit and observing the corresponding values of M_D and β . Our conclusion for the example of T Tauri is that the disk mass probably lies in the approximate range 0.03 to 0.07 $M_\odot$, knowledge of its actual value depending on the value adopted for β. Compare this range with the lower limits to disk masses listed in Table 4.

7 Conclusions

We have performed millimetre and submillimetre continuum observations of a sample of T Tauri systems in Taurus-Auriga. Comparison of model spectra with our data allow estimates to be made of the masses of the dust component of circumstellar disks. Many of our lower-bound estimates to disk masses exceed the minimum mass solar nebula, a result which is important to studies of the formation of planetary systems.

Any future progress in elucidating disk properties perhaps depends principally upon an improved knowledge of dust opacities and grain morphology. The fitting of model spectral energy distributions to single-point (spatially unresolved) continuum observations (AEF, Beckwith and Sargent 1991) will probably not yield such knowledge, though useful bounds may be set to the masses of disks in T Tauri systems. The correlation in Beckwith and Sargent (1991) of small χ^2 with large uncertainties in M_D and opacity index β is a good illustration of the difficulties we encounter when attempting to simultaneously constrain both disk masses and dust opacities (i.e. we find that good fits are not necessarily unique fits). One should also remember that dust opacity profiles are unlikely to be independent of radius in the disk, for it would seem unlikely that grain structure/composition would remain unchanged across a temperature range of between 1 and 2 orders of magnitude. Is it reasonable to speak of a single opacity profile without reference to location in the disk? Perhaps so, with regard to the millimetre-wave emission, the bulk of which arises in the outer disk regions. However, the possibility of radial dependence does introduce a further degree of uncertainty. At least two lines of attack present themselves. As pointed out by Beckwith and Sargent (1991), one can investigate mass opacities by combining measurements of disk masses and the distribution of material from line observations together with measurements of the distribution of optical depth from (spatially resolved) continuum maps. A more direct approach to investigating grain structure and properties will be available in the future, following the launch of ISO; the results of sensitive spectral observations with the LWS (Long-Wavelength Spectrometer — 45 to 180 μm) are awaited with much interest.

REFERENCES

Adams, F.C., and Shu, F.H., 1986, *Astrophys J.*, **308**, 836.

Adams, F.C., Lada, C.L., and Shu, F.H., 1987, *As- trophys. J.*, **312**, 788.

Adams, F.C., Lada, C.L., and Shu, F.H., 1988 (ALS) *Astrophys. J.*, **326**, 865.

Adams, F.C., Emerson, J.P., and Fuller, G.A., 1990 (AEF), *Astrophys. J.*, **357**, 606.

Adams, F.C., Ruden, S.P., and Shu, F.H., 1989, *As- trophys. J.*, **347**, 959.

Beckwith, S.V.W., and Sargent, A.I., 1991, *Astro- phys. J.*, **381**, 250.

Beckwith, S.V.W., Sargent, A.I., Chini, R.S., Güsten, R., 1990, *Astron. J.*, **99**, 924.

Cassen, P., and Moosman, A., 1981, *Icarus*, **48**, 353.

Cohen, M., 1973, Mon. Not. Roy. Astron. Soc., **164**, 395.

Cohen, M., 1974, Mon. Not. Roy. Astron. Soc., **169**, 257.

Cohen, M., 1983, *Astrophys. J.*, **270**, L69.

Cohen, M., and Schwartz, R.D. 1976, *Mon. Not. Roy. Astron. Soc.* **174**, 137.

Cohen, M., and Kuhi, L.V., 1979, *Astrophys. J. Suppl.*, **41**, 743.

Cohen, M., Harvey, P.M., and Schwartz, R.D., 1985, *Astrophys. J.*, **296**, 633.

Cohen, M., Emerson, J.P., and Beichman, C.A., 1989 (CEB), *Astrophys. J.*, **339**, 455.

Duncan, W.D., Robson, E.I., Ade, P.A.R., Griffin, M.J., and Sandell, G., 1990, *Mon. Not. R. astr. Soc.*, **243**, 126.

Elias, J.H., 1978, *Astrophys. J.*, **224**, 857.

Emerson, J.P., 1988, in *Formation and Evolution of Low-Mass Stars*, ed. A.K. Dupree and M.T.V.T. Lago (Dordrecht: Kluwer), p. 21.

Evans, N.J., Levreault, R.M., and Harvey, P.M., 1986, *Astrophys. J.*, **301**, 894.

Harvey, P.M., Thronson, H.A., and Gatley, I., 1979, *Astrophys. J.*, **231**, 115.

Herbig, G.H., and Bell, K.R., 1988, *Lick Obs. Bull.*, No. 1111.

Kenyon, S.J., and Hartmann, L., 1987, *Astrophys J.*, **323**, 714.

Mannings, V., and Emerson, J.P. 1992 (MNRAS, submitted)

Mendoza, E.E.V., 1966, *Astrophys. J.*, **143**, 1010. Mendoza, E.E.V., 1968, *Astrophys. J.*, **151**, 977.

Myers, P.C., Fuller, G.A., Mathieu, R.D., Beichman, C.A., Benson, P.J., Schild, R.E., and Emerson, J.P., 1987, *Astrophys. J.*, **319**, 340.

Rydgren, A.E., Strom, S.E., and Strom, K.M., 1976, *Astrophys. J. Suppl.*, **30**, 307.

Rydgren, A.E., and Vrba, F.J., 1983, *Astron. J.*, **88**, 1017.

Rydgren, A.E., Schmeltz, J.T., Zak, D.S., and Vrba, F.J., 1984, Publ. U.S. Naval Obs., Vol. XXV, Part I.

Shu, F.H., Adams, F.C., and Lizano, S., 1987, *Ann. Rev. Astron. Astrophys.*, **25**, 23.

Strom, S.E., Strom, K.M., Kenyon, S.J., and Hart- mann, L., 1988, *Astron. J.*, **95**, 534.

Strom, K.M., Strom, S.E., Edwards, S., Cabrit, S., and Skrutskie, M.F., 1989, *Astron. J.*, **97**, 1451.

Weintraub, D.A., Sandell, G., and Duncan, W.D.A, 1989, *Astrophys. J. (Letters*, **340**, L69.

Woody, D.P., Scott, S.L., Scoville, N.Z., Mundy, L.G., Sargent, A.I., Padin, S., Tinney, C.G., and Wilson, C.D., 1989, *Astrophys. J.*, **337**, L41.

Observational Constraints on a Proto-stellar Disc

D. Ward-Thompson
M.R.A.O., Cavendish Laboratory,
Madingley Road,
Cambridge, CB3 0HE

Abstract

Sub-millimetre continuum data are presented of the ρ Oph A dark cloud, and are combined with a new maximum entropy deconvolution of the IRAS data of the region. In addition to the known sub-millimetre source SM1, the data show strong sub-millimetre emission from a candidate protostar, VLA1623, which has a highly collimated bipolar outflow and strong radio emission, but appears to have no detectable infra-red emission. SM1 also has no infra-red emission, but has no radio emission or bipolar outflow either. It is hypothesised that SM1 is in an earlier evolutionary state than VLA1623, possibly pre-stellar. The envelope of VLA1623 is modelled, and seen to be consistent with a radial density distribution of $\rho(r) \propto r^{-1/2}$. This disagrees with theoretical predictions, but is not unique. There is no evidence in the data for any large-scale disc ($\sim$1000AU) around VLA1623. Rather, the data point to a "cored-apple" circumstellar structure. There is also no evidence in other authors' interferometer data for a smaller ($\sim$250AU) disc. It is speculated whether a disc is necessary for bipolar outflow collimation or generation, or if some other effect such as magnetic pinching is sufficient. However the data cannot rule out the presence of a small-scale disc ($\sim$80AU), which is optically thick at 2.7mm.

1 In search of protostars

Discs are now a widely-accepted facet of the evolution of young stellar objects (YSO's), however much remains unclear about the role which they play, how early in the evolutionary cycle they form, and whether they are necessary for the collimation and/or driving of bipolar outflows. In this paper I will concentrate on the nature of *proto*-stellar discs (ie: discs around protostars) and present some recent observations of a newly-discovered candidate protostar. Take as a working definition of a protostar:

A condensed object which will become a star, which contains as yet only a small fraction of the mass which it will contain when it reaches the main sequence.

A class of objects has been identified, which have been referred to as protostars (eg: Adams, Lada & Shu 1987), which are known technically as "Class I" sources (Lada 1987), based on their 1-10μm spectral index. These objects are optically invisible, were discovered by their near infra-red emission, and have steeply-rising infra-red spectra toward longer wavelengths. However, recent work has cast some doubt on the suggestion that Class I sources are true protostars as defined above:- Stahler & Fletcher (1991) modelled the luminosity function of embedded clusters and found that the expected fraction of embedded sources which are protostars is <1% for most of a young cluster's life. Therefore *protostars are rare*, whereas Class I sources are not so rare – eg: Wilking, Lada & Young
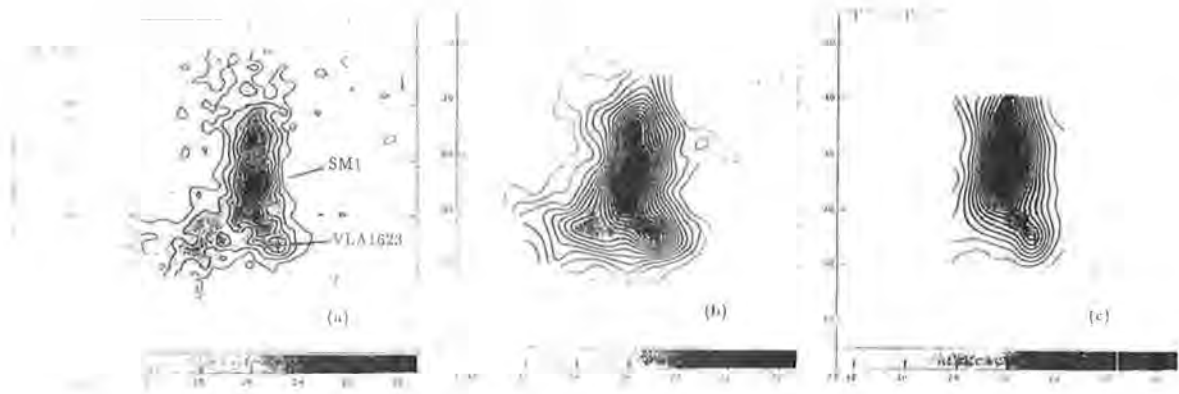
Figure 1: Sub-millimetre continuum isophotal contour maps superposed on grey-scale images of SM1 and VLA1623 at (a) 800μm, (b) 450μm and (c) 350μm. The resolution of all maps is 13 arcsec. The positions of SM1 and VLA1623 are marked. The other crosses mark the positions of GSS30 and S2.

protostars are rare, whereas Class I sources are not so rare – eg: Wilking, Lada & Young (1989) found that for the ρ Oph cluster, there were roughly equal numbers of Class I, II & II sources, so ~33% of the embedded sources were Class I.

Submillimetre luminosity is a direct measure of the mass of cold dust at a given temperature surrounding an object, and hence of the total mass of circumstellar material surrounding the protostar, and the younger a protostar, the more circumstellar material it should have, and hence the greater the sub-millimetre luminosity should be. Barsony & Kenyon (1992) found that the sub-millimetre luminosity of a sample of embedded sources in the Taurus dark cloud was not correlated with their near-infrared colours. Furthermore, they found that the submillimetre luminosity of Class I sources is not significantly greater than that of T Tauri stars (TTS), which are much more evolved objects. Irrespective of any model, protostars should have more circumstellar material than TTS. This is however complicated by the effects of temperature gradients.

Therefore we need to look for something younger than a Class I object if we are to find a true protostar, by the above definition. Such an object may not be detectable at all in the near-infrared, mid-infrared, or even in extreme cases in the far-infrared, and may possibly only be detected in the sub-millimetre and at radio wavelengths.

Protostars are generally believed to coalesce from density enhancements (clumps) in molecular clouds. Hydrostatic equilibrium of a clump is only possible if its mass M is less than a critical mass M_{crit} (Shu 1977) given by:

$$M_{crit} = 1.18 \frac{a^4}{G^{3/2}} P_{ext}^{-1/2}$$

where a is the isothermal sound speed. In this instance the radial dependence of density is $\rho(r) \propto r^{-2}$. If the mass of a clump exceeds the critical mass, then collapse to a protostellar object commences. The collapse begins at the centre and a collapse expansion
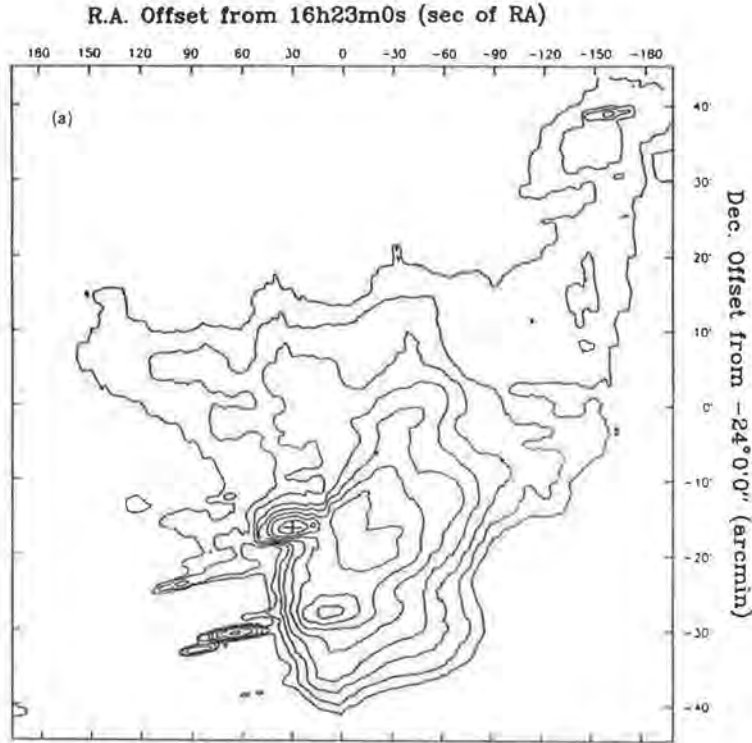
Figure 2: IRAS 12-μm image of the ρ Oph A region. The position of S1 is marked.

wave (CEW) travels outwards from the centre. Within the CEW the radial dependence of density is $\rho(r) \propto r^{-3/2}$ (Shu 1977). The accretion luminosity is given by L=GM$\dot{M}$/R (Adams, Lada & Shu 1987).

2 The ρ Oph dark cloud

The nearby (d=160pc) ρ Oph dark cloud was first mapped in SO by Gottlieb *et al* (1978), who found 2 dense cores, which were subsequently named ρ Oph A and B (Loren *et al* 1980). ρ Oph A & B and other dark clouds in the region are connected by filaments, which can be seen in ^{13}CO, and were christened 'the cobwebs of ophiuchus' (Loren 1989a&b). A small clump in one of the filaments hosts the bipolar outflow source IRAS16293 (Walker *et al* 1986).

A rich cluster of embedded IR sources fills the majority of the ρ Oph region (Wilking, Lada & Young 1989, and references therein), the brightest of which, Source 1 (Grasdalen, Strom & Strom 1973), lies near the peak of ρ Oph A. Source 1 (hereafter S1) is known to be an embedded B3 star with an associated HII region (André *et al* 1991, and references therein), responsible for heating an extended region of dust to T~30K, which was observed at 80μm and named IRS1 (Harvey, Campbell & Hoffmann 1979). S1/IRS1 was identified with the IRAS source 16235-2416 (Ward-Thompson *et al* 1989). Thus it appears that ρ
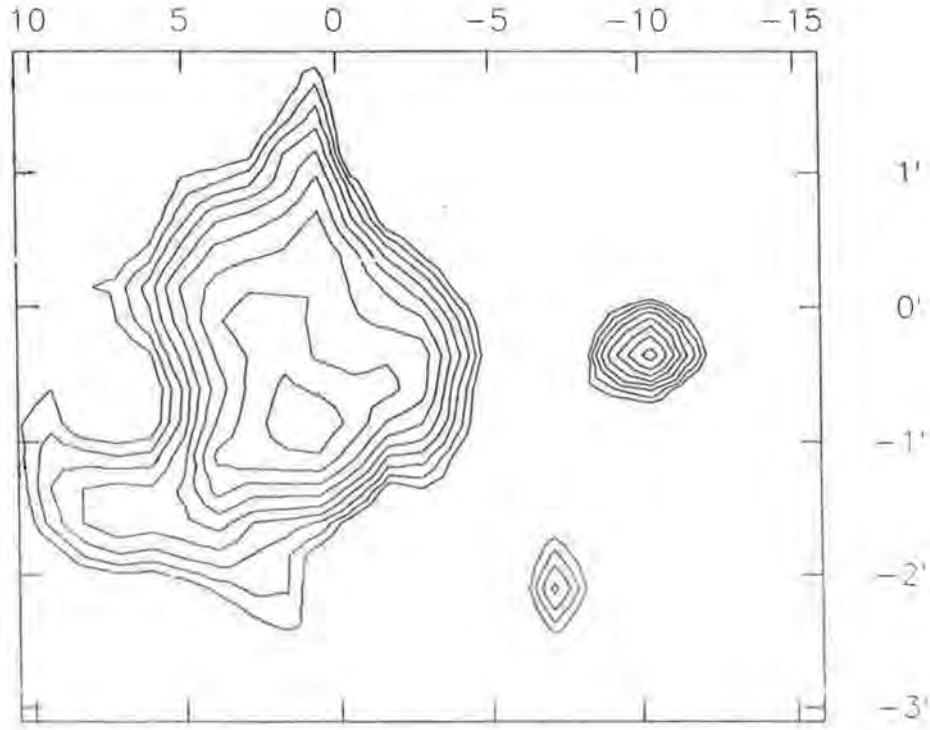
Figure 3: Maximum entropy reconstruction of the IRAS 12-μm data of the S1 region. The origin is at $16^h23^m30^s$, $-24^o16'0''$ and axes are marked in seconds of RA and arcminutes. Note the smaller scale of this map, and the higher resolution. The two point-like sources are GSS30 and S2, and the extended source is S1/IRS1.

Oph is a rich, nearby, star-forming region, and a good place to search for protostars.

The first sub-millimetre continuum search of ρ Oph was carried out by Ward-Thompson *et al* (1989), who discovered an emission peak near to the peak of ρ Oph A itself, which they named SM1. They mapped this peak at 350, 800 & 1100 μm and speculated that it may be a candidate protostar. However their observations lacked the spatial resolution to confirm this hypothesis.

The first (and so far only) bipolar outflow to be discovered in the core of ρ Oph A was reported by André *et al* (1990), and was seen to be centred to the south-west of the peak of SM1. Subsequently a 6-cm radio source – VLA1623.4-2418 (hereafter VLA1623) was found to lie at the centre of the bipolar outflow (Leous *et al* 1991).

Neither SM1 nor VLA1623 was detected in the IRAS raw data, and neither has any known near-IR association. It was speculated that they are therefore candidate protostars, and ideal for further study.

3   Sub-millimetre sources in ρ Oph A

Figure 1 (a) - (c) shows three sub-millimetre continuum isophotal contour maps superposed on grey-scale images of a roughly 2.5-arcmin square region around SM1 and

$\lambda/\mu\mathrm{m}$	SM1	VLA1623
800	6.7±1.5	3.0±1.0
450	37±9	25±5
350	70±20	22.5±7.5

Table 1: Source peak flux densities in Jy per 13-arcsec beam.

VLA1623. Figure 1(a) shows an 800-μm map, which has a resolution of 13 arcsec, and Figure 1 (b) & (c) show 450- & 350-μm maps respectively, smoothed to the same resolution. The maps were made using the James Clark Maxwell Telescope (JCMT) situated on Mauna Kea, Hawaii. Calibration was performed using the planet Uranus (for full details of calibration proceedure, mapping parameters etc, see André, Ward-Thompson & Barsony 1992 – hereafter AWB). The two sub-millimetre sources SM1 & VLA1623 are clearly resolved in all three maps. Source peak flux densities, measured in Jy per 13-arcsec beam, are listed in Table 1 for both SM1 & VLA1623.

SM1 appears to be located in the middle of an extended ridge-like structure running north-south which also contains other clumps (see Figure 1a). South of SM1 the ridge turns to the south-east to form an arc-like structure, whose centre appears to lie somewhere to the east, in the direction of S1. This may be indicating that S1 is interacting with the ridge in some way – either by means of its stellar wind or its HII region. VLA1623 appears to lie on the edge of the ridge furthest away from S1, and hence it is easier to define its properties than those of SM1, which is confused by the more extended structure.

Figure 2 shows an IRAS 12-μm image of the ρ Oph A region taken from Ward-Thompson et al. (1989). Note that this is a much larger region than is shown in Figure 1 ($\sim$1.5° square). S1/IRS1 (alias IRAS16235-2416) can be clearly seen along with a number of other sources (cf: Wilking, Lada & Young, 1989). However, SM1 & VLA1623 cannot be seen in any of the raw IRAS data due to their proximity to S1. Therefore it was decided to use a maximum entropy method (MEM) to deconvolve the IRAS raw data, in an attempt to resolve the two sub-millimetre sources.

Figure 3 shows a maximum entropy reconstruction of the IRAS data of the S1 region. This map is at a much larger scale than Figure 2, and has much greater resolution. No prior information was given to the maximum entropy routines about the sources in this field, however point sources are now seen which are coincident with the known IR sources S2 and GSS30 – neither of which have previously been detected in the IRAS data – and an extended source is seen at the position of S1/IRS1. MEM also recovered all IRAS sources in the field, and did not find any sources which were not previously known near-IR sources. The method has also been used on the IRAS data of M51 (Bontekoe et al 1991) and W49 (Ward-Thompson, Berry & Robson 1992), and is a very powerful technique for improving the resolution of IRAS data (see Narayan & Nityananda 1989 for a recent review of astronomical implementations of MEM).

There are no IRAS sources coincident with either SM1 or VLA1623. The same procedure was repeated with the IRAS data at 25, 60 & 100 μm with similar results. Upper
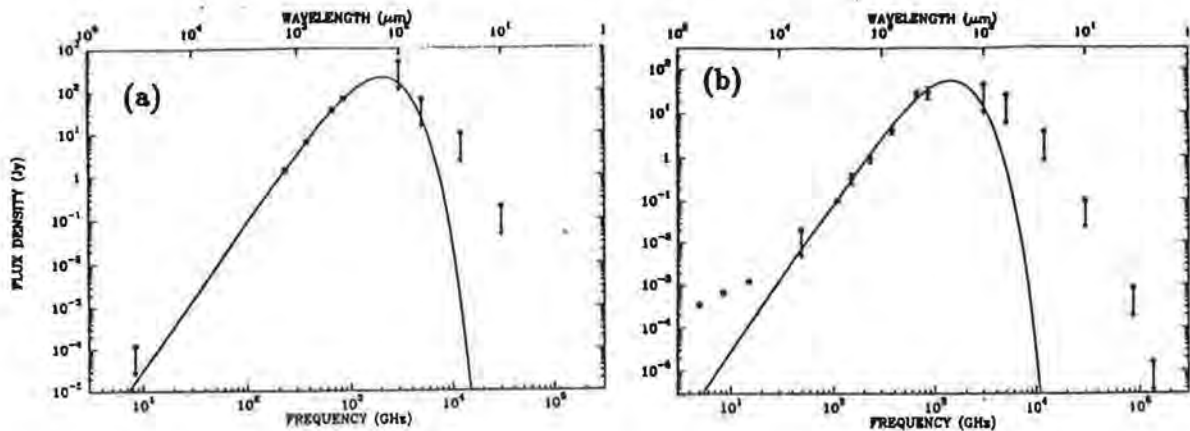
Figure 4: Spectral energy distributions of (a) SM1 and (b) VLA1623, plotted as log (flux density) against log (frequency). The IRAS upper limits come from the maximum entropy deconvolution, and the sub-millimetre datapoints come from this paper and AWB.

limits could therefore be placed on the IRAS flux densities of SM1 & VLA1623 which are much tighter than was previously possible (Ward-Thompson 1992). These flux densities, together with those in Table 1, and data taken from the literature (AWB and references therein), are plotted on Figure 4 (a) & (b) for SM1 & VLA1623 respectively. Also plotted on Figure 4 are single-temperature grey-body fits to the data, with, for SM1, T=27K and β=1.5, and for VLA1623, T=20K and β=1.5.

The fits suggest bolometric luminosities of order $4L_\odot$ and $0.75L_\odot$ for SM1 & VLA1623, and the sub-millimetre fluxes indicate circumstellar masses of $0.7\pm0.3M_\odot$ & $0.6\pm0.3M_\odot$ respectively. However, note that the mass of SM1 is more difficult to define (as mentioned above) due to its confusion by the extended ridge. The fact that SM1 (which is closer to S1) is warmer than VLA1623, may be indicating that S1 is the main source of heating for the ρ Oph A core, as hypothesised by Ward-Thompson et al (1989).

The total mass derived for the ρ Oph A core from these measurements (calculated within the lowest 800-μm contour of Figure 1(a)) is $\sim$10-15$M_\odot$. This is in very good agreement with the mass derived from CO isotope measurements by Loren, Wootten & Wilking (1990) of $12M_\odot$, and gives confidence in the derived masses of the two sources.

In summary, VLA1623 is a low-mass, low-luminosity, cold source, on the edge of the ρ Oph A core, which has a bipolar outflow, and is also seen in the radio continuum. SM1 is a similar but slightly warmer source (possibly due to external heating by S1), apparently in the centre of the ρ Oph A core, which has no outflow and no radio continuum emission from its peak. On the basis of this, it is hypothesised that VLA1623 is a candidate protostar, whilst SM1 is in an earlier, possibly pre-stellar phase (AWB). The remainder of this paper will concentrate on VLA1623.
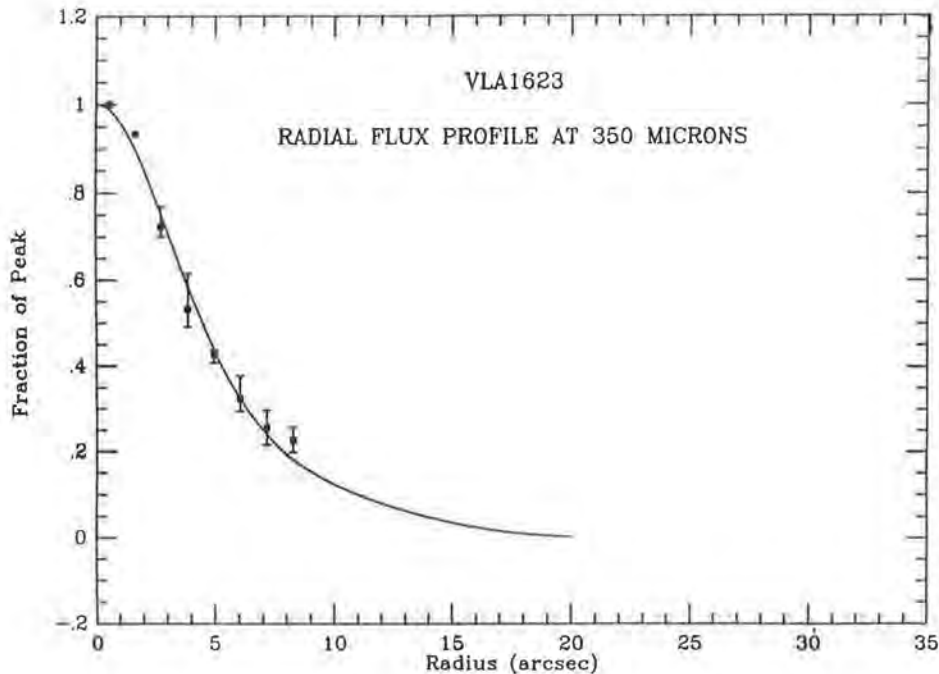
Figure 5: Azimuthally averaged radial flux density profile at 350μm of VLA1623 compared to the predictions of the Wolfire-Cassinelli model for a $\rho(r) \propto r^{-1/2}$ radial density profile (solid line).

4 The "protostar" VLA1623

If the luminosity of VLA1623 is due to infall and accretion alone, the equation quoted in section 1 can be used to derive the mass of the central core, or protostar, itself. Using a typical sound speed for ρ Oph of 0.35kms^{-1} (Adams, Lada & Shu 1987), the mass infall rate is 10^{-5}M$_\odot$/yr, and hence, for the luminosity found for VLA1623, the mass which has already accreted onto the core is $\sim$10^{-2}M$_\odot$. This means that the protostellar core contains only a few percent of the mass of the circumstellar envelope, and is consistent with VLA1623 being a true protostar.

The azimuthally averaged radial intensity profile of VLA1623 was compared to the planet Uranus, which had an apparent diameter of 3.5 arcsec at the time of the observations. It was seen that VLA1623 was more extended than Uranus, and had been partially resolved in the sub-millimetre data at all wavebands. The deconvolved FWHM of VLA1623 at 450μm is 11$\pm$4 arcsec, and a consistent result was obtained at 350 & 800 μm. All of the derived parameters of VLA1623 are listed in Table 2.

The dust radiative transfer code of Wolfire & Cassinelli (1986; 1987) was used to model VLA1623. This code fits both the spectral energy distribution and the radial intensity profile *simultaneously*, for a centrally heated core or YSO, given certain input parameters, and observational constraints, such as total luminosity and mass. It was found that the fits were most sensitive to the radial dependence of density $\rho(r)$, and further, that the best fit to the data was given by $\rho(r) \propto r^{-1/2}$ (AWB). Figure 5 shows the radial flux profile of VLA1623 compared to the $r^{-1/2}$ density profile, after it has been convolved with the

Parameter	Value
FWHM	$\sim$2000AU
T_d	20$\pm$5K
$\tau_{350\mu m}$	$\sim$0.2
N_H	$\sim 10^{24}\text{cm}^{-2}$
L_{bol}	0.75$\pm$0.25 L$_\odot$
M_C	0.6$\pm$0.3M$_\odot$

Table 2: Derived parameters of VLA1623.

JCMT beam, showing that it is consistent.

This is in *disagreement* with the theoretical prediction of $\rho(\text{r}) \propto \text{r}^{-3/2}$ for a collapsing protostellar object (Shu 1977). However, this is not the only such object with a shallow density gradient. An identical radial density power law was found for LkHα198 (Natta *et al* 1992) in a spherical envelope, although the data for this object also required an inner disc (or else strong emission from PAH's) to explain its near-IR spectrum.

5 Outflow without a disc?

Lin & Pringle (1990) proposed the existence of large-scale collimating discs around YSO's with radius $\sim$1000AU to explain the generation and collimation of bipolar outflows. No evidence was found in any of the sub-millimetre data of VLA1623 for a large-scale disc of this nature. On the contrary, the bulk of the circumstellar material lies in a roughly spherical envelope. To be undetected a disc would have to have a radius <250AU.

However, even a disc such as this has been ruled out by recent 2.7-mm interferometer observations at OVRO (André & Sargent 1992), which show that VLA1623 has **no** compact disc component such as that found in the case of L1551-IRS5 (Keene & Masson 1990). The data cannot rule out the presence of an edge-on disc which is geometrically thin, but optically thick at 2.7mm. Such a disc would require T<20K and R<80AU (AWB) to escape detection. So a disc such as those envisaged by Adams, Lada & Shu (1987) remains possible, provided it is extremely optically thick.

Instead, the sub-millimetre observations along with the bipolar outflow appear to point to a "cored-apple" geometry for VLA1623. In this model, the outflow clears a cavity along the axis of the apple, while infall occurs in all other directions (AWB). Such a structure may subsequently evolve into a disc.

If this hypothesis is correct, then a highly collimated bipolar outflow may be possible without the presence of a disc. Perhaps something similar to the hydromagnetic, centrifugal wind model of Pelletier & Pudritz (1992) could collimate the outflow. Although their model requires a disc initially, they subsequently find that 'magnetic pinching' serves to recollimate the outflow at some distance from the disc.

6 Conclusions

The candidate protostar VLA1623 has been mapped in the sub-millimetre and shown to have a spherical envelope with a shallow ($r^{-1/2}$) density gradient. Although it has a well-collimated bipolar outflow, it shows no evidence for a disc-like structure of the nature of that around the archetypal outflow source L1551-IRS5. Rather the data seem to indicate a 'cored-apple' geometry for the circumstellar material, with the outflow sweeping a cavity along the axis of the apple. If there is a disc around VLA1623 at the centre of the envelope it has to be optically thick at 2.7mm and have a radius <80AU.

References

Adams, F. C., Lada, C. J., & Shu, F. H. 1987, *ApJ*, **312**, 788

André, P., Martín-Pintado, J., Despois, D., & Montmerle, T. 1990, *A&A*, **236**, 180

André, P., Phillips, R. B., Lestrade, J. F., & Klein, K. L. 1991, *Ap.J*, **376**, 630

André, P. & Sargent, A. I. 1992, in prep

André, P., Ward-Thompson, D. & Barsony, M. 1992, *ApJ*, in press (AWB)

Barsony, M. & Kenyon, S. J. 1992, *ApJ*, **384**, L53

Bontekoe, T., Kester, D., Price, S., de Jonge, A. & Wesselius, P. 1991, *A&A*, **248**, 328

Gottlieb, C. A., Gottlieb, E. W., Litvak, M. M., Ball, J. A., & Penfield, H. 1978, *ApJ*, **219**, 77

Grasdalen, G. L., Strom, K. M., & Strom, S. E. 1973, *ApJ*, **184**, L53

Harvey, P. M., Campbell, M. F., & Hoffman, W. 1979, *ApJ*, **228**, 445

Keene, J. & Masson, C. R. 1990, *ApJ*, **355**, 635

Lada, C. J. 1987, in *Star Forming Regions*, Proc. IAU Symp. 115, 1 eds. Peimbert & Jugaku.

Leous, J. A., Feigelson, E. D., André, P., & Montmerle, T. 1991, *ApJ*, **379**, 683

Lin, D. N. C. & Pringle, J. E. 1990, *ApJ*, **358**, 515

Loren, R. B. 1989a, *ApJ*, **338**, 902

Loren, R. B. 1989b, *ApJ*, **338**, 925

Loren, R. B., Wootten, H. A., Sandqvist A., & Bernes C. 1980, *ApJ*, **240**, L165

Loren, R. B., Wootten, H. A., & Wilking, B. A. 1990, *ApJ*, **365**, 269

Narayan, R. & Nityananda, R., 1989, *ARA&A* **24**, 127

Natta, A., Palla, F., Butner, H., Evans, N. & Harvey, P. M. 1992, *ApJ*, **391**, 805

Pelletier, G., & Pudritz, R. E. 1992, *ApJ*, **394**, 117

Shu, F. H. 1977, *ApJ*, **214**, 488

Stahler, S. W., & Fletcher, A. 1991, in Proc. Vulcano Workshop, eds. Palla & Zinnecker

Vrba, F. J., Strom, S. E., Strom, K. 1976, *AJ*, **81**, 958

Walker, C., Lada, C., Young, E. T., Maloney, P., & Wilking, B. A. 1986, *ApJ*, **309**, L47

Ward-Thompson, D. 1992, in prep

Ward-Thompson, D., Berry, D. S. & Robson, E. I. 1992, *MNRAS*, **257**, 180

Ward-Thompson, D., Robson, E. I., Whittet, D. & Gordon, M. 1989, *MNRAS*, **241**, 119

Wilking, B. A., Lada, C. J., & Young, E. T. 1989, *ApJ*, **340**, 823

Wolfire, M. G. & Cassinelli, J. P. 1986, *ApJ*, **310**, 207

Wolfire, M. G. & Cassinelli, J. P. 1987, *ApJ*, **319**, 850

Circumstellar Envelopes
of Long-Period Variables

A. Heske
ISO Science Operations Team / ESA
P.O.Box 299
2200 AG Noordwijk zh
The Netherlands

Abstract

Long-Period Variables are characterised by two phenomena: Pulsation and mass loss. This paper reviews characteristics of these evolved stars and discusses the results of correlations between observational stellar (pulsational) and circumstellar parameters, which point to a significant impact of the pulsational period on dust formation in the envelope. It is proposed that stellar pulsation determines the structure of circumstellar envelopes and might also lead to a non-spherically symmetric geometry; detailed models of *pulsating* stars are clearly needed.

1 Pulsation and Mass Loss of Long-Period Variables

At late stages of their evolution most stars become cool giants or supergiants. A characteristic of these evolved stars is *variability*. Pulsating variables with periods ranging from 60 up to 2000 days form one group of variables stars - the *Long Period Variables* (LPVs). The detection of blue shifted components in atomic lines in optical spectra of evolved stars revealed another characteristic (Deutsch 1956): *Mass loss* by which stars build up a circumstellar envelope.

There is observational and theoretical evidence that all LPVs are surrounded by circumstellar envelopes. These envelopes were found to exhibit a large variety of spectral features which trace different components. In the following, a short overview is given; more details can be found in proceedings of three conferences on cool stars, stellar evolution and stellar pulsation (Menessier and Omont (eds.) 1990, Wallerstein (ed.) 1990, Cacciari and Clementini (eds.) 1990).

- *Dust*: Depending on the chemical composition (oxygen-rich or carbon-rich) characteristic features at 9.7 or 11.3 microns can be found. The continuum emission from the star beyond 10 microns is dominated by the contribution of the cool dust with temperatures below 800 K, for example the IRAS colours give an indication of the amount of dust in circumstellar envelopes.

- *Molecules*: The main tracers of the molecular component are carbon monoxide (CO) lines and hydroxyl (OH) maser lines. These lines originate in the expanding envelope, where the line width is determined by the expansion velocity. Depending on the optical depth of CO typical profiles from spherically symmetric envelopes can be described as either flat-topped / double-peaked (optically thin) or parabolic (optically thick) (Knapp and Morris 1985).

60

- *Atomic gas:* Due to stellar pulsation the structure of the atmosphere is mainly determined by shock waves, which can be traced for example by the highly variable hydrogen lines (e.g. Gillet, Maurice and Baade 1983).

The spectral features detected in circumstellar envelopes have been used to determine mass loss rates. They range from 10^{-8} (early K giants) to 10^{-5} $M_\odot$/yr (obscured OH/IR stars). However, the mass loss rate for a particular object can vary one order of magnitude or even more, where uncertainties are mainly introduced by poorly known parameters like distance of the object, density distribution in the envelope, gas-to-dust ratio and chemistry.

A consistent description of the mass loss process in pulsating long-period variables is the following scenario: 1) Material from the stellar atmosphere is first pushed out to several stellar radii by means of shocks (e.g. Willson and Bowen 1986) or acoustic waves (Pijpers and Habing 1989). 2) Grains are formed via condensation processes in the atomic and molecular gas (Gail and Sedlmayr 1986). 3) Finally, radiation pressure on grains causes the circumstellar material to expand (Kwok 1975).

2 Stellar versus Circumstellar Characteristics

Dynamical models have been developed using a set of time-dependent hydrodynamical equations coupled to the moment equations describing the dust formation (Fleischer, Gauger and Sedlmayr 1991). The scenario outlined in the previous section can be understood quantitatively by these models which link processes occurring in the stellar atmosphere to mass loss.

Since the structure of the stellar atmospheres depends on stellar parameters of LPVs, such as pulsational period and amplitude - ultimately on mass and radius - most questions concerning the evolution of LPVs might only be answered once these stellar parameters have been determined:

- Do all giants follow a similar path through the Asymptotic Giant Branch (AGB) to become Planetary Nebulae?

- On which parameters does the evolutionary path of a cool giant depend?

- What are the properties of the precursors of asymmetric planetary nebulae?

DATA
As stated earlier, two main characteristics describe the cool giant phase: Stellar pulsation and mass loss. In a first step towards understanding qualitatively the impact of stellar on circumstellar parameters, correlations between observational characteristics of the star and its circumstellar envelope were searched for.
The characteristics are:
for the star

- P - the stellar period.

- f - the ratio between the rise time from the minimum to the maximum of the light curve (Vardya 1988) and P.

61

for the circumstellar envelope

- v_{exp} - the expansion velocity, derived from molecular lines.

- $I_{9.7}$ - the intensity of the silicate dust feature, being the ratio of the peak flux at $9.7\mu m$ to the flux of the underlying continuum, as defined by Mitchell and Robinson (1981).

For about 100 stars expansion velocities, based on CO or OH measurements, and periods have been retrieved from the literature (Mattei 1983, Herman and Habing 1985, Knapp and Morris 1985, Wannier and Sahai 1986, Sivagnanam et al. 1989, Heske 1989). For most of the sample stars f values were available (Herman and Habing 1985) or were derived from the visual light curves (Mattei 1983). For the measurements of the $9.7\mu m$ intensities the IRAS low resolution spectra (IRAS Science Team 1986) have been used.

RESULTS
Expansion velocity versus stellar period (FIG.1)
For periods below 400 days the expansion velocity is confined to a range between 4 and 14 km/s, for periods longer than 600 days the velocity remains rather constant between 10 and 30 km/s. In the transition region between 400 and 600 days there is a large scatter in the v_{exp} values. The distribution suggests that there are two groups of variables, each characterised by a typical expansion velocity. The v_{exp} - P relation thus can be described as a step function where the transition between the two groups occurs at a period of 500 days.

- "rapid" long period variables (P < 500 d) with typically $v_{exp} = 10$ km/s.

- "slow" long period variables (P > 500 d) with typically $v_{exp} = 20$ km/s.

According to models of grain condensation the velocity of the expanding envelope is determined by grain properties (e.g. size) and the dust condensation radius (Kwok 1975, Bowen 1988). Small outflow velocities can be the result of a large dust condensation radius or large grains, which would be the case for the "rapid" long period variables (Mira variables, carbon-rich stars and supergiants); smaller grains or smaller condensation radii would result in a larger outflow velocity, which would be the case for the "slow" group (OH/IR stars). For each group of variables there seems to exist a typical condensation radius and/or a typical size of the grains. In the transition region between 400 and 600 days the dust condensation parameters are not determined: For similar periods highly different expansion velocities can be found.

Intensity of silicate feature versus stellar period (FIG.2)
The distribution of $\log I_{9.7}$ vs. P shows that for periods up to about 500 days (Miras, supergiants and a few OH/IR stars) the silicate feature can be found in emission, beyond (OH/IR stars) it only appears in absorption. The results of model calculations of silicate feature intensities ($\log I_{9.7}$) as a function of optical depth of the dust by Mitchell and Robinson (1981) revealed a similar sequence.

The model intensities of the silicate feature for a constant dust density throughout the envelope are indicated in Fig.2 by dashed lines. For an outer envelope radius of $10^6 R_*$ (R_2) the feature can never be observed in emission; for $100R_*$ (R_1) emission is expected for low optical depths of the dust and pure absorption for optical depths higher than
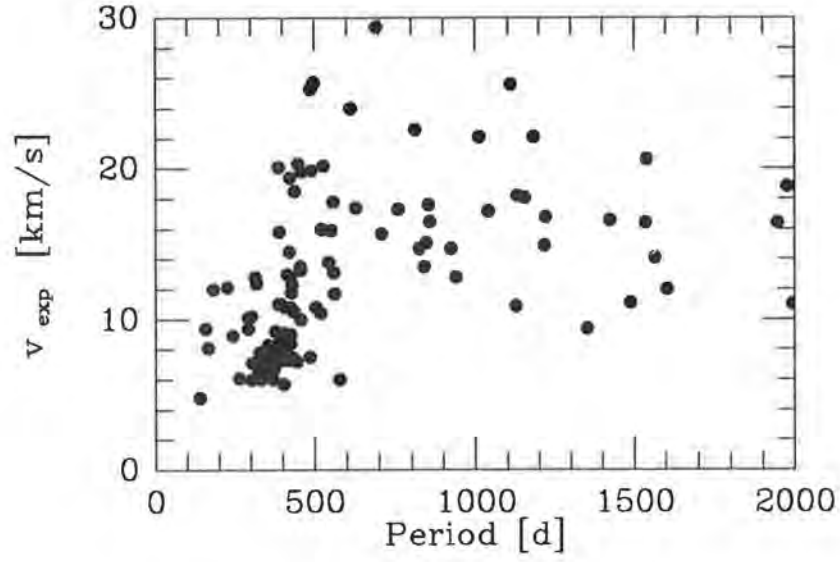
Figure 1: Expansion velocity versus stellar period.
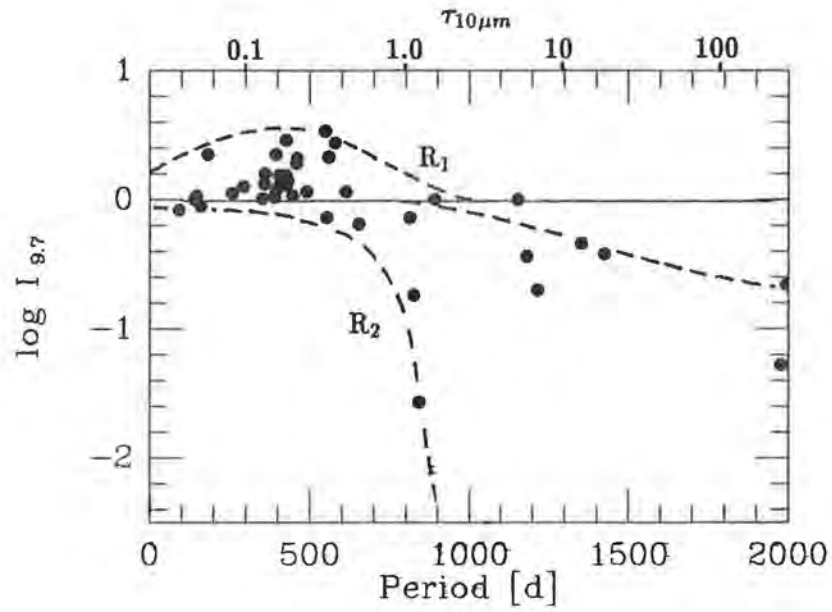
Figure 2: Intensity of the 9.7μm feature versus stellar period
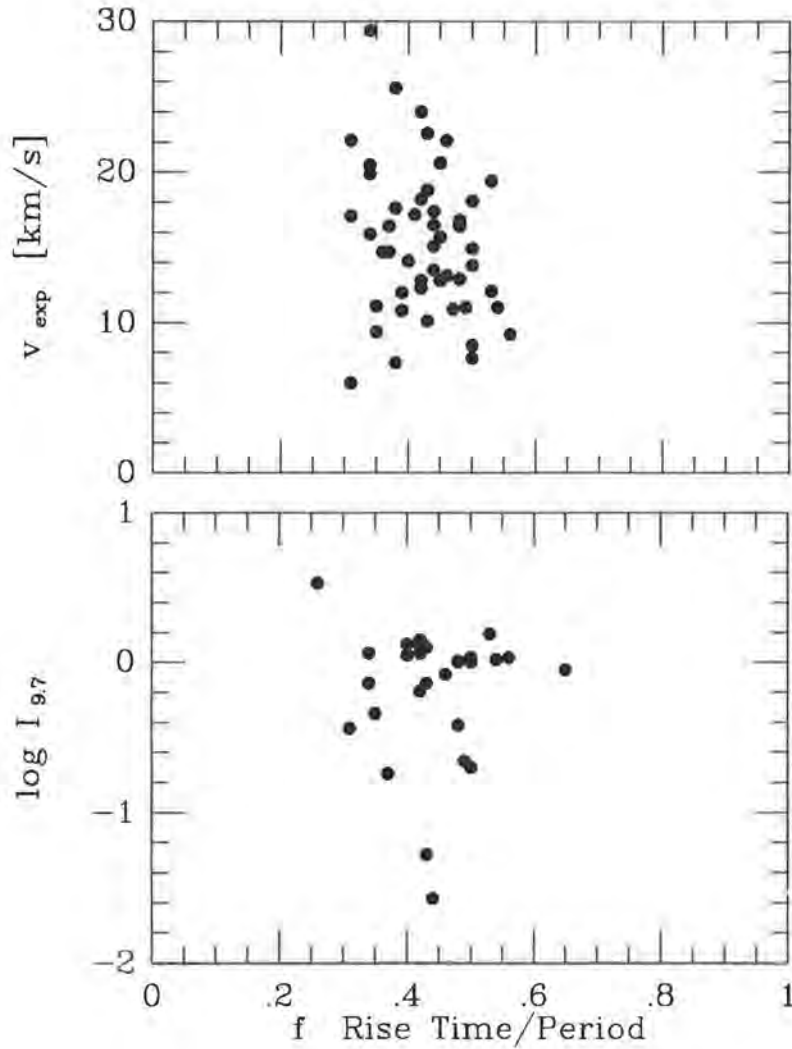
Figure 3: Upper - Expansion velocity versus f. Lower - log $I_{9.7}$ versus f.

unity. The data follow the same pattern as the model intensities which suggests that with increasing period the optical depth of the dust increases.

The combination of the results from Fig.1 and 2 indicates that LPVs with rather short periods are surrounded by an optically thin dust envelope expanding with a low velocity; the dust envelope around LPVs with longer periods is optically thick and expands with a higher velocity. It can be concluded that the pulsational period has a major impact on the dust formation in the circumstellar envelope.

Intensity of silicate feature and expansion velocity versus f (FIG.3)

The sample of stars for which f values were determined includes oxygen- and carbon-rich Mira variables and OH/IR stars. The f values are confined to a range between 0.2 and 0.7. In contrast to the previous relations no correlation of v_{exp} or $I_{9.7}$ with f has been found.

The main parameters that describe pulsation are the period and the amplitude. Whereas the period can be observed directly, the amplitude can only be traced indirectly

via an appropriate spectral feature. The f value can serve as such a tracer. The fact that no correlations between f and v_{exp} or $I_{9.7}$ are found is taken as an indication that similar pulsational amplitudes can lead to highly different characteristics of the circumstellar envelope.

INTERPRETATION WITHIN A NEW MODEL

In a recent study of the pulsational behaviour of long-period variables, these stars were modelled as a driven keplerian oscillator, i.e. the star consists of a pulsating core - 'interior' - which drives the surrounding stellar material - 'mantle' (Icke, Frank and Heske 1992). The calculations show that such a driven oscillator causes weak chaos. The most important parameters in the model are the mass, which determines the period, and the amplitude of the oscillation of the 'interior' and the 'mantle'. This model can account for observed characteristics of long-period variables, such as regular and irregular variability, increasing mass loss rates at the end of the evolution on the AGB. However, one of the main results is that stars with similar spectral features do not necessarily have to be in the same evolutionary phase nor have their stellar parameters to be similar (weak chaos). This led to the conclusion that stars which start out with only slightly different parameters can show very different variability and follow a completely different evolutionary path.

The presence, and absence, of correlations between stellar and circumstellar parameters support the results from those model calculations: The highly different circumstellar features for similar f values (Fig.3) and the step function in the v_{exp} - P plot (Fig.1). The result of increasing optical depth of the dust with increasing period (Fig.2) might also be understood with previous models which predict increasing mass loss as the star evolves. However, from the driven oscillator model it is clear that a sequence as in Fig.2 should not be directly translated into an evolutionary sequence. Stars which exhibit a similar intensity of the 9.7μm feature may have a similar mass rather than the same age.

3   Discs around Long-Period Variables?

A large fraction of planetary nebulae show a non spherically symmetric geometry (e.g. Icke, Preston and Balick 1989). The various shapes of these planetary nebulae can be modelled numerically by a fast low density wind running into the remnant circumstellar envelope with an asymmetric density distribution (Icke 1992). Such a non-spherically symmetric envelope must have been built up during evolutionary phases preceeding the planetary nebula stage, i.e. when stars are long-period variables. It would be expected that a similar fraction of these stars show aspherical mass loss.

The CO line offers an indirect method to detect asymmetric mass loss. At high spectral resolution, higher than 1 km/s, any deviation of the profile from the expected flat-topped, double-peaked or parabolic profiles would indicate a non-spherically symmetric geometry of the envelope.

One example is the CO(1-0) line observed in TX Psc, a carbon-rich semi-regular variable, a narrow peak is superimposed on a broad component (Heske 1989). The CO spectrum is reproduced in Fig.4. Follow-up mapping observations revealed extended CO emission over more than 40 arcsec in diameter (Heske, te Lintel Hekkert and Maloney 1989). The distribution of the integrated CO(1-0) line emission shows a feature which

TX Psc

0.5

0.

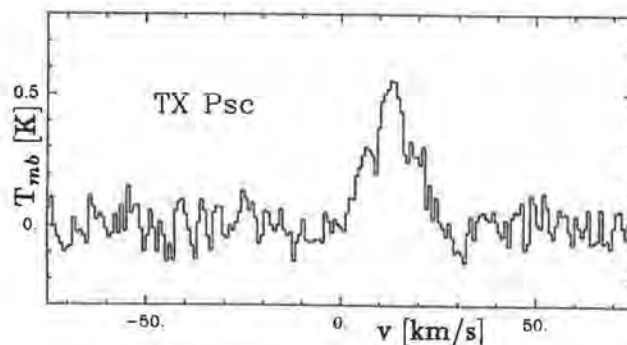T_{mb} [K]

-50.   0.   50.

v [km/s]

Figure 4: TX Psc - high resolution spectrum of CO(1-0).

would not be expected for the emission distribution from a spherically symmetric envelope (Fig.5, the contour units are K·km/s): The peak emission is elongated.

The first star where observational evidence for a non-spherically symmetric envelope has been detected was V Hya (Tsuji et al. 1988), like TX Psc a carbon-rich semi-regular variable. TX Psc is the second example of a LPV where an indication of an asymmetric circumstellar envelope has been found.

4 Conclusions and Outlook

The problem of non-spherically symmetric mass loss from Long-Period Variables is still rather unexplored on the observational side. To get more insight, new candidates for asymmetric circumstellar envelopes should be searched for and their spectral characteristics would have to be compared with those from LPVs with spherically symmetric envelopes. Such a comparison of stellar characteristics is expected to give hints of the origin of an asymmetric structure.

The difficulties in studying non-spherically symmetric envelopes around LPVs rise from the fact that these envelopes, in contrast to planetary nebulae, are still rather compact and asymmetry is less pronounced. To investigate the geometry of those envelopes mapping in the CO(1-0) and (2-1) lines with high spectral resolution and high signal-to-noise would be needed. However, this type of observation is very time consuming since CO lines from most stars are relatively weak.

With imaging at different infrared wavelengths the distribution of the dust in the envelope could be studied directly. Due to the strong contrast between stellar and circumstellar infrared emission from LPVs, detectors of a high dynamic range would be needed. ISO, the Infrared Space Observatory (see paper elsewhere in these proceedings), will offer this possibility.

On the theoretical side, the understanding of the structure of dynamical atmospheres and envelopes around Long-Period Variables has continuously been increased in the last few years. At this point, the results of recent models of stellar atmospheres and stellar pulsation as well as the correlations between stellar and circumstellar characteristics discussed in this paper point to the direction into which further steps should be taken: To
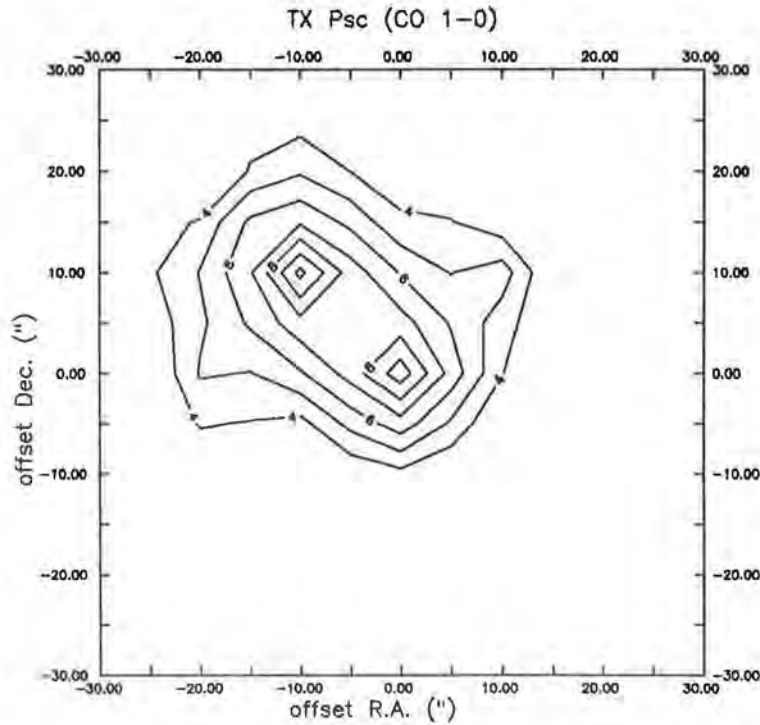
TX Psc (CO 1−0)

Figure 5: TX Psc - Contour map of the integrated CO(1-0) intensities.

reveal evolutionary paths of Long-Period Variables and to understand asymmetric mass loss, detailed models of *pulsating* stars and their evolution are needed.

References

CONFERENCE PROCEEDINGS

Cacciari, C., Clementini, G. (eds.) 1990 *"Confrontation between stellar pulsation and evolution"*, Astron.Soc.Pacific Conf. Series Vol.11

Menessier, M.O., Omont, A. (eds.) 1990 *"From Miras to Planetary Nebulae: Which path for stellar evolution?"*, Editions Frontières

Wallerstein, G. (ed.) 1990 *"Cool stars, stellar systems and the sun"*, Sixth Cambridge Workshop, Astron.Soc.Pacific Conf. Series Vol.9

INDIVIDUAL PAPERS

Deutsch, A. 1956, *Astrophys..J.* **123**, 210

Fleischer, A.J., Gauger, A., Sedlmayr,E. 1991 *Astron. Astrophys.* **242**, L1

Gail, H-P., Sedlmayr, E., 1986, *Astron. Astrophys.* **166**, 225

Gillet, D., Maurice, E., Baade, D. 1983, *Astron. Astrophys.* **128**, 384

Herman, J., Habing, H.J. 1985, *Reports on Progress in Physics*, ESTEC/ESA

Heske, A., te Lintel Hekkert, P., Maloney, P.R., 1989, *Astron. Astrophys.* **218**, L5

Heske, A. 1989 *Astron. Astrophys.* **229**, 494

Icke, V., Frank, A., Heske, A. 1992 *Astron. Astrophys.* **258**, 341

Icke, V. 1991 *Astron. Astrophys.* **251**, 369

Icke, V., Preston, H.L., Balick, B. 1989 *Astron. J.* **97**, 462

IRAS Science Team 1986, *Astron. Astrophys. Suppl. Ser.* **65**, 607

Knapp, G.R., Morris, M., 1985, *Astrophys.J.* **292**, 640

Kwok, S., 1975, *Astrophys.J.* **198**, 583

Mattei, J.A. 1983, *AAVSO Report* **38**, Cambridge, Mass.

Mitchell, R.M., Robinson, G. 1981, *Monthly. Not. Roy. Astr. Soc.* **196**, 801

Sivagnanam, P., Le Squeren, A.M., Foy, F., Tran Minh, F. 1989, *Astron. Astrophys.* **211**, 141

Tsuji, T., Unno, W., Kaifu, N., Izumiura, H., Ukita, N., Cho, S., Koyama, K. 1988 *Astrophys. J.* **327**, L23

Vardya, M.S., 1988, *Astron. Astrophys. Suppl.Ser.* **73**, 181

Willson, L.A., Bowen, G.W. 1986, in:*3rd Trieste workshop on relationship between chromospheric / coronal heating and mass loss*, (eds. R.Stalio, J.Zirker), p.127

DISKS AROUND EVOLVED STARS?
(BIPOLAR NEBULAE AND SN 1987A)

PHILIPP PODSIADLOWSKI
Institute of Astronomy, Cambridge CB3 0HA

ROBIN E. S. CLEGG
Royal Greenwich Observatory, Cambridge CB3 0EZ

ABSTRACT   We review the observational evidence for disk-like out-flows from evolved stars and discuss theoretical ideas for their origin. Disk-like structures are seen around AGB stars, bipolar proto-planetary nebulae, planetary nebulae and SN 1987A. Most of these structures are consistent with an equatorially enhanced radial outflow, but some show the signature of rotation, consistent with rotating disks. Theoretical models fall into two classes: single-star and binary models. Primordial disks, non-radial pulsations and magnetic fields are the main ingredient in the major single-star scenarios, while binary interaction can affect stellar outflows in at least three different ways (stellar merging, common-envelope ejection and gravitational wind interaction). We estimate that at least $\sim 35\%$ of all stellar outflows from evolved stars are affected by binary interaction.

1. INTRODUCTION

One of the main topics of this workshop are protostellar disks as they are commonly observed in star-forming regions. Their origin is easy to understand: a typical star-forming core has too much angular momentum to collapse directly into a protostar. Any matter that is accreted onto the protostar therefore first has to pass through a disk where its excess angular momentum can be dispersed by viscous processes. For evolved stars, the situation is completely different. Since during its evolution, a star continues to lose angular momentum by various processes (most of the angular-momentum loss already occurs in the pre-main-sequence phase), any evolved, single star will be a slow rotator. It would therefore be surprising to find disk-like structures around evolved stars (unless such structures are remnants of protostellar disks). Nevertheless, there is ample observational evidence that just such disk-like structures exist.

Some of the evidence is quite indirect and, in some cases, other interpretations are possible. This review has two purposes. The first is to summarize the observational evidence for disk-like structures around evolved stars and the second to systematically discuss the various ideas that have been advanced to explain them. One of the main question we want to address is whether such disks are the result of some intrinsic property of single stars (like rotation, pulsations or magnetic fields) or whether they require an external agent in the form of a companion star.

2. OBSERVATIONAL EVIDENCE FOR DISKS

Throughout this paper, we will use the term "disk" rather loosely. Unlike protostellar disks, the disk-like structures around evolved stars are not necessarily Keplerian disks. In most cases, the observational evidence is consistent with radial outflows which are strongly enhanced in the equatorial direction. (An equatorial outflow is kinematically fundamentally different from Keplerian rotation.) On the other hand, there are some systems which show the kinematical signature of rotation.

Most of the evidence for disks around evolved stars comes from systems that have already evolved beyond the asymptotic giant branch (AGB) and are either in the planetary nebula stage or in the transition to it. We have grouped the evidence for disks in five classes and present them in a sequence of evolutionary order. We start with disks around AGB stars, followed by disks around proto-planetary nebulae and disks around different types of planetary nebulae. The final class, containing the nebula around SN 1987A as its single member, does not fall into this order, but may nevertheless be an instructive example for this phenomenon. (For related reviews, see Morris 1990; Olofsson 1992.)

2.1 Disks around AGB stars

The evidence for disk-like structures around AGB stars is rather sparse, since their circumstellar envelopes (CEs) can rarely be resolved spatially. In the cases where the geometry of CEs can be resolved, it is usually consistent with spherical symmetry. Maser maps (based on H_2O, SiO or OH maser emission) occasionally show a ring-like or elongated geometry for the emission region

(e.g., W Hya [Reid and Menten 1990]; R Aql [Lane et al. 1987]; OH26.5+0.6 [Bowers and Johnston 1990]), but in most cases are consistent with a spherical geometry (Olofsson 1992).

A noticeable exception is the late-type carbon star IRC +10216 (= CW Leonis), which is a strong and extended, nearby IR source. Its large, intrinsic polarization already suggests that the observed light is scattered light from a CE and that the central star is obscured by an opaque disk (Serkowski 1972). This picture has been largely confirmed by infrared (IR) Michelson interferometry (McCarthy et al. 1980) and speckle interferometry (Dyck et al. 1987). The IR image is highly flattened at $2.2-5\,\mu$m with an aspect ratio between the major and minor axis of about 2. On the other hand, at $10.3\,\mu$m the image is almost circular; it shows only a small asymmetry ($\sim 10-20\,\%$) with a major axis perpendicular to the the major axis at shorter wavelengths. A plausible model for IRC +10216 can be constructed, in which the $2.2\,\mu$m emission is scattered light from two bipolar lobes, while the $10.3\,\mu$m emission is thermal radiation from an equatorial disk seen at relatively high inclination (Dyck et al. 1987). In this model, IRC +10216 would be a likely progenitor for a bipolar planetary nebula.

The M3–5 supergiant VY Canis Majoris also shows strong evidence for a circumstellar disk around an evolved star (note that VY CMa has occasionally been considered a protostar because of its proximity to a star-forming region; e.g., Herbig 1970). Interferometry maps (McCarthy 1979) and OH maser maps (Moran et al. 1977) show an elongated geometry for the CE which is consistent with a circumstellar disk.

The carbon star V Hydrae is a particularly interesting object. A CO radio map (Kahane et al. 1988) shows a bipolar geometry for the CE. In addition, the optical photospheric spectrum suggests that V Hya is rotating with $v\sin i$ between 10 and 20 km s^{-1}. This implies that V Hya is rotating close to break-up. However, since such a star would have been broken up on the main sequence, this system can only be understood if V Hya has or had a binary companion which provided a source of angular momentum and helped to spin it up (see Sec. 5.1, 5.5). V Hya may therefore provide direct evidence for a possible link between rapid rotation of the central star (induced by a binary companion) and anisotropic outflows.

2.2 Bipolar Proto-Planetary Nebulae

Bipolar proto-planetary nebulae (PPN) constitute a relatively well defined class of objects which show evidence for non-spherical outflows (see, e.g., Morris 1987). They are believed to be transition objects between the AGB and the planetary nebula (PN) phase. In comparison to their probable descendants, bipolar PNe, they are relatively rare. This suggests that the lifetime of the PPN phase is relatively short ($\sim$ few 10^3 yr). PPNe generally are reflection nebulae; their central stars appear to be hidden by disk-like structures. The inferred spectral types of these central stars vary from O to M.

An excellent representative of this class is the PPN CRL 2688 ("Egg Nebula"). In the optical, it is a strongly bipolar reflection nebula consisting of two egg-shaped lobes separated by a dark lane (Ney et al. 1975). The inferred spectral type of the hidden central star lies between F2I and F5I (Crampton et al. 1975; Cohen and Kuhi 1977). The chemical composition of the envelope resembles that of a carbon star (see the references in Bieging and Nguyen-Quang-Rieu 1988). The obscuring dark lane has been mapped in HCN by Bieging and Nguyen-Quang-Rieu (1988). The HCN emission is strongly centrally concentrated, but shows faint extensions along the dark lane. No HCN emission is seen from the reflection nebula. This morphology suggests a toroidal density distribution for the HCN emitting gas. The velocity field, as measured in HCN, supports this picture. Its most important feature is a velocity gradient of 2 km/s along the dark lane. The most straightforward interpretation of this velocity gradient is that it is caused by a rotating circumstellar disk. The inferred specific angular momentum, J/M, is $\sim 7 \times 10^{21}$ cm^2 s^{-1}, which corresponds to a minimum (Keplerian) disk size of ~ 100 AU (see Sec. 5.3). Thus CRL 2688 may provide strong evidence for a rotating circumstellar disk.

The OH/IR star OH231.8+4.2 ("Rotten Egg" or "Kalabash Nebula") provides another interesting example of this class. It is surrounded by a narrow IR bipolar nebula with Herbig-Haro-like objects. The inferred spectral type of the central star, which is hidden within an equatorial dust disk, is M9 III (Cohen 1981; Morris 1981). The outflow velocity (as determined from OH maser emission) increases from ~ 10 km s^{-1} in the equatorial plane to ~ 200 km s^{-1} in the polar direction (Bowers 1991). The large polar velocity and the narrow collimation of the outflow (Reipurth 1987) can only be understood, if the central system is a binary consisting of a red giant and a more compact

companion which provides the source of the fast outflow (see Morris 1987 and Sec. 5.3). The presence of a blue companion star is also indicated by an excess in the blue continuum from the reflection nebula (Cohen et al. 1985). Because of its probable binary nature, OH231.8+4.2 may provide an important link between evolved binaries (in particular symbiotic binaries like R Aqr [Solf and Ulrich 1985]) and bipolar PNe.

The IR source IRAS 09371+1212 resembles OH231.8+4.2 in many respects. Because of its strong ice feature, it is also known as the "Frosty Leo Nebula" (Forveille et al. 1987; Rouan et al. 1988). Unlike OH231.8+4.2, the bipolar lobes are not collimated, but consist of the two hemispheres of a single spherical envelope which are separated by a sharply defined dark lane. Thus, IRAS 09371+1212 provides particularly good evidence for a disk-like structure around a bipolar PPN, which in this case must be seen almost edge-on.

2.3 Butterfly Planetary Nebulae

"Bow-tie" or "butterfly" planetary nebulae are presumably the descendants of bipolar PPNe. They form a distinct class of PNe (see Sec. 3), comprising $\sim 10 - 20\%$ of all PNe. A large fraction of butterfly PNe are chemically classified as type I PNe (Peimbert 1978), i.e., as helium- and nitrogen-rich PNe. Their geometry is strongly bipolar and has the appearance of an hourglass, where the ionized gas is constrained at the waist by a disk of cool material. Significant effort has been spent on imaging this cool and largely neutral component (Rodríguez 1989). It has been detected in a number of objects as thermal CO emission, shock-excited H_2 emission, OH maser line emission or as 21-cm HI emission.

A prime example of this class is NGC 2346 (for other examples, see, e.g., Icke et al. 1989). It has been classified as a "middle butterfly PN" (in Balick's [1987] classification scheme; see Sec. 3). In Hα and [NII], the central region has the appearance of a tilted ring. A molecular envelope has been detected both in CO (Healy and Huggins 1988) and H_2 (Zuckerman and Gatley 1988). The geometry of the CO emission is oblate with a major axis perpendicular to the bipolar axis. The H_2 emission lies outside and closely traces the ionized gas of the PN. It is peaked near the waist of the butterfly nebula. This strongly supports the picture in which the expanding PN shell is obstructed by a disk of material in the equatorial plane (also see Meaburn et al. 1985) and where

the H_2 emission is excited by the shock interaction of the PN shell with the circumstellar envelope, in particular the equatorial disk. Interestingly, the central star of NGC 2346 is a main-sequence A star, which presumably is the companion of the undetected, hot component which ionizes the nebula. Thus, at least in the case of NGC 2346, the butterfly geometry may be directly connected with the binary nature of the progenitor system (a point we will return to again in Sec. 5).

2.4 Elliptical Planetary Nebulae

Elliptical PNe are a second, more common class of PNe which show evidence for non-spherical envelopes. The molecular envelopes (as seen, for example in CO) often have a toroidal (disk-like?) geometry. It is generally believed that this neutral gas torus constrains the expansion of the HII region in the equatorial plane. This leads to a collimation of the flow and explains the larger velocities in the polar direction commonly observed in elliptical PNe (see, e.g., Balick et al. 1987). Emission peaks in the ionized component along a PN's minor axis provide direct evidence for a constraining torus, since the shock-excited emission should be strongest along the direction of maximum impediment.

A typical example of an elliptical PN is NGC 7027. The emission from the ionized component shows strong emission peaks along the nebula's minor axis (Masson 1989). A molecular envelope (as seen in CO [Bieging et al. 1991]) encloses the ionized portion of the nebula. The CO emission is very clumpy, which suggests that the AGB mass loss was neither spherically symmetric nor uniform in time. The overall geometry of the molecular envelope is axisymmetric and is aligned with the symmetry axis of the ionized component. The inner part of the envelope, just outside the HII region, has the geometry of a torus, although not necessarily the geometry of a disk.

NGC 3132 represents another interesting example. The H_2 emission of the elliptical shell of the PN is strongly peaked along the minor axis (Storey 1984), which again suggests the presence of a toroidal envelope constraining the nebula in the equatorial plane. This toroidal envelope has been mapped in CO by Sahai et al. (1990). Most interestingly, the velocity distribution of the CO emission has a velocity gradient of 5 km s^{-1} along the plane of the inferred torus. Just as in the case of CRL 2688 (Sec. 2.2), this may be interpreted as

the signature of rotation. However, the specific angular momentum of matter in the torus ($J/M \sim 7 \times 10^{22}$ cm^2 s^{-1} [Sahai et al. 1990]) would in this case be uncomfortably large and imply a minimum (Keplerian) disk size of 0.05 pc (see Sec. 5.3).

2.5 The Bipolar Nebula around SN 1987A

SN 1987A is surrounded by a complex, but well-structured nebula which is now glowing in recombination radiation (excited by the supernova UV flash). Since the whole nebula was ejected in the final stages of the evolution of the presupernova system, it provides a direct imprint of the late evolution of the progenitor. The nebula consists of three main components. A ring of material ($\sim$ 1.6 lt. yr across) makes up the central portion of the nebula (Wampler et al. 1990; Jacobson et al. 1991). Two elliptical loops protrude from the northern and the southern portion of the ring, and the northern part of the nebula is bounded by a structure that has the appearance of Napoleon's hat (Wampler et al. 1990). The whole nebula is strongly axisymmetric and all parts share a common axis of symmetry. The ring and the elliptical loops resemble some bipolar PNe, and several attempts to model this nebula based on an interacting-wind model (Sec. 3) have been published (Luo and McCray 1991; Wang and Mazzali 1992; Lundqvist 1992). The ring could be the product of an equatorial outflow (excretion disk?) which was swept up by the energetic wind in the supernova progenitor's final blue-supergiant phase (Podsiadlowski 1991). Detailed hydrodynamical models (e.g., Lundqvist 1992) also require a disk-like structure for the mass loss from the progenitor in its red-supergiant phase. Thus, the ring around SN 1987A may provide the best evidence to date for a disk-like structure around an evolved star. The physical reason for this mass-loss asymmetry is not yet clear. However, the ring and several other anomalies may suggest that the progenitor system was a binary, either at the time of the explosion or at least in the not-too-distant past (Podsiadlowski 1992).

3. THE SHAPING OF PLANETARY NEBULAE

Before we review the theoretical ideas to explain non-spherical mass loss from evolved stars, it is worth while to make a small excursion and discuss the shap-

ing of PNe. A very successful to account for the variety of observed shapes has been the interacting wind model developed mainly by Kwok and his collaborators (e.g., Kwok et al. 1978; Volk and Kwok 1985; and also Pikel'ner 1968, 1973; Kahn and West 1985). In this model, the PN shell is produced by the interaction of two winds. The first wind is the cool, slow wind emitted by the nebula's AGB progenitor. It has a typical mass-loss rate $\dot{M} \sim 10^{-5} M_\odot$ yr^{-1} and a wind velocity $v \sim 10$ km s^{-1}. After the AGB star has lost all (or almost all) of its envelope, the central degenerate-dwarf core is exposed and a hot wind starts to emanate from this hot core (with $\dot{M} \sim 10^{-7}$–$10^{-8} M_\odot$ yr^{-1} and $v \sim 10^3$ km s^{-1}). This fast wind will now snowplow into the earlier slow wind and sweep it up into the bright shell which produces the spectacular display of a planetary nebula. The model requires an additional ingredient, since most planetary nebulae are axisymmetric, but very non-spherical ($\sim 20\%$ are spherical, $\sim 30\%$ are elliptical, $\sim 30\%$ are bipolar, and $\sim 20\%$ are butterfly). It is probably the density contrast (i.e., the ratio of the density in the equatorial plane to the density in the polar direction) in the slow AGB wind that determines the final geometry of the PN. This is the basis of the empirical classification scheme by Balick (1987). It has two classification parameters: the first is the initial density contrast in the AGB wind (no, mild or strong) which determines the morphological class of the PN (spherical, elliptical or butterfly), and the second is the evolutionary stage of the PN (early, middle or late). The majority of all PNe can be well classified by this scheme. An important theoretical issue is the relation between the density contrast and the resulting morphological class. The studies by Balick et al. (1987) and Icke et al. (1989), largely confirmed by the fully hydrodynamical calculations by Soker and Livio (1989), show that a spherical PN results from a density contrast ~ 1, an elliptical PN from a density contrast ~ 2 and a butterfly PN from a density contrast ~ 10 ($\gtrsim 5$). Icke et al. (1989) emphasize that a continuous variation of the density contrast can produce most observed PN morphologies. While this has been a great success for the interacting-wind model, the model does not and cannot explain the origin of the large density contrasts which are responsible for elliptical and butterfly PNe. In particular, the large density contrast required to produce butterfly PNe suggests that the AGB mass loss resembles more an equatorial (disk-like?) outflow than an oblate wind. The physical mechanism(s) that could explain these large density contrasts will be

the subject of the remainder of this review.

4. SINGLE-STAR SCENARIOS

Can a single AGB star produce a disk-like outflow? AGB envelopes are only loosely bound, and we should expect that every AGB wind will be spatially anisotropic and varying in time (as is often observed). However, to produce a disk-like outflow, one requires a mass-loss mechanism that has a well-defined symmetry axis. Several such mechanisms have been proposed, and we will now discuss them in turn.

4.1 Primordial Disks?

Perhaps the simplest model to explain the observed disk-like structures is that they are relics of protostellar disks (Matese et al. 1989; Pringle 1989). Such a model has to overcome several problems. One is that such disks are not observed around main-sequence stars (apart from Vega-like disks which contain very little [observable] mass). In addition, the composition of the observed disk-like outflows frequently shows the signature of nuclear processing, which implies that at least part of the material must have undergone nuclear processing in the star and been ejected subsequently. Matese et al. (1989) solve these problems by suggesting that the protostellar disk material condenses out into comets, which are practically invisible (except for their possible role in replenishing the dust grains in Vega-like disks). As the central star evolves up the giant and asymptotic-giant branch, these comets start to sublimate because of the increasing central luminosity and associated flux temperature, injecting visible dust grains into a circumstellar disk. In addition, these dust grains can now act as nucleation cores for the condensation of dust grains out of the (asymptotic) giant wind, which contains nuclear-processed material. Even though the stellar wind may be perfectly spherically symmetric, the dust production will thus be strongly amplified in the comet plane. This model could potentially explain many of the apparent disk-like structures discussed in Sec. 2. However, in order to be dynamically important and to affect the shaping of strongly bipolar PNe, the disk mass has to be comparable to the mass in the PN shell (at least several tenths of a $M_\odot$). Such large disk masses are not inconsistent with the masses inferred for protostellar disks, but

may be increasingly difficult to hide around ordinary stars. On the other hand, the discovery of such massive comet disks would lend credence to this general idea.

4.2 Rapid Rotation?

Rapid rotation of the wind-emitting star is another mechanism that could produce an equatorially enhanced outflow (e.g., Calvert and Peimbert 1983). However, for rotation to be dynamically important, the surface rotation velocity has to be a significant fraction of the star's break-up velocity (e.g., Poe and Friend 1986). This is not possible for a single evolved star. Even if the star was a rapid rotator on the main sequence, it could only be a slow rotator in a subsequent giant phase (if the star's specific angular momentum remains constant, the ratio of its surface velocity to the break-up velocity decreases approximately as $\sim R^{-1/2}$, where R is the stellar radius). In addition, a star's specific angular momentum tends to decrease during its evolution because of efficient magnetic braking, which stars are likely to encounter during various evolutionary phases. Thus, rotation cannot be important for producing disk-like outflows unless there is a source of angular momentum. A binary companion could provide such a source, since mass transfer or tidal locking can provide a means by which orbital angular momentum is converted into spin angular momentum (see Sec. 5.1).

4.3 Non-Radial Pulsations

Non-radial pulsations may also be able to produce non-spherical winds, provided that cool giant winds are driven by acoustic modes (e.g., Pijpers and Habing 1989). Such a model still requires a source for the asymmetry. Pijpers (1992) has suggested that evolved stars could have rapidly rotating cores which may drive axisymmetric acoustic modes into the overlying envelopes and ultimately lead to equatorially enhanced outflows. He is presently investigating whether the propagation of non-radial modes through a spherical envelope leads to an enhancement or a diminution of the asymmetry. We will have to wait for these results, before we will be able to assess the importance of this scenario.

4.4 Magnetic Fields

Magnetic fields are another important factor that can affect the geometry of stellar winds (Pascoli 1992). To be dynamically important, the wind Alfvén velocity has to be of the order of the break-up velocity. For a typical AGB star, this means that the surface magnetic field has to be of order a few Gauß. Such values may not be unreasonable, since much larger magnetic fields have been inferred from observations of masers around several AGB stars (Barvainis et al. 1987; Cohen 1992). However, it is not entirely clear how representative these maser magnetic field strengths are for the whole wind-driving region. In any case, a strong stellar dynamo is required to generate a magnetic field of $\sim 1\,\mathrm{G}$. Pascoli (1992) suggests that this dynamo is situated near the bottom of the convective envelope of the AGB star (with a magnetic field $B \sim 2 \times 10^3\,\mathrm{G}$ at a distance $r \sim 10^{11}\,\mathrm{cm}$) from the center. This dynamo generates toroidal bubbles (not in equilibrium with the ambient medium) which start to rise. As the bubbles float to the surface, their magnetic field decreases as r^{-1}. When they encounter the steep density gradient near the surface (in a transition zone), they rapidly expand and drive a disk-like, magnetized wind.

This model leaves several questions open. One is the question of the origin of the strong dynamo. In addition, even if such a dynamo exists, how will such a system avoid magnetic braking, which here should be very efficient and rapidly slow down the star, until the dynamo is too weak to affect the outflow? Just as in the case of rotation, it seems that the model requires a source of angular momentum (which a dynamo converts into magnetic energy). Again a binary companion could be the solution. RS CVn binaries provide an excellent example for binary-induced magnetic activity (e.g., Rodonò 1992). In these systems, the primary subgiant is tidally locked to the orbit, and the magnetic activity is presumably caused by tidally induced dynamo action.

5. BINARY SCENARIOS

Since the vast majority of all stars are believed to be members of binary systems (e.g., Abt and Levy 1976, 1978; Kraicheva et al. 1978, 1979; Duquennoy and Mayor 1991) and since binary interaction can affect stellar mass loss in a variety of ways, it seems only natural that the non-spherical structures frequently seen around evolved stars could be connected with binary evolution

(e.g., Paczyński 1985; Iben, 1989; Eggleton 1990). On the other hand, Zuckerman and Aller (1986) and Zuckerman and Gatley (1988) have argued that duplicity is generally not important for the shaping of PNe. Their conclusion is based on two main arguments. The first is that only a minority of PNe ($\sim 20\%$) can be classified as circular PNe. The majority is either bipolar ($\sim 50\%$) or elliptical ($\sim 30\%$). However, binaries which are sufficiently close to affect the mass loss from AGB stars are not common enough to account for 80 % of all systems. Since therefore not all asymmetrical PNe can be the result of binary interaction, Zuckerman and Aller (1986) conclude that duplicity may not play an important role in general. The second argument is that strongly bipolar PNe (in particular, butterfly nebulae) tend to be found at lower galactic latitude than the average PN (Zuckerman and Gatley 1988). This suggests that they are connected with a massive-star population rather than with a binary population.

We do not think that these arguments are cogent. In fact, the second argument appears to be a *non sequitur*. Even if butterfly PNe were connected with more massive stars — the evidence is actually not very strong — this would not rule out the possibility that they are all binaries; they may just be *massive binaries*. The first argument, while stronger, is also not without counter-arguments. The most extreme view is represented by Paczyński (1985) who has argued that duplicity may be a prerequisite for the PN phenomenon and that all PNe are the product of binary evolution. This hypothesis is probably too extreme. Nevertheless, one should remember that a large fraction of all stars are found in relatively close binaries and that mass loss rates are often found to be enhanced in interacting binaries. As a consequence, PNe in binaries may be more conspicuous. This may introduce an important selection effect, although it will be difficult to assess quantitatively. One can also reverse the argument. Since we know that close binaries are common and since most types of binary interaction tend to generate axisymmetric flows, we should expect that duplicity plays an important role in the shaping of at least some PNe (also note that bipolar outflows are often observed around interacting binaries; see, e.g., Solf 1984).

The truth probably lies somewhere between these extremes. A binary mechanism may only be required for PNe that need extremely large density contrasts in their AGB outflows. Perhaps all butterfly PNe ($\sim 10-20\%$) and

most other bipolar PNe ($\sim 30\%$) have close-binary progenitors, while the majority of elliptical and all circular PNe have single or wide-binary progenitors.

In the following, we will discuss systematically how binary interaction can affect the outflows from evolved stars and, in Section 6 we will return to the question of binary- versus single-star scenarios.

5.1 Rapid Rotation

In Sec. 4.2 we concluded that an evolved star can only be rotating rapidly, if there is a source of angular momentum. A binary companion can provide such a source, provided that orbital angular momentum can be converted into spin angular momentum. Tidal locking and mass transfer provide two possible conversion mechanisms.

The rotation of any star that is close to filling its Roche lobe will be tidally locked to the orbit, i.e., the star's rotation period will be synchronous with the orbital period (provided that the binary mass ratio, $q \equiv M_2/M_1$ is larger than ~ 0.2; Sparks and Stecher 1974). We can write the ratio of the rotation velocity, $v_{\rm rot}$, to the break-up velocity, $v_{\rm break}$, of a tidally locked star as

$$\frac{v_{\rm rot}}{v_{\rm break}} = (1 + q)^{\frac{1}{2}} \left(\frac{R_1}{a}\right)^{\frac{3}{2}},$$

where R_1 is the radius of the tidally locked star (star 1) and a is the binary separation. For a star that almost fills its Roche lobe, this ratio varies from 0.33 (for $q = 1$) to 0.41 (for $q = 0.2$). Thus, any tidally locked star that is close to filling its Roche lobe will rotate at a significant fraction of its break-up velocity. Since, in addition, its mass-loss rate is likely to be significantly enhanced compared to that of a single, non-rotating star (e.g., Tout and Eggleton 1988), this effect alone may be able to produce strong, equatorially enhanced outflows.

Mass accretion can also produce a rapidly rotating star, since a star has to accrete only a few % of its own mass to accrete enough angular momentum to be spun up to break-up velocity (e.g., Packet 1981). However, in order to produce a rapidly rotating *evolved* star by accretion, the accreting star already has to be a giant, when mass transfer begins. This requires somewhat special conditions for the possible binary parameters (the masses have to be very close and the orbital period relatively long and in a narrow range). Therefore, accretion can only be important in a small fraction of all systems (perhaps in a few %).

81

5.2 Gravitational Focusing

The presence of a companion star will also affect any wind emanating from an evolved primary, because it provides an attractive force to gravitationally focus the wind even if the wind is spherically symmetric in the primary's reference frame (Fabian and Hansen 1979; Morris 1981; Kolesnik and Pilyugin 1986; Pilyugin 1987). The various proposed scenarios differ significantly in their assumptions, and none of them can be considered fully realistic.

For example, Morris (1981) argues that the primary is not in synchronous rotation with the orbit (in order to avoid that material that is focused by the companion is accreted by the companion). In this case, a typical gas stream from the primary that is deflected by the companion towards the orbital plane may hit an opposing gas stream when it reaches the midplane, producing a strong shock in the orbital plane and losing all of its vertical momentum. The result of this interaction is disk-like outflow from the system.

On the other hand, Kolesnik and Pilyugin (1986) assume that the primary is rotating synchronously and that all the material that comes within a Bondi-Hoyle radius of the companion is accreted by the companion. Thus, in this model, the density is diminished (!) in the equatorial plane. In fact, Kolesnik and Pilyugin (1986) conclude that, when the wind ejection velocity is much less than the binary orbital velocity, all of the matter ejected in the equatorial plane is accreted by the companion, and that there is no outflow in the equatorial plane at all. Such a model does not seem to be consistent with the evidence for disk-like structure around evolved stars and PNe discussed in Sec. 2.

Finally, Pilyugin (1987) considers the competing effects of accretion by the secondary and rotation of the primary (see Sec. 5.1) and finds that the outflows can either be equatorially enhanced or diminished.

5.3 The Circumbinary Disk Model

The simple binary models above cannot account for all the features of all PPNe and PNe. For example, they cannot explain the large velocities observed in the bipolar flows of some PPNe (e.g., OH 231.8+4.2; Sec. 2.2) and the large rotation rates inferred for some circumstellar outflows (e.g. CRL 2688 [Sec. 2.2]; NGC 3132 [Sec. 2.4]). The latter can best be seen by determining the equivalent Keplerian disk radius implied by the inferred specific angular

momentum for these disk-like structures. The specific angular momentum, J/M, can be directly related to a Keplerian disk radius, R_{Kep}, by the relation

$$\frac{J}{M} \simeq 2\pi \sqrt{G \, M_s \, R_{\text{Kep}}},$$

where G is the gravitational constant and M_s the mass of the system. Adopting a characteristic system mass $M_s \simeq 5 \, M_\odot$, one finds a Keplerian disk radius of $\sim 100 \, \text{AU}$ for CRL 2688 (with $J/M \sim 7 \times 10^{21} \, \text{cm}^2 \, \text{s}^{-1}$) and $\sim 10,000 \, \text{AU}$ for NGC 3132 (with $J/M \sim 7 \times 10^{22} \, \text{cm}^2 \, \text{s}^{-1}$). This means that the mass outflow must be rotating with the local Keplerian velocity up to this radius (as, for example, in an excretion disk of this size). The simple gravitational focusing model is not consistent with such a large disk radius, since the gravitational effects become negligible within a few binary separations (at larger distances, material is freely streaming and the specific angular momentum is conserved).

These considerations among others led Morris (1987) to modify his original binary model, mainly by also including the effects of accretion onto the secondary. If the accreted material has too much angular momentum to fall directly onto the secondary, an accretion disk will form. This disk will grow by viscous processes and will eventually, when the disks grows beyond the secondary's Roche lobe, form an excretion disk surrounding the whole binary. As the disk grows, it intercepts an increasing fraction of the mass lost from the wind and may, according to Morris, grow to very large size. Thus, this model may be able to explain the large inferred rotation rate seen in the outflow from CRL 2688, although it may have difficulties in accounting for the much larger rotation rate inferred for the outflow from NGC 3132. In addition, Morris hypothesizes that the accretion disk around the secondary could be the source of an energetic bipolar wind. It seems that such a model is ideally suited to explain the bipolar PPN OH 231.8+4.2 (Sec. 2.2). OH 231.8+4.2 may therefore provide strong support for this scenario.

5.4 Common-Envelope Models

In all binary models discussed so far, the binary was either detached or semi-detached. However, binary interaction can affect the stellar outflows in much more dramatic ways. The most dramatic is by common-envelope evolution.

When a star with a deep convective envelope (e.g., all giants) fills its Roche lobe, mass transfer is generally dynamically unstable, if the mass of

the primary exceeds a large fraction ($\sim 0.7-1$) of the mass of the secondary (Paczyński 1970). The reason is that the radius of the Roche lobe usually shrinks when mass is transferred from the more massive to the less massive component, while the radius of a star with a deep convective envelope tends to increase when mass is taken off adiabatically. Thus, a Roche-lobe-filling giant will overfill its Roche lobe by an increasingly larger amount, which is inherently unstable and leads to a mass-loss runaway. On the other hand, the companion star cannot accrete at the same rate at which mass is transferred. The excess material will pile up on top of the secondary, and the secondary itself will grow to giant dimensions and soon fill its own Roche lobe. Beyond this point, all mass lost from the primary will flow into a common envelope which surrounds both binary components (Paczyński 1976). The common envelope consists mainly out of the material of the giant's envelope. Immersed in it are the core of the giant and the more-or-less unaffected companion star, orbiting about the common center of mass. However, the orbiting binary core experiences dynamical friction and frictional drag because of its motion relative to the common envelope and the two binary components start to spiral towards each other (on a characteristic timescale of $10^3 - 10^4$ yr). A large fraction ($\sim 1/3$ [Livio and Soker 1988]) of the orbital energy released by the spiral-in process is deposited in the envelope and, in effect, heats the envelope. There are now two possibilities. The first is that the orbital energy deposited in the envelope exceeds the envelope's binding energy. In this case, the envelope will be ejected, producing a bright PN display and leaving behind a very compact binary nucleus. The second possibility is that the energy deposited in the envelope is not sufficient to unbind the envelope. In this case, the immersed secondary will at some point fill its own Roche lobe and will start to be dissipated/disrupted. As a result, the secondary will be completely dissolved and, in the end, the system will have coalesced completely into a single star. This merged system has some highly unusual properties. It will be a rapidly rotating giant (see Sec. 5.5), and the composition of the envelope may show chemical anomalies, since it is likely that the envelope will be completely mixed with material that has undergone some nuclear processing. Common-envelope ejection should generally occur in initially wide binaries (because of the smaller binding energy of the common envelope), while complete coalescence should occur in initially relatively close binaries (because of the larger

envelope binding energy). For typical binary distributions, coalescence should be more frequent than common-envelope ejection.

We would expect that any outflow from a common-envelope system will be axisymmetric and highly non-spherical. Since the envelope itself is rotating with near break-up velocity, any wind from the system will not only be enhanced, but also concentrated towards the equatorial plane (e.g., Bodenheimer and Taam 1984; Livio and Soker 1988). However, the details of the common-envelope phase are not well understood theoretically, and different authors have emphasized different mass-loss mechanisms. Livio et al. (1979) argue that, during the early common-envelope phase when the envelope is still co-rotating with the immersed binary, the envelope fills the critical surface through the outer Lagrangian point, L2. This leads to a low-velocity outflow through L2 and the formation of a ring around the system, which will subsequently diffuse out into an excretion disk. Later on, when the binary core is orbiting relative to the envelope, the spiraling-in binary is likely to strongly perturb the surrounding envelope, for example, by inducing a powerful magnetic dynamo (Bieging and Nguyen-Quang-Rieu 1988) or exciting non-radial pressure modes (Soker 1992a). In the first case, this may lead to a strong, magnetically coupled outflow (perhaps necessary to explain systems like CRL 2688 [Bieging and Nguyen-Quang-Rieu 1988]) and, in the second case, to an additionally enhanced equatorial mass loss. Finally, the strong deformation of the common envelope, when its mass has decreased to less than $\lesssim 10^{-3} \, M_\odot$, may lead to a collimation of the mass loss along the rotation axis and produce the fast jets seen or inferred in several PNe (Soker 1992b).

On the observational side, Bond and Livio (1990) conclude that $\sim 15\,\%$ of all PNe have close-binary cores (with periods less than a few days), confirming that common-envelope ejection leads to the formation of a significant fraction of all PNe. The real fraction could even be much higher, since it is extremely difficult to detect binary cores with periods of weeks to months (Bond and Livio 1990). The morphologies of most PNe are either butterfly/elliptical or peculiar (i.e., do not fall in any well-defined class). This is consistent with the above theoretical picture (Bond and Livio 1990). A notable exception is Sp 1 which is perfectly round. Bond and Livio (1990) have suggested that this could be a toroidal PN seen almost pole-on.

5.5 The Merger Model

In the discussion of common-envelope evolution in Sec. 5.4, we mentioned that one of its likely outcomes is the complete coalescence of the two stars. This provides another mechanism to produce non-spherical outflows from evolved stars. Even though this channel has received fairly little attention in the past (e.g., Bond and Livio 1990; Eggleton 1990), it may in fact be one of the most common. As noted above, the merged system will be a single star that is rotating near break-up. Thus, immediately after coalescence, we expect the stellar wind to be strongly enhanced and directed preferentially in the equatorial plane — just as desired. However, magnetic braking by a magnetically coupled wind, carrying away spin angular momentum, is also likely to be important in this phase and will slow down the star efficiently. If this effect is combined with the evolutionary expansion of the star, we suspect that the star will eventually become a slowly rotating giant again. Except for possible chemical anomalies, it will then look like an ordinary single giant, but it may still be surrounded by a disk of previously ejected material. FK Comae stars are rapidly rotating giants (Bopp and Stencel 1981) and are believed to be merged binaries. V Hya (see Kahane et al. 1988 and Sec. 2.1) may be an excellent example of a very evolved merged system, although one can probably not rule out that it still has a close binary companion.

6. CONCLUSIONS

To conclude the review, let us now return to the question of how important binary interactions are for producing disk-like outflows around evolved stars and, in particular, for the shaping of PNe. In the previous section, we showed that there are three different evolutionary channels which are all expected to produce axisymmetric, but non-spherical outflows. The occurrence of a particular channel depends on the initial binary parameters, most importantly on the initial period. Binaries with relatively short periods (perhaps with periods $\sim 10\,\mathrm{d} - 1\,\mathrm{yr}$) are likely to experience a common-envelope phase and to coalesce (see, e.g., FK Comae and V Hydrae). Systems with somewhat longer periods ($\sim 1\,\mathrm{yr} - 10\,\mathrm{yr}$) will also undergo a common-envelope phase, but should be able to eject their envelopes (e.g., NGC 2346). While systems with even longer periods ($\sim 10 - 100\,\mathrm{yr}$) will not experience Roche-lobe overflow, their

winds may still influenced by binary interaction (e.g., OH 231.8+4.2). If we use the rule-of-thumb that the orbital period distribution for binaries is flat in $\log P$ and that each decade of $\log P$ contains 10 % of all binaries, we can estimate the frequencies of the various channels as $\sim$ 15 % for merging, $\sim$ 10 % for common-envelope ejection and $\sim$ 10 % for detached, interacting systems (note that the estimate for common-envelope ejection is in approximate agreement with the observational estimate by Bond and Livio [1990]). Even though these estimates are very crude and ignore important selection effects, they show that the outflows from a significant fraction of all stellar systems (at least $\sim$ 35 %) are affected by binary interaction. We therefore have to conclude that binary interaction is likely to be important, not only to explain disk-like outflows around evolved stars, but also for the shaping of PNe (although probably not in all cases).

REFERENCES

Abt, H. A., and Levy, S. G. 1976, ApJS, 30, 273

Abt, H. A., and Levy, S. G. 1978, ApJS, 36, 241

Balick, B. 1987, AJ, 94, 671

Balick, B., Preston, H. L., and Icke, V. 1987, AJ, 94, 1641

Barvainis, R., McIntosh, G., and Predmore, C. R. 1987, Nature, 329, 613

Bieging, J. H., Wilner, D., and Thronson, H. A., Jr. 1991, ApJ, 379, 271

Bieging, J. H., and Nguyen-Quang-Rieu 1988, ApJ, 324, 516

Bodenheimer, P., and Taam, R. E. 1984, ApJ, 280, 771

Bond, H. E., and Livio, M. 1990, ApJ, 355, 568

Bopp, B. W., and Stencel, R. E. 1981, ApJ, 247, L131

Bowers, P. F. 1991, ApJS, 76, 1099

Bowers, P. F., and Johnston, K. J. 1990, ApJ, 354, 676

Calvert, N., and Peimbert, M. 1983, Rev. Mexicana Astr. Ap., 5, 319

Cohen, M. 1981, PASP 93, 288

Cohen, M. 1992, private communication

Cohen, M., Dopita, M. A., Schwartz, R. D., Tielens, A. G. G. M. 1985, ApJ,

297, 702

Cohen, M., and Kuhi, L. V. 1977, ApJ, 213, 79

Crampton, D., Cowley, A., and Humphreys, R. M. 1975, ApJ, 198, L135

Duquennoy, A., and Mayor, M. 1991, A&A, 248, 485

Dyck, H. M., Zuckerman, B., Howell, R. R., and Beckwith, S. 1987, PASP 98, 99

Eggleton, P. P. 1990, in From Miras to Planetary Nebula: Which Path for Stellar Evolution?, ed. M. O. Mennessier and A. Omont (Gif sur Yvette Cedex, Editions Frontières), p. 513

Fabian, A. C., and Hansen, C. J. 1979, MNRAS, 187, 283

Forveille, T., Morris, M., Omont, A., and Likkel, L. 1987, A&A, 176, L13

Healy, A. P., and Huggins, P. J. 1988, AJ, 95, 866

Herbig, G. H. 1970, ApJ, 163, 557

Iben, I., Jr. 1989, in IAU Symp. 131, Planetary Nebulae, ed. S. Torres-Peimbert (Dordrecht, Kluwer), p. 505

Icke, V., Preston, H. L., and Balick, B. 1989, AJ, 97, 462

Jacobson, P. et al. 1991, ApJ, 369, L63

Kahane, C., Maizels, C., and Jura, M. 1988, ApJ, 328, L25

Kahn, F. D., and West, K. A. 1985, MNRAS, 212, 837

Kolesnik, I. G., and Pilyugin, L. S. 1986, Sov. Astr., 30, 169

Kraicheva, Z. T., Popova, E. I., Tutukov, A. V., and Yungel'son, L. R. 1978, Sov. Astr., 22, 670

Kraicheva, Z. T., Popova, E. I., Tutukov, A. V., and Yungel'son, L. R. 1979, Sov. Astr., 23, 290

Kwok, S., Purton, C. R., and FitzGerald, M. P. 1978, ApJ, 219, L125

Lane, A. P., Johnston, K. J., Bowers, P. F., Spencer, J. H., Diamond, P. J. 1987, ApJ, 323, 756

Livio, M., Salzman, J., and Shaviv, G. 1979, MNRAS, 188, 1

Livio, M. and Soker, N. 1988, ApJ, 329, 764

Lundqvist, P. 1992, preprint

Luo, D., and McCray, R. 1991, ApJ, 379, 659

Masson, C. R. 1989, ApJ, 336, 294

Matese, J. J., Whitmire, D. P., and Reynolds, R. T. 1989, Icarus, 81, 24

McCarthy, D. W., Jr. 1979, in IAU Coll. No. 50, High Angular Resolution Stellar Interferometry, ed. J. Davis and W. J. Tango (University of Sydney), p. 18-1

McCarthy, D. W., Jr., Howell, R. R., and Low, F. J. 1980, ApJ, 235, L27

Meaburn, J., Walsh, J. R., Morgan, B. L., Hebden, J. C., Vine, H., and Standley, C. 1985, MNRAS, 213, 35p

Moran, J. M., Ball, J. A., Yen, J. L., Schwartz, P. R., Johnston, K. J., and Knowles, S. H. 1977, ApJ, 211, 160

Morris, M. 1981, ApJ, 249, 572

Morris, M. 1987, PASP 99, 1115

Morris, M. 1990, in From Miras to Planetary Nebulae: Which Path for Stellar Evolution, ed. M .O. Mennessier and A. Omont (Gif sur Yvette Cedex, Editions Frontières), p. 520

Ney, E. P., Merrill, K. M., Becklin, E. E., Neugebauer, G., and Wynn-Williams, C. G. 1975, ApJ, 198, L129

Olofsson, H. 1992, in ESO/CTIO Workshop, Mass Loss on the AGB and Beyond, preprint

Packet, W. 1981, A&A, 102, 17

Paczyński, B. 1970, in Mass Loss and Evolution in Close Binaries, ed. K. Gyldenkerne & R. M. West (Copenhagen, Copenhagen Univ. Press), p. 139

Paczyńksi, B. 1976, in IAU Symp. No. 73, Structure and Evolution of Close Binary Systems, ed. P. P. Eggleton, S. Mitton, and J. Whelan (Dordrecht, Reidel), p.75

Paczyński, B. 1985, in Cataclysmic Variables and Low-Mass X-Ray Binaries, ed. D. Q. Lamb and J. Patterson (Dordrecht, Reidel), p1

Pascoli, G. 1992, PASP 104, 350

Peimbert, M. 1978, in IAU Symp. No. 76, Planetary Nebulae, ed Y. Terzian

(Dordrecht, Reidel), p. 409

Pikel'ner, S. B. 1968, Astrophys. Lett., 2, 97

Pikel'ner, S. B. 1973, Astrophys. Lett., 15, 91

Pijpers, F. P. 1992, private communication

Pijpers, F. P., and Habing, H. J. 1989, A&A, 215, 334

Pilyugin, L. S. 1987, Sov. Astr., 31, 282

Podsiadlowski, Ph. 1991, Nature, 350, 654

Podsiadlowski, Ph. 1992, PASP 104, 1

Poe, C. H., and Friend, D. B. 1986, ApJ, 311, 317

Pringle, J. E. 1989, in Theory of Accretion Disks, ed. F. Meyer (Dordrecht, Kluwer, p. 105

Reid, M. J., and Menten, K. W. 1990, ApJ, 360, L51

Reipurth, B 1987, Nature, 325, 787

Rodonò, M. 1992, in IAU Symp. No. 151, Evolutionary Processes in Interacting Binary Stars, ed. Y. Kondo, R. F., Sisteró, and Polidan, R. S. (Dordrecht, Kluwer), p. 71

Rodríguez, L. F. 1989, in IAU Symp. No. 131, Planetary Nebulae, ed. S. Torres-Peimbert (Dordrecht, Kluwer), p. 129

Rouan, D., Omont, A., Lacombe, F., and Forveille, T. 1988, A&A, 189, L3

Sahai, R., Wootten, A., and Clegg. R. E. S. 1990, A&A, 234, L1

Serkowski, K. 1972, private communication (as quoted by Dyck et al. 1987)

Soker, N. 1992a, ApJ, 386, 190

Soker, N. 1992b, ApJ, 389, 628

Soker, N. and Livio, M. 1989, ApJ, 339, 268

Solf, J. 1984, A&A, 139, 296

Solf, J., and Ulrich, H. 1985, A&A, 148, 274

Sparks, W. M., and Stecher, T. P. 1974, ApJ, 188, 149

Storey, J. W. V. 1984, MNRAS, 206, 521

Tout, C. A., and Eggleton, P. P. 1988, ApJ, 334, 357

Volk, K., and Kwok, S. 1985, A&A, 153, 79

Wampler, E. J. et al. 1990, ApJ, 362, L13

Wang, L., and Mazzali, P. A. 1992, Nature, 355, 58

Zuckerman, B., and Aller, J. H. 1986, ApJ, 301, 772

Zuckerman, B., and Gatley, I. 1988, ApJ, 324, 501

Is Mass Loss From Red Giant Stars Dust Driven ?

J. A. Yates
University of Manchester
Nuffield Radio Astronomy Laboratories
Jodrell Bank, Macclesfield, Cheshire SK11 9DL.

Abstract

Long period variable stars on the Asymptotic Giant Branch are observed to be losing mass in the form of cool dusty molecular stellar winds at rates from 10^{-7} to $10^{-4} M_\odot yr^{-1}$. The driving force for this mass loss is thought to be radiation pressure on dust particles. The dust transfers its momentum to gas molecules via collisions. This paper discusses the existing evidence for this scenario. New results, from analysis of 22GHz H_2O maser observations made by MERLIN, show that the crucial acceleration past the stellar escape velocity of the central star takes place in the inner circumstellar envelope around the central star. The analysis of the velocity fields of the circumstellar envelopes of VX Sgr and VY CMa using the model described by Chapman & Cohen (1986) will be discussed.

1 Introduction

Long period variable stars (LPVs) are found on the Asymptotic Giant Branch of the H–R diagram. Their typical physical parameters are as follows :- $R_* \sim 10^{11}$–10^{12}m; $M_* \sim 0.8$–10 $M_\odot$; $T_{surface} \sim 2000$–3000 K. These stars undergo radial pulsations with periods of 300–3000 days. They are losing mass to the ISM at rates of between 10^{-7} to $10^{-4} M_\odot yr^{-1}$. The more massive stars have longer periods and greater mass loss rates. The circumstellar envelopes (CSEs) of these stars can be optically thin (miras) or optically thick (OH–IR stars). This phase of stellar evolution is thought to last 10^5 years. It is thought to be the main mechanism for replenishing the ISM with gas and dust.

This article will review, and add to, the evidence that the process of mass loss seen in these stars is essentially radiation driven. This was first proposed by Goldreich & Scoville (1976). They proposed that radiation pressure on dust, and the subsequent collisions of the dust with gas, radially accelerates material past the stellar escape velocity and away from the star, out into the ISM. Their model was further refined by Bowen (1988) who incorporated the radial pulsations of the photosphere into the model. Chapman & Cohen (1986) used observations of several different maser transitions observed towards the supergiant VX Sgr to measure the velocity field in its CSE and see how it compared with the model proposed by Goldreich & Scoville (1976). They also showed that in the case of VX Sgr the critical acceleration of the material past the stellar escape velocity V_{esc} takes place in the inner CSE in which the 22GHz water masers are found.

In section 3 the evidence for acceleration past V_{esc} the inner CSE will be outlined. This is based upon 22GHz H_2O maser MERLIN observations of the physical structure of this region. Section 4 will briefly outline the evidence for the existence of dust in CSEs and consider one example of observational evidence that supports the assertion that it is the agent by which photon momentum is transferred to gas molecules in the CSEs of LPVs. Section 5 will formally outline the model of Goldreich & Scoville (1976), and discuss the contributions made by Chapman & Cohen (1986) and Bowen (1988). Also it will consider more recent work on the role of dust in causing radial acceleration in CSEs. In Section 6 other mechanisms that could cause the observed radial acceleration will be discussed. The conclusions and further work will be given in section 7. First, in section 2, I will outline why, and how, circumstellar masers are used to trace the radial velocity field in CSEs.

2 Masers As Velocity Field Probes

At the moment the velocity fields of the CSEs of these stars are investigated using, primarily, spectral line interferometric observations of their circumstellar 43GHz SiO, 22GHz H_2O, and OH 1612MHz maser emission. Because of their different inversion and radiative decay properties, we can use these masers to probe different regions of the CSE. This allows us to build up a comprehensive picture of the physical structure and velocity field of a CSE. The 43GHz SiO maser arises high in the extended stellar atmosphere. The maser emission is centred on the stellar velocity. There is no correlation between the stellar mass loss rate and the expansion velocity of the SiO masing region. Gas is not undergoing radial acceleration in this region. Dust has yet to form. This maser traces the physical conditions on the inner edge of the dust condensation zone. It is quenched if T < 1200 K and $n_{H_2} > 10^{16}m^{-3}$ (Elitzur (1992), and references therein). SiO begins to condense out of the extended stellar atmosphere in these conditions and form dust particles. This maser is a probe of the region where mass loss is established. The 22GHz H_2O maser is detected in the inner CSE. Its pumping mechanism has been successfully modelled by Cooke & Elitzur (1985). The maser is quenched if $n_{H_2} > 10^{15}m^{-3}$. It is seen in the temperature range 300 to 900 K. The maser region is bounded by well defined inner and outer radii. The inner boundary is determined by collisional quenching (Cooke & Elitzur 1985). This maser is seen in an expanding thick shell around the star with inner and outer radii typically being 10^{12} and 10^{13}m respectively. The OH 1612MHz maser is found in the outer CSE at a distance from the central star of 10^{14} to 10^{15}m. It has an IR pumping scheme (Elitzur 1982). This maser is quenched if n_{H_2} exceeds $4 \times 10^{11}m^{-3}$ and if the medium is optically thin at 119μm. These control the size of the inner and outer radii, respectively, of the OH 1612MHz maser emission zone.

Interferometric observations in spectral line mode of these masers have been made towards LPV stars. Maps of the maser emission described above are to be found in Lane (1984), Lane et al. (1987), and Bowers, Johnston & Spencer (1983). Kinematic analysis of the masers' doppler velocities and relative positions allows velocity–radius diagrams of the maser distribution to be plotted. Figure 1 shows the simplest case of a thin shell with single expansion velocity. Different radial velocities correspond to different slices through the shell in this case, and the plot of radius vs velocity is simply an ellipse

(Cohen 1989). Chapman & Cohen (1986) analysed observations of the 3 maser transitions described above and the OH 1665/7 MHz mainline maser transitions and performed such an analysis. Figure 2 summarizes their results. The OH 1612MHz masers trace the expected radius–velocity ellipse, but the other masers have more complex radius–velocity signatures. These can be interpreted in terms of a smooth increase in expansion velocity with distance from the central star. From Figure 2 it can be seen that the SiO maser emission is close to the star and has an expansion velocity of $\sim$2 km s^{-1}. The H$_2$O maser emission is seen in a thick shell further out. The OH 1612MHz maser emission is seen in a thin shell at a much greater distance from the star than the other two masing regions. The information this plot provides about the velocity field of the CSE of VX Sgr was used to test the validity of the model proposed by Goldreich & Scoville (1976) (see section 5.1 and Figure 5).
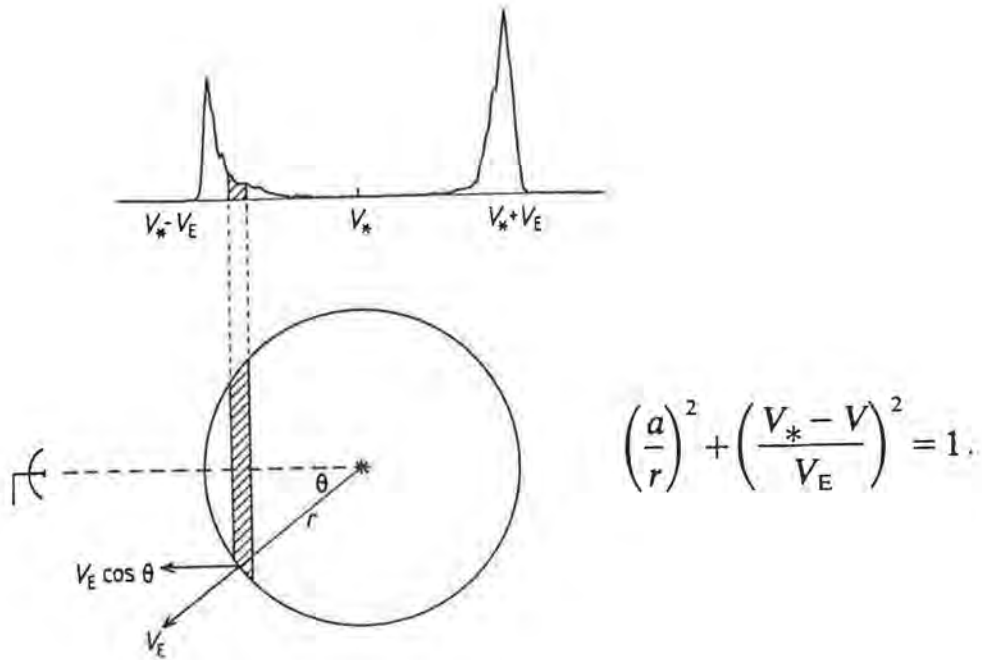

$$\left(\frac{a}{r}\right)^2 + \left(\frac{V_* - V}{V_E}\right)^2 = 1.$$

Figure 1: A typical OH 1612MHz spectrum and an outline of the Thin–Shell Model (Cohen 1989). For a uniformly expanding thin shell each radial velocity corresponds to a slice through the maser shell perpendicular to the line of sight. The radial velocity V and radius a ($a = r \sin \theta$) of such a slice are related by the equation of an ellipse, which is given in this figure.
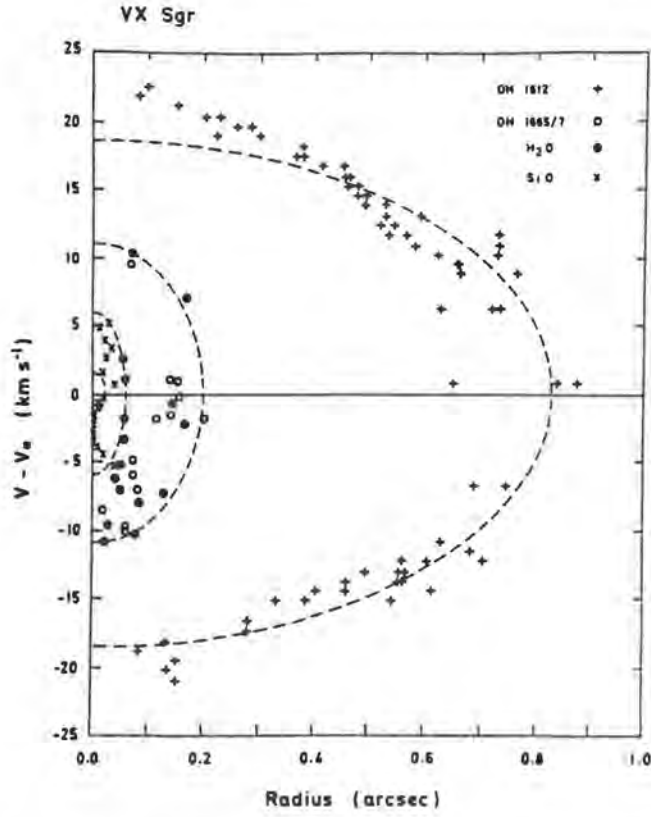
Figure 2: The Velocity–radius diagram made from maps that were made from the 6 maser transitions observed towards VX Sgr (Chapman & Cohen 1986). The maser symbols are given in the top right hand corner of the diagram. Three distinct masing regions are clearly seen for the SiO, H_2O, and OH 1612MHz masers.

3   The Inner CSE : As Seen By 22GHz H₂O Maser Emission.

3.1   Physical Structure

We have mapped the 22GHz H$_2$O maser emission seen towards three mira variables and three supergiant stars (Yates & Cohen 1992). Their integrated line emission maps are shown in Figure 3. The extent of the emission region generally increases with mass loss rate. The miras have relatively simple structures compared to the supergiants. The supergiants have complex structures. There is evidence for circumstellar discs, especially around VY CMa. Both VY CMa and NML Cyg show evidence of bipolar outflows in the form of weak H$_2$O maser features situated symmetrically each side of the central star. These features are well separated from the main body of H$_2$O emission (circumstellar disc) and in the case of VY CMa are found to lie above and below the circumstellar disc. It is clear that the structure of the inner CSE is not spherically symmetric. There is clear evidence for toroidal and disc–like structures in this region.

3.2   Velocity Field Analysis

For VY CMa, S Per, RT Vir, and IK Tau it was possible to plot velocity–radius diagrams of the H$_2$O masers. These are presented in Figure 4. The dashed ellipses represent the inner and outer radii of the masing region. The expansion velocity of an ellipse is the point where the ellipse intersects the velocity axis. The escape velocities at the inner and outer radii are also given in Figure 4. In all four cases the circumstellar material is bound to the star at the inner radius ($V_{exp} < V_{esc}$), but unbound at the outer radius ($V_{exp} > V_{esc}$). Thus the expansion velocity increases with radius through the H$_2$O maser region.

4   Dust

The main evidence for the existence of dust comes from the observed IR silicate line at 9.7 μm, IRAS colour–colour plots, and recent 11 μm interferometry results (Bester 1991). The 9.7 μm is always observed whether in emission (miras) or absorption (OH–IR stars). It shows that stellar radiation is being absorbed by silicate dust in the CSE. IRAS colours for these sources show a clear IR excess over the black body spectrum between 12 and 60 μm. This is because the dust is re–radiating stellar photons at IR frequencies. The interferometry data at 11 μm show dust to within 3R$_*$ of the stellar surface of the mira O Ceti. This places dust close to its theoretical condensation zone of 2 to 3R$_*$.

There is some direct observational evidence that radiation pressure acting on dust grains influences mass loss from OH–IR stars. Lewis, Eder & Terzian (1990) report that a clear correlation is seen between the expansion velocities of CSEs of a sample of OH–IR stars (derived from their OH 1612MHz spectra) and their IRAS (25–12)μm colours. Lewis, Eder & Terzian (1990) argue that this correlation is seen because the dust, which has been "energised" by stellar photons from the central star, does actually cause the the radial acceleration observed in CSEs.
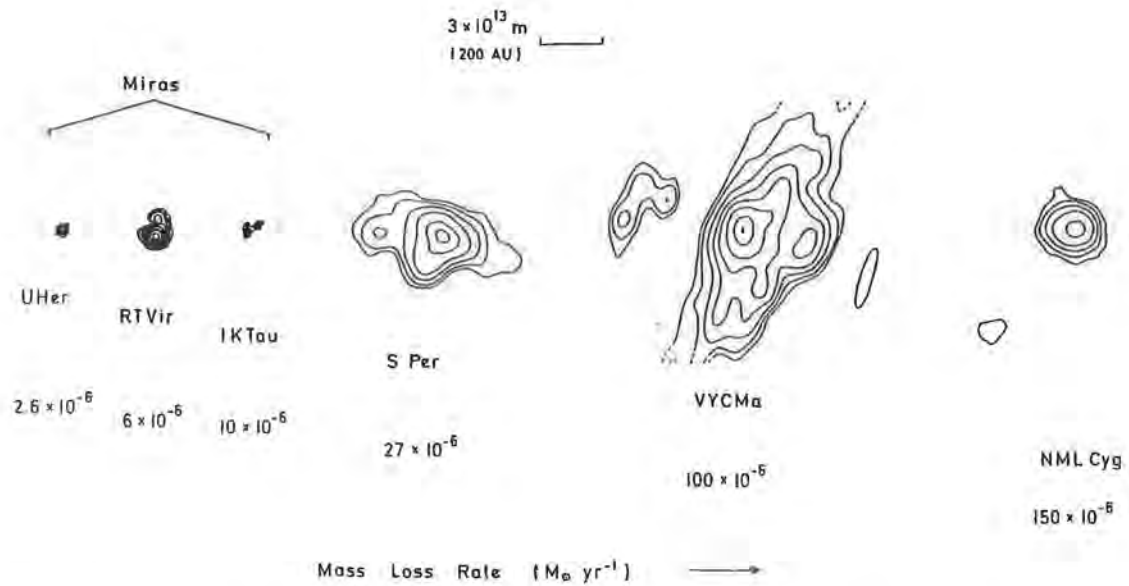
Figure 3: 22GHz H_2O maser integrated line emission maps of the inner CSEs of U Her, RT Vir, IK Tau, S Per, VY CMa and NML Cyg from Yates & Cohen (1992). They are presented in order of increasing mass loss rate. It is seen that envelope size generally increases with increasing mass loss rate. The mass loss rates are from Bujarrabal, Gomez-Gonzalez & Planesas (1989), Knapp *et al.* (1982), Gehrz & Woolf (1971), and Zuckerman & Dyck (1986).
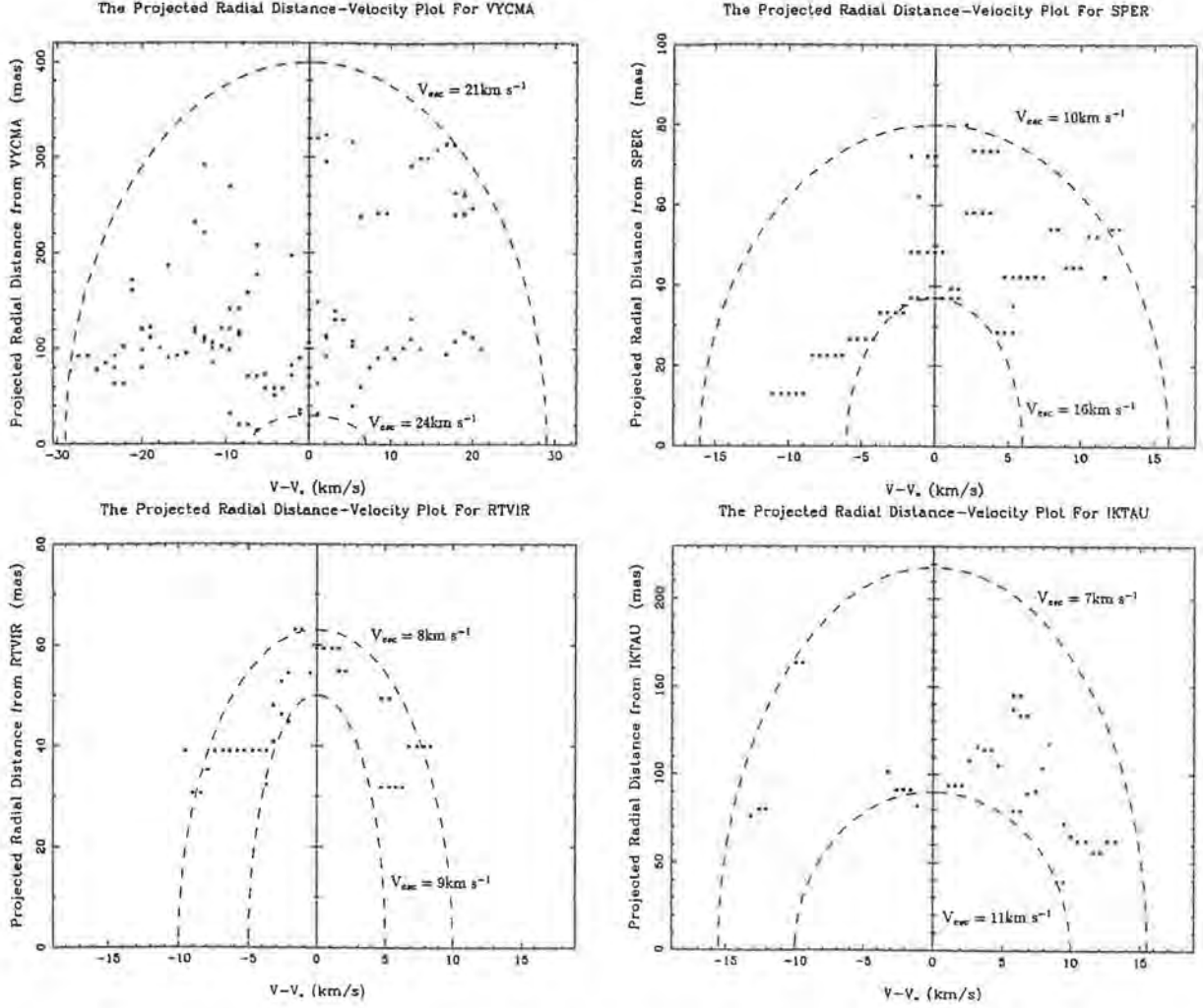
Figure 4: Velocity–radius plots of the 22GHz H_2O maser distributions about VY CMa, S Per, RT Vir, and IK Tau (Yates & Cohen 1992). The black dots are the individual maser spots. The dashed ellipses show the inner and outer radii of the maser distributions. The escape velocity V_{esc} at each radius is also given. The masses and distances used to determine V_{esc} are listed in table 4 of Yates & Cohen (1992).

5 Modelling The CSE Velocity Field

5.1 Modelling the Expanding Wind

Goldreich & Scoville (1976) proposed that radial acceleration is caused by radiation pressure which acts on dust grains that condense in the extended outer atmosphere of the central star. **Dust grains transfer photon momentum to the gas molecules by collisions with the gas molecules.** The gas flow is supersonic, hence the thermal pressure term in an equation of motion becomes unimportant. Goldreich & Scoville (1976) proposed the following equation of motion for gas and dust particles in the CSE,

$$\nu \frac{d\nu}{dr} = \frac{\kappa(r)L_*}{4\pi r^2 c} - \frac{GM_*}{r^2}.$$ (1)

ν is the radial gas velocity, L_* is the stellar bolometric luminosity, M_* is the stellar mass, and r is the radial distance from the star. $\kappa(r)$ is the dust opacity per unit mass and is defined as follows,

$$\kappa = \frac{\sigma_{gr} n_{gr} Q}{\rho} m^2 kg^{-1}.$$ (2)

σ_{gr} is the cross section of the grains, n_{gr} is their number density, Q is the radiation pressure efficiency factor, and ρ is the gas density. If all the dust condenses out at $2R_*$ κ is constant. However observations of the CSE of IRC+10011 during a lunar occultation showed that κ increases from the stellar surface to about $10R_*$ (Goldreich & Scoville 1976). They modelled κ as,

$$\kappa(r) = \Gamma(1 + \frac{\Delta r^2}{(10R_*)^2 + r^2}).$$ (3)

Γ and Δ are model dependent parameters.

Chapman & Cohen (1986) tested this model with their analysis of the velocity field of VX Sgr. In Figure 5 the expansion velocity is plotted against radial distance from the star. Two curves are shown. The dashed curve describes the motion of a dust particle if κ is constant after $2R_*$. The full curve is the motion of a particle if κ is modelled as follows,

$$\kappa(r) = \Gamma(1 + \frac{Ar^2}{B^2 R_i^2 + r^2}).$$ (4)

R_i is the inner radius of the CSE and Γ is the initial dust opacity. The parameter A controls the terminal velocity and dust opacity and B controls $d\kappa/dr$. A similar analysis has been done for VY CMa (Yates & Cohen 1992) and is shown in Figure 6. Both figures show that the assumption that κ is constant in the equation of motion is not valid. The model velocity field reaches the terminal velocity too soon in both cases. κ increases with distance from the star out to $100R_*$. This is probably due to grain growth which increases the cross–sectional area of the dust. In the inner CSE this is probably due to collisions of the dust particles and to dust still condensing out of the gas. In the OH 1612MHz region all the dust should have condensed out of the gas and collisions will be rare. In this region the formation of ice mantles on the dust (Justtanont & Tielens 1992) will increase κ. This analysis does suffer from a lack of good reliable data, especially 43GHz SiO and OH
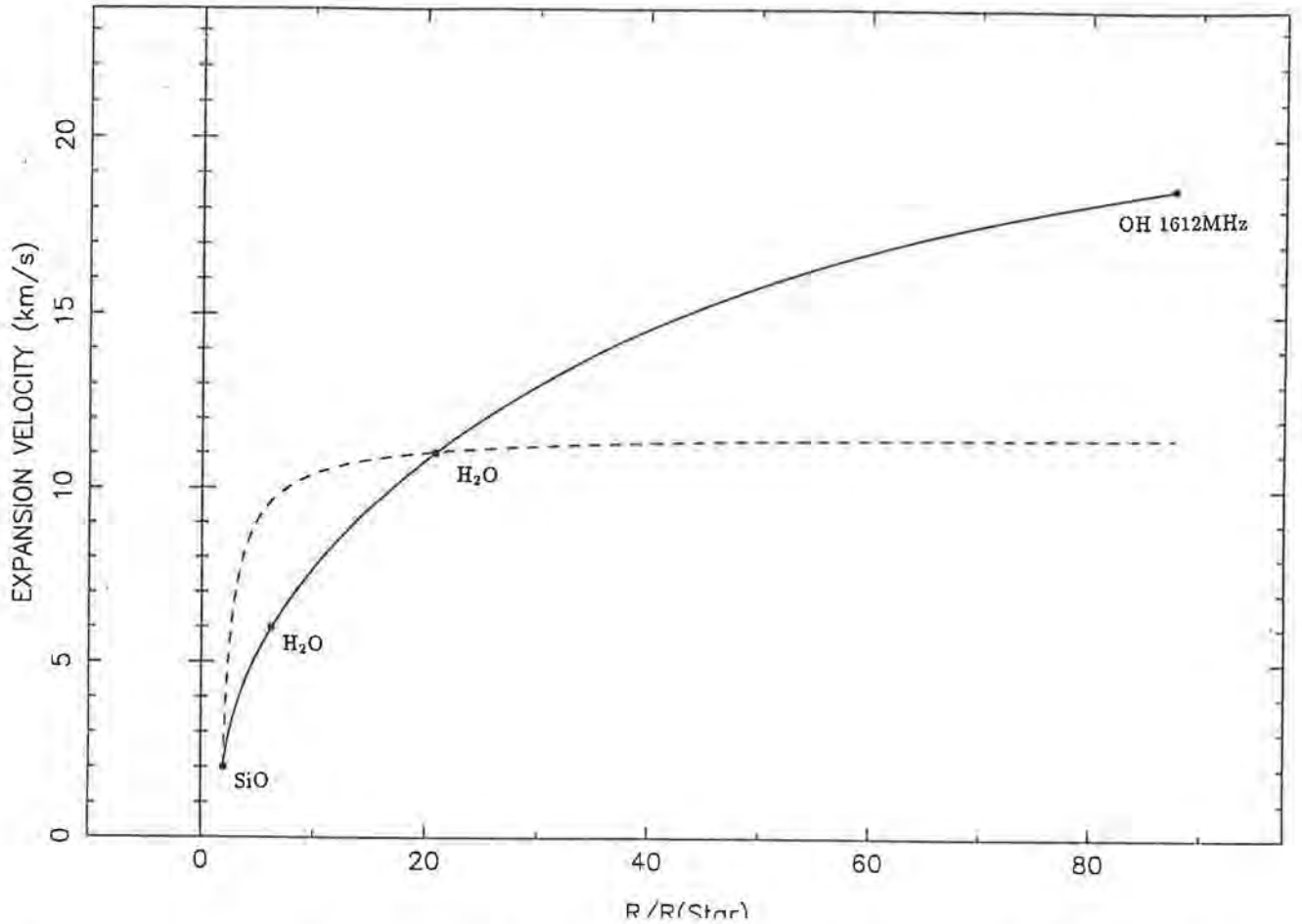
Figure 5: V_{exp} plotted against R/R_* for VX Sgr (Chapman & Cohen 1986). The dashed line is a fit to the SiO data point and the 11 km s^{-1} H$_2$O point assuming κ is constant. The κ calculated from this is 0.04 m^2 kg^{-1}. The bold line is a fit to the data points with $\kappa = \kappa(R)$ (equation 4). The model parameters calculated from the fit to the four points are $\Gamma = 0.033$ m^2 kg^{-1}, A=17.9, and B=28.8.

mainline data. To solve the equation of motion using the $\kappa(r)$ proposed by Chapman & Cohen (1986) at least four reliable data points are required. The OH mainline points in Figure 6 are an example of the problems we face.

5.2 Incorporating Radial Pulsations

The model of Goldreich & Scoville (1976) did not address how the SiO particles got to the region where they could condense out of the stellar photosphere (2 to 3R$_*$). Radiation pressure cannot drive gas in sufficient quantities from the stellar atmosphere and observations of SiO masers (Lane 1984) show SiO molecules to be still in the gaseous state at 2R$_*$. However observational evidence provided by Hinkle, Scharlach & Hall (1984) showed cyclical motions of cool gas in the extended outer layers of the photospheres of several miras. The measured velocities of 20 km s^{-1} are sufficient to take material 2 to 5R$_*$ above the photosphere. These cyclical motions are due to the radial pulsations of the stellar atmosphere. The expansion is adiabatic, so the gas cools and becomes less dense, so allowing dust to form. Bowen (1988) proposed that acceleration of circumstellar
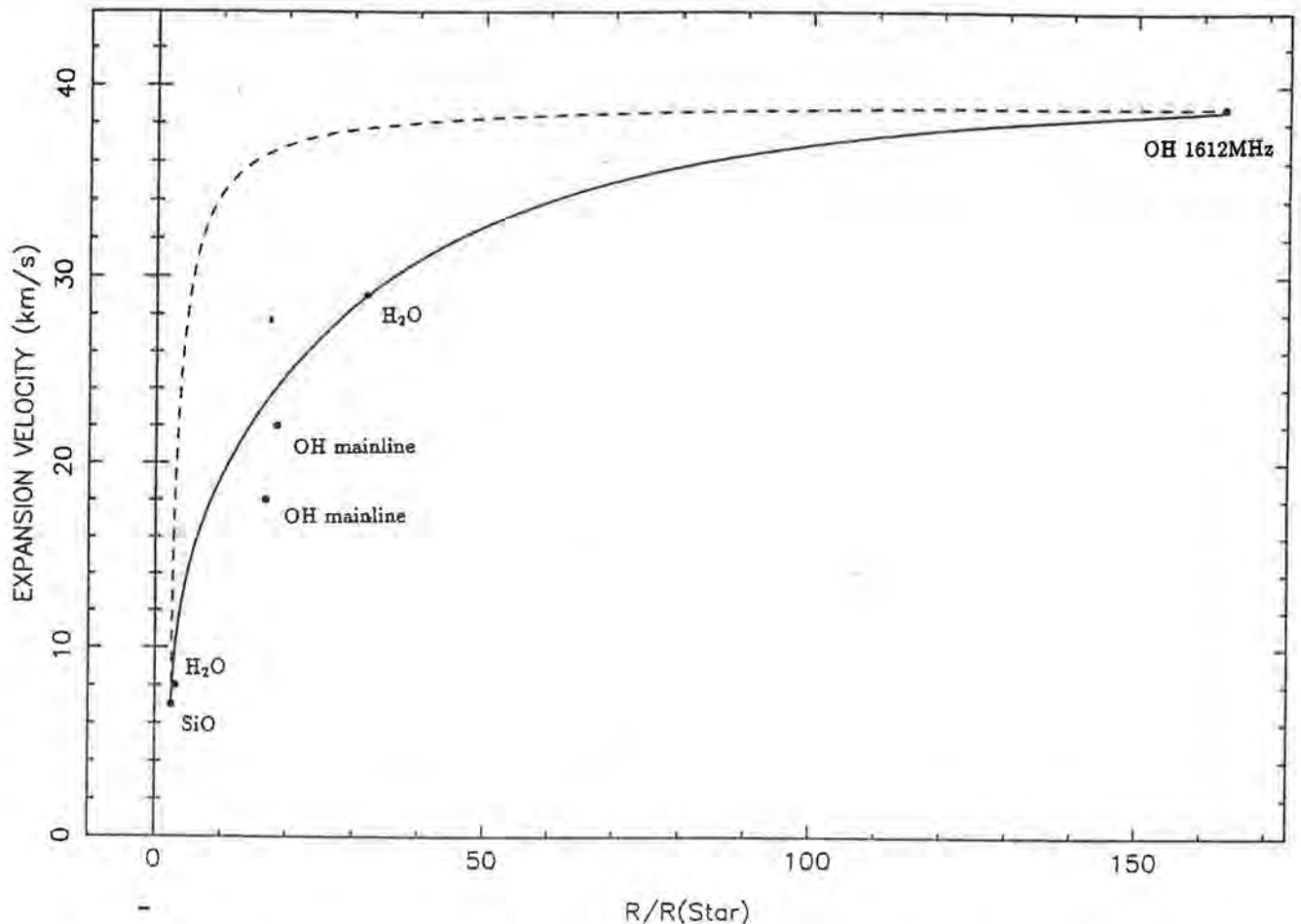
Figure 6: V_{exp} plotted against R/R$_*$ for VY CMa (Yates & Cohen 1992). The dashed line is a fit to the SiO data point and the OH 1612MHz data point assuming κ is constant. The κ calculated from this is 0.123 m^2 kg^{-1}. The bold line is a fit to the data points with $\kappa=\kappa(R)$ (equation 4). The model parameters calculated from the fit to the SiO, H$_2$O, and OH 1612MHz points are $\Gamma = 0.045$ m^2 kg^{-1}, A=21.4, and B=16.2. The SiO point is derived from Lane (1982); the H$_2$O points are from Yates & Cohen (1992); the OH mainline points are derived from Benson & Mutel (1982); the OH 1612MHz point is from Bowers, Johnston & Spencer (1983).

material and the subsequent mass loss results from the combined effects of atmospheric extension by shocks, followed by radiation pressure on the newly formed dust grains which is accompanied by collisional momentum transfer to the gas. Bowen (1988) modelled the motion of gas with and without dust. He found that the gas around a typical mira type star failed to achieve V_{esc} unless dust was present. Dust forms in the shock enhanced densities of the cool outer regions. It serves as an effective agent for transferring momentum from the radiation field of the star to the gas. Using this work Berryer (1991) calculated a minimum grain flux of $10^{31} s^{-1}$. At this flux dust will cause an accelerating outflow that will achieve V_{esc}. Fleischer, Gauger & Sedlmayr (1991) have included dust formation, dust growth and evaporation in Bowen's model. This is a good first attempt at modelling the variation of the dust opacity from theoretical considerations.

6 Other Mechanisms for Acceleration

6.1 Sound

The alternative main mechanism proposed for causing the observed radial acceleration in LPVs is sound. Pijper & Habing (1989) proposed that the mass loss rates and low terminal velocities of LPVs can explained by radial acoustic waves. The energy flux in these waves should be a few per cent of the thermal energy flux and the dissipation length of the wave is $\geq$ R$_*$ (a weakly dissipating sound wave). Their model velocity fields were similar to those of Goldreich & Scoville (1976), Chapman & Cohen (1986), and Yates & Cohen (1992). These acoustic waves produce a slow wind which accelerates over a long distance. Pijper & Habing (1989) claim that dust is not required to drive the observed mass loss. If there are a range of wavelengths present in the CSE, the wave–vectors acquire non–radial components. This can cause the CSE to have an aspherical structure and inhomogenities in the wind (masers?).

6.2 Radial Pulsations

Judge & Stencel (1991) proposed that long–period photospheric variations can drive stellar winds. They calculated that more than enough energy exists in long-period variations to account for wind energy losses and have suggested a program to study correlations between photospheric flux variations and chromospheric and wind diagnostics.

6.3 Gradual Dust Formation

Bowers (1992) pointed out that the natural progression often quoted in the literature:- $V_{max}(\text{SiO}) < V_{max}(\text{H}_2\text{O}) < V_{max}(\text{OH 1612MHz})$ is not always the case. This would cause problems for the present models of smooth radiative acceleration of dust up to a terminal velocity (assuming $R_{SiO} < R_{H_2O} < R_{OH1612}$). Also Bowers (1992) claims that there is no sudden change of velocity between any of the species which might be attributed to a sudden burst of dust formation at a given radius. He argues that dust formation is a gradual process and that gas is being accelerated *within* the SiO maser shell. He makes the important point that non–uniform/chaotic processes could be important for causing outflow.

7 Conclusion

The 22GHz H$_2$O maser emission of LPVs provides evidence for acceleration past the escape velocity in a specific region of the CSE (Chapman & Cohen (1986) and Yates & Cohen (1992)). In the near future theoretical work on extended stellar atmospheres and CSEs will benefit from the recent completion of the MERLIN upgrade and the VLBA. These two interferometers will provide much better spectral line data on maser emission with which to test kinematic models. The recent discovery of the sub–mm water maser lines at 96, 232, 321 GHz (Menten & Melnick 1991) and the 325 GHz (Yates, Cohen & Hills 1992), should allow us to put limits on the physical conditions in the inner CSE (Neufeld & Melnick 1991). The appearance of FIR spectral line interferometers will allow us to

observe dust in velocity space. This will allow us to see if gas motions (maser observations) and dust motions (FIR observations) in a CSE are related. Modelling velocity fields semi-empirically e.g. (Chapman & Cohen 1986) and theoretically e.g. (Fleischer, Gauger & Sedlmayr 1991) will provide two approaches to understanding the behaviour of dust grains in CSEs. It will tell us how the dust affects the bulk dynamics of the outflow and help us understand the processes of dust formation and growth in different parts of the CSE. A complete treatment should include nucleation; growth, from nucleation until saturation, of the dust grains; the dependence of Q on grain size; momentum and energy coupling of the grains to the gas; grain dynamics, and sputtering, at supersonic velocities. Also the role of non–linear processes (chaos) in establishing and driving outflow should be investigated. The body of evidence for radiation (dust) driven winds is large and still increasing. Developments in theory, and new observations, will allow us to show that radiation (dust) driven winds are the major cause of the radially accelerated outflows seen around long period variable stars.

References

Benson, J. M. & Mutel, R. L., 1982. *Astrophys. J.*, **253**, 199.

Berryer, N., 1991. *Astr. Astrophys.*, **249**, 181.

Bester, L., 1991. *Astrophys. J.*, **367**, L27.

Bowen, G. H., 1988. *Astrophys. J.*, **329**, 299.

Bowers, P. F., Johnston, K. J. & Spencer, J. H., 1983. *Astrophys. J.*, **274**, 733.

Bowers, P. F., 1992. *Astrophys. J.*, **309**, L27.

Bujarrabal, V., Gomez-Gonzalez, J. & Planesas, P., 1989. *Astr. Astrophys.*, **219**, 256.

Chapman, J. M. & Cohen, R. J., 1986. *Mon. Not. R. astr. Soc.*, **220**, 513.

Cohen, R. J., 1989. *Rep. Prog. Phys.*, **52**, 883.

Cooke, B. & Elitzur, M., 1985. *Astrophys. J.*, **295**, 175.

Elitzur, M., 1982. *Rev. Mod. Phys.*, **54**, 1225.

Elitzur, M., 1992. *Astronomical Masers*, Kluwer Academic Publishers.

Fleischer, A. J., Gauger, A. & Sedlmayr, E., 1991. *Astr. Astrophys.*, **242**, L1.

Gehrz, R. D. & Woolf, N. J., 1971. *Astrophys. J.*, **165**, 285.

Goldreich, P. & Scoville, N., 1976. *Astrophys. J.*, **205**, 144.

Hinkle, K. H., Scharlach, W. & Hall, D., 1984. *Astrophys. J. Supp. Series.*, **56**, 1.

Judge, P. G. & Stencel, R. E., 1991. *Astrophys. J.*, **371**, 357.

Justtanont, K. & Tielens, A. G. G. M., 1992. *Astrophys. J.*, **389**, 400.

Knapp, G. R., Phillips, T. G., Leighton, R. B., Lo, K. Y., Wannier, P. G., Wootten, H. A. & Huggins, P. J., 1982. *Astrophys. J.*, **252**, 616.

Lane, A. P., Johnston, K. J., Bowers, P. F., Spencer, J. H. & Diamond, P. J., 1987. *Astrophys. J.*, **323**, 756.

Lane, A. P., 1982. *PhD thesis*, University of Massachusetts.

Lane, A. P., 1984. In: *IAU Symposium no. 110*, 329, eds Fabtini, Kellerman & Setti, D. Reidal.

Lewis, B. M., Eder, J. & Terzian, Y., 1990. *Astrophys. J.*, **362**, 634.

Menten, K. & Melnick, G., 1991. *Astrophys. J.*, **377**, 647.

Neufeld, D. A. & Melnick, G. J., 1991. *Astrophys. J.*, **368**, 215.

Pijper, F. P. & Habing, H. J., 1989. *Astr. Astrophys.*, **215**, 334.

Yates, J. A. & Cohen, R. J. 1992. In preparation.

Yates, J. A., Cohen, R. J. & Hills, R. E. 1992. In preparation.

Zuckerman, B. & Dyck, H. M., 1986. *Astrophys. J.*, **304**, 394.